UNIVERSITY OF
BIRMINGHAM

Laser Based Manufacturing of Optical Diffusers

By

Tawfiq Alqurashi, M.Sc.

A thesis submitted to
The University of Birmingham
For the degree of
DOCTOR OF PHILOSOPHY

Nanophtonics Group
School of Engineering
College of Engineering
and Physical Science
University of Birmingham
September 2018

ABSTRACT

High-quality optical diffusers provide a solution for a variety of applications requiring Gaussian and non-Gaussian intensity distributions, including usage in aerospace, for displays, imaging systems, and for biomedical optics. Advances in laser machining processes have enabled the rapid production of efficient optical diffusers. Three types of laser machining processes: CO_2, nanosecond, and femtosecond laser machining were utilized to fabricate the optical diffusers, mainly on float glass on which these processes produced nano and microfeatures allowing the light to be scattered. Also the float glass is an inexpensive material compared to fused silica and quartz glasses. But some other diffractive optical devices were fabricated on polycarbonate (PC) material. The reason the optical diffusers were not fabricated on polycarbonate (PC) and polyethylene terephthalate glycol (PETG) materials is that the areas treated with the laser became opaque, not allowing light to be scattered thoroughly.

Furthermore, we describe the design and experimental realization of mechanically stretchable and tunable optical diffusers. These intrinsically designed diffusers (based on cylindrical lenslet and micro tip arrays) were made directly on elastomer material using laser ablation. The dimensions of both the tips and the lenslet arrays play a critical role in the distribution of illumination and wettability resistance. By stretching the diffusers mechanically along the lenslet arrays, diffusion angle tuning was achieved along with a revisable change between hydrophilic to superhydrophobic states providing self-cleaning properties. These multifunctional diffusers constitute an important step towards integration with flexible materials or devices, such as stretchable organic light-emitting diodes (OLEDs) and polymer light-emitting diodes (PLEDs).

Acknowledgements

In the name of God the most Merciful and Beneficent

First and Foremost, praise be to Allah “Alhumidillah” for giving the strength, inspiration, ability, knowledge, and his blessing to undertake and conduct this scientific research study. Even his continuous grace and mercy during my life. Also, my deepest appreciation to all my family members without them I could not come to this stage.

I would like to thanks and express my deep and sincere gratitude to my supervisor **Dr. Haider Butt**, senior lecturer, School of engineering, the University of Birmingham for his encouragement, guidance and support during my Ph.D. program research. He is always there when I need him and kept track on improving my research skills, for that reason he is being an excellent supervisor. This thesis was completed with the support and encouragement of numerous people including **Prof. Stefan Dimov, Dr. Ali K. Yetisen, Dr. Umair Muhammed Hussain, Dr. Pavel Penchev and Dr. Aydin Sabouri**.

I would like to thank Leverhulme Trust, Saudi Arabia Cultural Bureau in London, Shaqra University, Wellcome Trust, King Abdullah bin Abdulaziz and the Saudi Government for the research funding.

Publications

Peer-reviewed Journal Publications

1- **Alqurashi, T**., et al., Nanosecond pulsed laser texturing of optical diffusers. AIP Advances, 2017. 7(2): p. 025313.
2- **Alqurashi, T**., et al., Femtosecond laser directed fabrication of optical diffusers. RSC Advances, 2017. 7(29): p. 18019-18023.
3- **Alqurashi, T**., et al., Femtosecond laser ablation of transparent microphotonic devices and computer-generated holograms. Nanoscale, 2017, 9, 13808-13819.
4- **Alqurashi, T**., et al., Laser inscription of pseudorandom structures for microphotonic diffuser application. Nanoscale, 2018, 10, 7095-7107.
5- **Alqurashi, T**., et al., Laser inscription of microfludic devices for bilogical assays. ACS Appl. Mater. Interfaces, 2019, 11, 13, 12253-12260.
6- **Alqurashi, T.** and Haider Butt, Highly flexible, stretchable, super hydrophobic and tunable optical diffusers. ACS Central Science, 2019 5 (6), 1002-1009.
7- **Alqurashi, T**., et al., Crystal Powder for Tunable Optical Diffuser. Under review.

Conference/Proceedings

1- **Alqurashi, T**., Ultrashort pulses laser directed manufacturing of glass diffusers, Photon 16, University of Leeds, 2016.
2- **Alqurashi, T**., Holographic ink-based optical devices, Photon 16, University of Leeds, 2016.
3- **Alqurashi, T**., Micro-structured surfaces for manufacturing photonic diffuser, PERCAT LES & EPS Research conference, University of Birmingham, 2017.
4- **Alqurashi, T**., Laser inscription of pseudorandom structures for microphotonic diffuser application, Nanotech, SETCOR Conference & Exhibition, Dubai, 2017.
5- **Alqurashi, T**., Laser directed manufacturing of optical diffuser, 5th Mechanical Engineering symposium, University of Birmingham, 2016.

Table of Contents

Table of Figures

Tables

Nomenclatures

T_α	Ablation Temperature	**I**	Intensity
α	Absorption Coefficient	**J**	Joule
V_α	Ablation Velocity	z_{max}	Maxima
θ	Angle	**MHz**	Mega Hertz
ϕ	Arbitrary Phase	**μ**	Micro
A	Area	**μJ**	Micro-Joule
°C	Celsius	**ε**	Nominal Strain
dB	Decibel	**P**	Power
°	Degree	**p**	Pressure
ρ	Density	**R**	Reflectivity
D	Diameter	**n**	Refractive Index
δ	Elongation	**d**	Spacing
E	Energy	**k**	Thermal Conductivity
f	Focal Length	**t**	Time
F	Force	**T**	Transmission/Temperature
C_p	Heat Capacity	**V**	Velocity
Q	Heat Flux	**W**	Watt
H_S	Heat of Sublimation	**λ**	Wavelength
h	Height	k_1, k_0	Wavevectors

Abbreviations

AFM	Atomic force microscope	**FWHM**	Full width at half maximum
Ra	Average Roughness	**HD**	Hatch Distance
CO_2	Carbon Dioxide	**IF**	Infinite-Focus
cm	Centimeter	**LMP**	Laser Micro Processing
CMOS	Complementary Metal-Oxide-Semiconductor	**LASER**	Light amplification by simulated emission of radiation
CGH	Computer-Generated Holography	**LED**	Light-Emitting Diode
CW	Continuous wave	**LCD**	Liquid Crystal Displays
DOD	Diffractive Optical Device	**MOPA**	Master Oscillator Power Amplifier
DOE	Diffractive Optical Element	**ms**	Millisecond
dpi	Dot-per-Inch	**NS**	Nanosecond
EBL	Electron Beam Lithography	**Nd;YG**	Neodymium Yttrium-Aluminum-Garnet
FFT	Fast Fourier Transform	**1/2/3D**	One/two/three-dimensional
FS	Femtosecond	**OLED**	Organic Light-Emitting Diode
FEG	Field Emission Gun	**PC**	Polycarbonate
FEA	Finite Element Analysis	**PDMS**	Polydimethylsiloxane
FEM	Finite Element Method	**PLED**	Polymer Light-Emitting Diode
FZP	Fresnel Zone Plates	**SEM**	Scanning Electron Microscope

Chapter 1: INTRODUCTION

1.1 Optical Diffuser Principles

An optical diffuser is a device or an element that is used to diffuse, scatter or diffract light in a certain way to transmit a soft or shaped light in a wide range of illumination and display applications. As a result of diffusing light, an optical diffuser reduces or eliminates the zero-order bright spot, which is the part of the energy from the incident beam passing through the optical diffuser without being scattered. It also enables the efficient transformation of incoming light beams into the desired diffraction of the outgoing light shape. This desired diffraction of the light shape can be categorized based on its intensity distribution profile (scatter shape) into two distinct characteristics: Gaussian-like shape and non-Gaussian-like shape (**Figure 1a-c**). To understand both shapes, the Gaussian shape inevitably needs to be identified and clarified. In mathematics, the Gaussian distribution simply refers to a normal distribution, familiar in statistics, and it has a random variable. For this reason, the Gaussian-like shape has a random variable distribution along the diffusion angle, resulting in light being refracted in a random direction. This is presumed to be without affecting the homogenizing light distribution, in this case, meaning the intensity profile presents a smooth scattering.

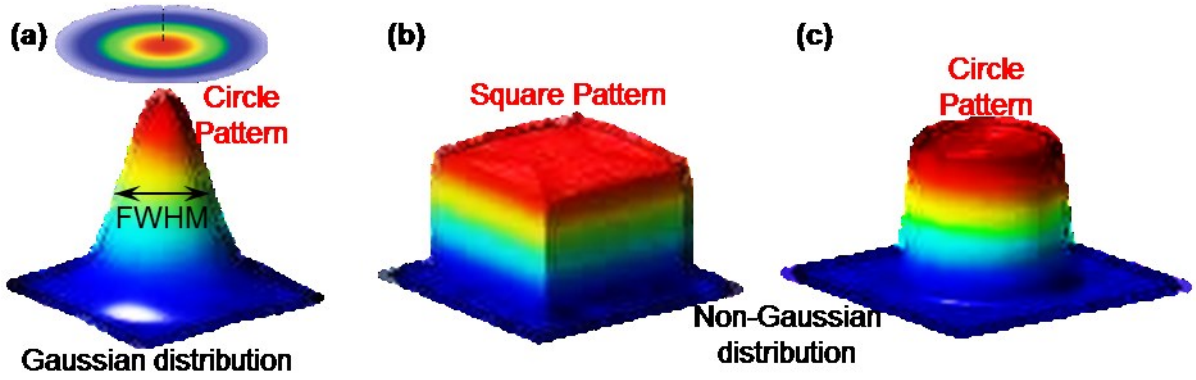

Figure 1. The intensity distribution of an outgoing light shape after passing through an optical diffuser: (a) the Gaussian-like distribution; (b, c) non-Gaussian distribution with square and circle shapes, respectively.

Gaussian-like shape diffusers often produce a circular light pattern with the independent variable of a Gaussian intensity profile, the scatter shape. Due to the independent variable of the Gaussian intensity profile, an inherently superior parameter was introduced to describe the width of a bump on the Gaussian distribution, called a full width at half maximum (FWHM). It is given by the difference between two extreme values of these independent variables on a curve at which the dependent variable reaches half its maximum (**Figure 1a**). This FWHM allows the denotation of a new term for optical specification among other Gaussian diffusers. On the other hand, non-Gaussian-like shaped diffusers often produce a wide range of light patterns; such as linear, elliptical and square patterns with several intensity profiles, ranging from a Lambertian scattering to a top hat shape. For Lambertian scattering, it has a non-Gaussian shape because its light distribution is uniformly and precisely scattered in terms of its profile, following a cosine relationship with the polar angle of the scattered illumination. This relationship state with Lambert's law is shown in Equation 1, where $I_{diffuse}$ represents the intensity of the incident light at the particular wavelength; k_d

represents the diffused reflectivity of the surface at that wavelength; and I_{light} represents the intensity of the incoming light at the particular wavelength. [1]

$$I_{diffuse} = k_d I_{light} \cos(\theta) \qquad \text{Equation 1}$$

1.2 **Huygens' Principle and Diffraction**

The diffraction is based upon the propagation of electromagnetic waves through a medium with a varying refractive index, or a slit that is comparable in size to its wavelength. Here, light is described as an electromagnetic wave that consists of synchronized oscillation of electric field E and magnetic field B that propagates at the light speed of 3×10^8 m.s^{-2} in a vacuum. Diffraction is a concept that is firstly described using Huygens's Principle which is defined as the bending of a wave around obstacles. This principle states that every point on a wave front can be considered as a new source of secondary wavelets that spread out in the outward direction at the same speed of the wave itself. Therefore each individual point is the centre of its own circular wave front which expands the light source as shown in Figure 2 [2, 3].

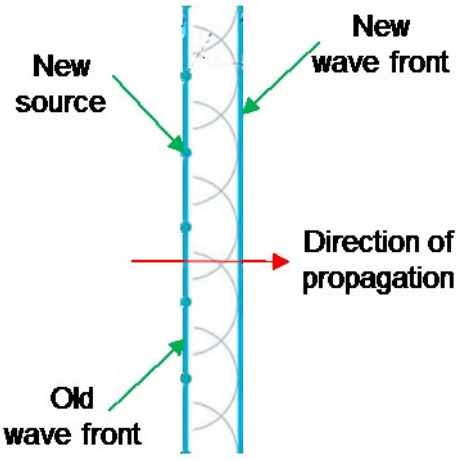

Figure 2. Huygens's principle applied to straight wave front. Each individual point propagates a circular wavelet that moves in the direction of propagation.

According to Maxwell's equations (Equations 2-4), spatially varying electric fields are associated with specific changes over time in the electric field [4]. These oscillations of the two fields are perpendicular to each other and perpendicular to the direction of the wave propagation, forming a transverse wave. The wavefront of electromagnetic waves is emitted from a light source such as a laser. This laser emits monochromatic light through a process of optical amplification by stimulated emission of photons. The laser travels through matter and under goes reflection, transmission or absorption, when it interacts with matter. For this reason, the light-matter interaction depends on the light's wavelength and the object's properties and size [5]. Snell's law describes the relationship between the incident and a refracted light wave, when light interacts with matter. Equation 5 states that the ratio of incident and refraction angles is equal to the ratio of phase velocities or refractive index.

Maxwell-Faraday law: $\nabla \times \mathbf{E} = \partial \mathbf{B} / \partial t$ Equation 2

Maxwell-Ampère law: $\nabla \times \mathbf{B} = \mu_0 \varepsilon_0 \partial \mathbf{E} / \partial t$ Equation 3

Gauss's law: $\nabla \cdot \mathbf{E} = 0$ Equation 4

Snell's law: $\frac{sin\,\theta_2}{sin\,\theta_1} = \frac{v_2}{v_1} = \frac{n_1}{n_2}$ Equation 5

In addition, light scattering is another form of propagation of light in which light is scattered by particles. Rayleigh describes the elastic scattering of light from particles whose diameter is less than about one-tenth of the wavelength of the incident light. The scattering can occur when light travels through transparent solids, liquids and gasses containing particles. These particles absorb light and emit this light absorbed radially. Therefore the particle become new source of light and acts as small radiating units. Because the particles are randomly positioned, the scattered light is observed at particular positions with randomly light phases. As a result, the amount of scattering is the sum of the squares of the amplitude and proportional to the inverse fourth-power

of wavelength and the sixth-power of particle sizes. In detail, the intensity of the light scattered by Rayleigh is described in Equation 6, where I_0 is the normal light intensity before the light travels through particle, θ is the scattering angle, R is the distance to the particles, λ is the wavelength of the light, n is the refractive index and d is the diameter of the particle [6-8]. Otherwise, Mie describes the elastic scattering of light from particles whose diameter is comparable to the wavelength range. Similarly, the particles absorb light but Mie differs from Rayleigh scattering in respect of emission: the particle emits this light absorbed into more directional rather than radial. The more of the light is scattered in the forward direction when the particle size becomes larger [9].

$$I = I_0 \left(\frac{1 + \cos\theta^2}{2R^2} \right) \left(\frac{2\pi}{\lambda} \right)^4 \left(\frac{n^2 - 1}{n^2 + 2} \right)^2 \left(\frac{d}{2} \right)^6 \qquad \text{Equation 6}$$

1.3 **Types of Diffusive media and their Limitations**

The Gaussian and non-Gaussian shapes are image formation which is created by the propagation of light through a diffusive media. There are two distinct types of diffusers in terms of diffusive media that achieve an optical diffusion. These diffusive media are either from a volume or a surface; for this reason, they are called volumetric diffusers and surface relief diffusers. In volumetric diffusers, the diffusion of light depends on a diffusing element that is ordered or disordered inside the bulk or volume of the diffuser. Generally, controlling the distribution of diffusive elements inside the volume is difficult; such as growing devitrite crystal [10], recording a laser speckle pattern into a photopolymer volume [11], or adding micro-polymer filler into a transparent volume [12-14]. These added polymer microspheres were reported with a small diffusion angle in the range of 10°-50°; while growing devitrite crystals achieved up a 120° diffusion angle. However, these crystals have been observed to be

uncontrollable and they have different arrangements, resulting in various scatter shapes along an exact diffuser. A further issue is that a devitrification process cannot produce ultra-thin diffusers due to the requirement of sufficient thickness to grow more devitrite crystals, facilitating a wide angle of light diffusion. Commercially, an opal diffuser was produced by Edmond Optics and offers a near Lambertian distribution; but the level of diffusion causes a large amount of scattering loss, around ~70% of transmission efficiency.

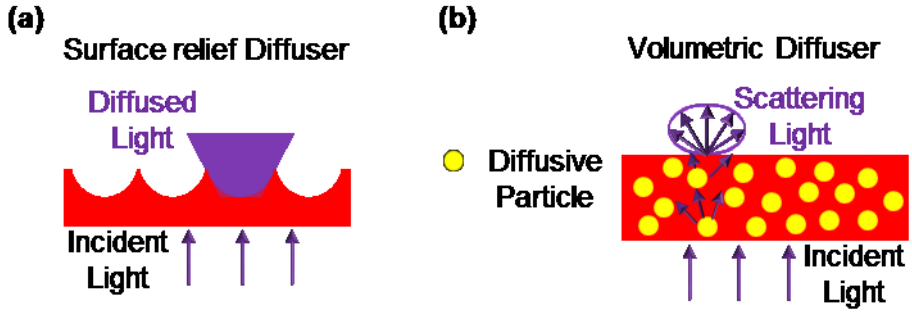

Figure 3. *The propagation of light through different diffusive media of optical diffusers: (a) surface relief diffuser; and (b) volumetric diffuser*

Therefore, the surface relief provided significant research in enhancements of diffractive optical design and manufacturing processes; which have reduced undesired orders and minimized the zero-order bright spot, while improving uniformity and achieving higher diffractive efficiency. The most common types of the diffractive optical devices are 1/2D diffraction grating, Fresnel zone plate (FZP) lens, optical diffusers, computer-generated holograms etc. The 1/2D diffraction gratings are normally designed to disperse the incident light beam into multi-bright spot with a specific angle and direction. They are based on the diffraction grating Equation 7, where d is the distance between the periodic structures; θ_m is the angle of diffracted light measured from normal incidence; n represents the order of the bright spot; and λ represents the wavelength of the incident beam. For a FZP lens, it consists of a series of radially

symmetric rings which alternate between opaque and transparent. It diffracts light around opaque zones following Equation 8 below: where f is a focal lens: d is a radius of the ring; n is a number of rings; and λ is wavelength [15, 16]. A computer generated hologram is based on an array of opaque and transparent aligned pixels, allowing the creation of constructive interference and a diffraction pattern formation [17]. An optical diffuser is designed from random rough surfaces to well-defined optical microstructures [18, 19]. In terms of fabrication, all of these diffractive optical devices have a lack of scientific research with direct laser machining into plastic material which has a high light transmission efficiency, high-impact resistance, is lightweight, and effective wettability resistance [20, 21].

$$\mathrm{d}\sin\theta\mathrm{m} = \mathrm{n}\lambda \qquad \text{Equation 7}$$

$$\mathrm{f} = \mathrm{d}^2/\mathrm{n}\lambda,\ (\mathrm{n} = 1,2,3\ldots) \qquad \text{Equation 8}$$

1.4 **Motivation and Limitation in Fabrication**

So far many manufacturing processes have been studied to fabricate optical diffusers, including: ultrasonic embossing [22], acid treatment [23], hot embossing [24], electrospray processes [25, 26]. These processes are non-traditional machining with low-cost machinery, compared to ultraprecision processes; but the processes involve either are non-direct fabrication, or they require a mould, so that they are quite time-consuming. A holography processes have been used to record the diffusion of light on silver halide (AgHal) and photopolymers [27], silver halide sensitized gelatin (SHSG) [28], azobenzene polymer [29] or ink materials [30] to produce a holographic diffusers. The reported diffusers suffer from low failure thresholds, hence can only operate on low laser powers. Also they have limited diffusion angle field of view and they cannot withstand to the chemical reaction or physical contact which results in distortion of

optical diffusers. In commercial products, sandblasting and polishing processes were utilized to produce a ground optical diffuser having a Gaussian-like shape. These processes are economical and simple for mass-production, but they are incapable of controlling and manufacturing customised surface structures on the diffuser surfaces. Therefore, they provide limited optical diffusers profiles with diffusion angles between 35° and 60° [31].

Lithography is one of the most promising fabrication processes for optical diffusers, presented in both scientific research and for commercial products. It provides the most solutions for customized tailoring of the characteristics of non-Gaussian diffusers, such as diffractive and engineered diffusers [32]. One of the advantages is that the lithography process is capable of producing deep analogue surface-relief structures on the master element, where these structures are based on arrays of optical microstructures [33, 34]. Subsequently, the fabricated master is used to replicate the optical diffuser pattern on a variety of materials and substrates[32]. The fabricated diffusers from the lithography process offer circular, square and a line distribution of top-hat patterns with a 90% transmission efficiency. However, this process relies on a mask and it requires multistep processes to achieve the desired optics; making it difficult to fabricate an optical diffuser directly without being time consuming. In some cases, depending on the required pattern size, it takes between an hour to several days for only the mask fabrication [35]. For this reason, a new advanced machining process needs to be introduced in the fabrication of optical diffusers to limit all of these mentioned issues.

In our case, optical diffusers require a new advanced micromachining process, allowing direct fabrication on a hard or soft materials that provides great emphasis on high accuracy and process control. Laser machining is one of the most promising direct

processes that utilizes a thermal process capable of high accuracy ablation on a wide range of materials. The specification of an optical system, the temporal modes of the laser used, and equipment hardware configuration are significantly important to develop robust, high-volume manufacturing solutions [36-38]. There are two types of common mediums used in the laser machining process: carbon dioxide (CO_2), and neodymium yttrium-aluminium-garnet (Nd:YAG) lasers. The CO_2 lasers have the highest laser power with great efficiency without sacrificing the superiority of the laser beam. It has a continuous wave (CW) laser producing a beam of infrared light with the principal wavelength band centring on 9.40 μm and 10.40 μm but the strongest laser transition occurs at 10.6 μm [39]. With the other medium, Nd:YAG lasers have a shorter wavelength of around 1 μm, making them appropriate for reflective materials because of their higher near-infrared light absorption compared to the CO_2 lasers [40]. In spite of the Nd:YAG lasers having low-beam powers, they can be operated in pulsed mode, ranging from the microsecond to the femtosecond to enable high-peak powers [41]. However, the shorter pulse reduces the effect of the heat damage on the materials, resulting in high micro and submicron accuracy [42].

The principle of material removal during laser machining consists of different three steps: melting (CW CO_2 laser), vaporization (femtosecond laser [43, 44] and nanosecond laser [45]) and chemical degradation (UV excimer laser [46] or excimer laser lithography [47]). This degradation breaks the chemical bonds and degrades the laser exposed materials. During laser machining, a high energy density laser beam is focused on a precise area of the work piece which absorbs the thermal energy. This allow to heat and transform the work piece into a melted, vaporized or chemically changed state [41, 42, 48]. In terms of physical phenomena, the laser light interacts with all materials through absorption, transmission, scattering, and reflection. However,

the most effect in the material is only probable through the absorption of the laser beams. Therefore, thermal and optical properties of the materials, for example thermal conductivity, thermal diffusivity and absorptivity have a significant effect on the quality characteristics of the machining process. Hard and brittle materials, such silicon and glass, have poor machinability with conventional fabrication. Therefore, they benefit from the advantage of laser machining where there is no mechanical contact between the machining tool and the fabricated materials [40]. These various laser machining processes have been of great interest in the related fabrication of optical devices, such as the cleaving of optical fibres [49, 50]; the cantilever fibre sensor [51]; fibre-based Fabry-Perot cavities (FFPC) [52]; the optical waveguide [53-55]; Fresnel and cylindrical lenses [15, 56-58] and diffraction gratings [59, 60]. However, there is a lack of research in fabricating optical diffusers by using a laser machining, which allows direct fabrication of optical diffusers on float glass and polymers in low-cost with rapid productions.

1.5 **Thesis Outline and Aims**

This thesis aims to contribute to designing and fabricating low-cost optical diffuser devices directly on transparent materials using direct laser machining processes. To date, there is a lack of research on laser machining process fabricating of an optical diffuser. This has encouraged us to carry on the development of optical diffusers on transparent materials; float glass, polycarbonate (PC), polyethylene terephthalate glycol (PETG) and polydimethylsiloxane (PDMS) elastomer, using three types of laser machining processes: CO_2, nanosecond and femtosecond lasers. Therefore, changing lasers and the transparent materials causes several challenges and issues to arise regarding the laser machining of these transparent materials, and how it affects the optical properties. This is finding a new way to form nano and microstructure directly on solid and soft surfaces for making optical diffusers. In Chapter five, a novel methodology has been invented to detect the homogenization of the diffused light from an outgoing diffraction beam. Furthermore, an innovative optical diffuser has been pioneered on elastomer material which is highly flexible, stretchable and mechanically tunable with superhydrophobic characteristics.

In order to achieve the fabrication of these optical diffusers the following steps have been addressed:

1- An investigation of three laser machining processes on transparent materials, in terms of the effect of the optical properties.
2- Optical modelling of corresponding diffractive optical devices such as 1/2D diffraction gratings, Fresnel zone plates (FZP), and computer-generated holograms, in the visible spectrum.

3- Using three types of direct laser machining processes: femtosecond, nanosecond and CO_2 lasers, to fabricate optical diffusers onto transparent materials.
4- Probing and measuring surface characterization of the fabricated diffusers and analysing the measurement results.
5- Testing optical characterization of the fabricated diffusers, analysing and interpreting the results.
6- Inventing a novel methodology, described in Chapter 5, to find out the homogenization of the diffused light at the outgoing diffracted beam.
7- Inventing a new type of flexible, stretchable and mechanically tunable optical diffuser, presented in chapter 6, based on elastomer material.
8- Demonstrating the interesting utility of the fabricated devices in industrial applications.

This thesis is organized in seven chapters, based on five publications:

Chapter 1 introduces the research topic and some background; provides a review of the literature related to the optical diffusers and their fabrications, and evaluates them. Finally, it includes the thesis outline and aims.

Chapter 2 presents the fabrication of optical diffusers on float glass by using femtosecond (FS) laser machining. The surface morphologies of optical diffusers were scanned by using scanning electron microscope (SEM) and their surfaces were discussed. Also, the surface roughness was measured and analysed by using Alicona G5 InfiniteFocous (IF) system to provide their average roughness (Ra). Then, the performance of optical diffusers based on the measurements of reflection and

transmission efficiencies, and the diffusion angles were performed and analysed. Finally, visualization of the three dimensional optical diffusion were captured using various wavelengths of monochromatic light. With glass being an inexpensive material, the proposed technique has a lot of potential for producing cost-effective, large-area optical devices. The process benefits from the flexibility of the laser writing method and enables the production of tailored and optical diffusers.

My contribution to this chapter was of conceiving the idea, designing the optical experimental setups and leading the research. This technique allowed to find a new way of fabrication of optical diffuser on float glass with FS laser processing in a short time period compared to laser lithography. R.A provided SEM images and PP did laser writing onto the samples for around one hour. I wrote the first draft of the paper. All authors proofread the writing of the manuscript.

Chapter 3 describes the fabrication of diffractive optical devices using FS laser machining directly on a transparent polycarbonate (PC) substrate due a high light transmission efficiency and an effective wettability resistance compared to the float glass. These diffractive optical devices, transmission 1D/2D gratings, Fresnel zone plate lenses, and computer-generated holograms were designed and calculated theoretically. Then they were produced directly on a transparent polycarbonate (PC) substrate using laser machining for the first time. Next, the optical properties of the devices including light transmission, angle-dependent resolution, and light polarization effects were investigated and the measurement was recorded. Subsequently, the optical properties of the grating were validated through a geometrical engineering theory of diffraction model, comprising phase modulation. Finally, the wettability resistance of the diffractive optical devices was carried out and investigated by the droplet of the contact angle measurement.

I conceived the idea of this paper, designed the optical experimental setups and led the research direction to allow a fast fabrication of self-cleaning optics. Y.M simulated computer generated hologram and PP did laser writing onto the samples for one hour. I wrote the first draft of the paper. All authors proofread the writing of the manuscript.

Chapter 4 introduces the fabrication of optical diffusers on float glass by using nanosecond laser machining which is low-cost and highly productive pulsed laser system compared to FS laser in Chapter 3. This nanosecond pulsed laser-induced micro-texturing surfaces to fabricate an optical diffuser for the first time. The research was conducted by point-to-point micro-texturing of a float glass surface in a spiral shape. The laser machining parameters, the number of pulses, and their speed and power, initially played a significant role on surface features. Therefore, the optical characteristics of the diffusers including broadband light transmission, angle-resolved monochromatic light diffusion and broadband light polarization effects were carried out and the measurements were investigated.

My contribution conceived the idea of this chapter, designed the optical experimental setups and provided the research direction to allow fabrication of the optical diffuser with nanosecond laser processing; having the advantage of being a low-cost and high throughput pulsed laser system compared to FS laser. RP did laser writing onto the samples for a half hour. I wrote the first draft of the paper. All authors proofread the writing of the paper.

Chapter 5 demonstrates the fabrication of optical diffusers on float glass by using CW CO2 laser, which is highly economical laser system as compared to pulsed laser machining in previous chapters. This laser machining patterned surface-relief

pseudorandom microstructures directly on the float glass surfaces, either on one side or both sides. These microstructures were visualized as three-dimensional under an optical microscope and they were captured. The captured image was processed through FFT simulation by reading out the image to design a predictable optical diffuser. A model of glass surface peeling was also developed to prevent its occurrence during the fabrication process. Further investigation on pseudorandom microstructures was characterized with optical microscopy, Raman microscopy, and polarization response. A numerical simulation of the temperature distribution from the CO_2 laser was carried on the float glass. Finally, a novel methodology for identifying the speckle pattern was performed and the speckle pattern was recorded using a high-resolution imaging camera with a complementary metal-oxide-semiconductor (CMOS) sensor.

My contribution to this project was conceived the experimental idea for the fabrication of optical diffuser using CW CO_2 laser, utilising the lowest cost of the laser systems, and designed the optical experimental setups and provided research direction under supervision of H.B. A.A did FEM simulation and I fabricated the samples. I wrote the first draft of the paper. All authors proofread the writing of the paper.

Chapter 6 presents the design and experimental realization of the pioneering, mechanically stretchable and tunable optical diffusers. These diffusers were made directly on elastomer material, which is based on the fabrication of cylindrical lenslet and tip arrays, by using a CW CO_2 laser. The cylindrical lenslet and tip were constructed with varied dimensions, which plays a critical role in the distribution of light and wettability resistance. The constructed cylindrical lenslet and tip were confirmed under the optical microscope. After that, the mechanical stretching of the diffusers was carried out to evaluate the distribution of light and wettability resistance.

My contribution to this chapter was of conceiving the idea for the fabrication of flexible and stretchable optical diffuser with low surface wettability for the first time. I designed the optical experimental setups, interpreted the data and provided research direction under the supervision of H.B. I wrote the first draft of the paper and H.B proofread the writing of the paper.

Chapter 7 concludes and summarises the main research in this thesis, finding the limitations of the current work and suggesting some possible future research.

Chapter 2: Femtosecond Laser Directed Fabrication of Optical Diffusers

Published article

Tawfiq Alqurashi, Pavel Penchev, Ali K. Yetisen, Aydin Sabouri, Rayan M. Ameen, Stefan Dimova and Haider Butt

RSC Advances, 2017. **7**(29): p. 18019-18023.

This chapter introduces the fabrication of optical diffusers on float glass by using femtosecond (FS) laser machining.

Author Contributions

T.A. conceived the idea, deigned the optical experimental setups and provided research direction. R.A provided SEM images and PP did laser writing onto the samples for one hour. T.A. wrote the first draft of the paper. All authors proofread the writing of the manuscript.

2.1 **Abstract**

The optical diffusers are widely used in various optical instruments. In this study, a method for fabrication of optical diffusers through femtosecond laser machining is demonstrated. Float glass surfaces were ablated, forming nanoscale ripples with dimensions comparable to the wavelength of visible light. It was found that these structures produce highly efficient and wide field of view diffusers. The machining patterns altered the diffusion characteristic and a maximum diffusion angle of 172˚ were achieved with optimum machining parameters. The transmission performance of the diffusers were measured to be around 30% (average) across the visible range. With glass being an inexpensive material, the proposed technique has a lot of potential for producing cost effective large area optical devices. The process benefits from the flexibility of the laser writing method and enables the production of tailored and holographic diffusers.

2.2 **Introduction**

Optical diffusers are widely used in a myriad of optical devices, including liquid crystal displays (LCDs), light-emitting diodes (LEDs), light sources, and random lasers [12, 61]. Generally, optical diffusers can be classified into two main categories. The particle diffusing type which has the particles inside the diffuser [10, 62] and the surface-relief type consisting of microstructures on surfaces. The most widely used surface-relief structures include microlenses [63], pyramids [64] and textured surfaces [65, 66]. Most applications of these types of diffusers can be observed in filament lamp [67], LEDs [68] and fibre optics [54]. Fabrication of textured surfaces through femtosecond (FS) laser ablation is a rapidly growing area of interest [69-71]. This fast and potentially viable method can produce micro and nanoscaled ripples onto the substrate surfaces and thus change their physical properties [72-74]. Such surface texturing results in modified wettability, conductivity and optical reflection/ transmission properties [75].

The fabrication of optical diffusers by femtosecond laser sources have not been exploited as it has challenges when compared to nanosecond pulsed lasers which exhibit excessive burrs due vaporized material [76]. Direct laser processing received intensive research as result of fast growing optoelectronic market [77-79]. Additionally, FS laser patterning is a deterministic process. First, it has limited thermal effect because the laser pulse ends before the electrons thermally excite any ion and also the heat diffusion outside the focal area is minimized. This leads to reduced heating caused by expansion effects and an increase in its patterning precision as compared to other laser sources [80, 81].

Here, we report the development of glass-based optical diffusers via FS laser patterning. FS laser ablation was used to produce both nano- and microstructures (~20 μm) to increasing the roughness of the glass surfaces, which randomly diffused the

transmitted light. The present method differs from other techniques used for producing diffusers, where a pulsed laser is used for patterning a photoresist layer on glass or plastic substrate [30]. Optical scattering from the textured glasses substrate was examined by angle-resolved spectral measurements. The optical response was characterized in the visible spectrum.

2.3 **Results and Discussion**

Femtosecond laser writing of glass diffusers

For producing the optical diffusers, float glass slides were textured using an in house FS laser microprocessing platform. The surface structures were produced on glass substrates by controlling the FS laser beam's polarization and hatch directions. Figure 1(a) shows the schematic diagram of the laser machining setup that includes an ultrashort ytterbium-doped fiber laser (0.8 W, 1030 nm, 310 fs, 100 kHz), a telecentric lens with a focal length of 100 mm and a 3D optical beam deflection system for scanning surfaces with high dynamics. The working envelope defined by the scan head and the focusing lens was 35 mm (x) × 35 mm (y) × 6 mm (z). Furthermore, the focal beam spot diameter was approximately 30 μm. The glass substrate was scanned at speed of 200 $mm.s^{-1}$ with a hatch distance of 4 μm while the pulse energy was 8 μJ. Figure 1(b) shows the typical surface morphology resulting on the substrate after the FS laser processing.

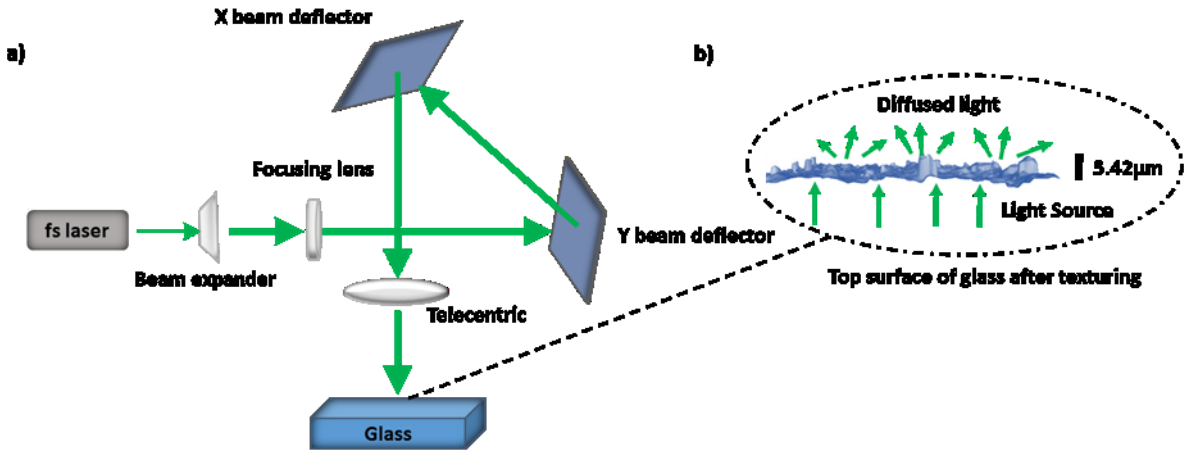

Figure 1. Fabrication of optical diffusers via FS laser patterning. (a) Schematic diagram of the laser setup. (b) the textured surface and the resulting light diffusion.

Various laser parameters were utilised to texture the glass substrates (Figure 2). The surface morphology of textured glass was analysed by using a high resolution of optical microscopy and average roughness (Ra) was measured by using Alicona G5 InfiniteFocous (IF) system. In Figure 2a, the samples represented by h1-3 were textured using circular polarization with varying hatch directions from horizontal, vertical and at 45°, respectively. Figure 2(b) shows the surface roughness of the diffusers along with the cross-sectional images of the fabricated samples. Side views of diffusers illustrate the difference in the surface topography produced by various laser processing parameters. The morphologies and arrangements of both micro- and nano-scale structures produced are highly dependent on the FS laser process parameters, including hatch direction [72, 82]. Figure S1 in supporting information shows the 3D map of the nanoripples produced.

Another set of samples (h4-6) was produced after changing the laser polarization to linear. The size and number of surface structures were reduced when the hatch direction was changed to vertical. In general, the surface structures on all samples had

non-uniform overlaps. The average surface roughness was between 375 to 424 nm (Figure 2b). The vertical hatch direction produced the lowest average roughness of 375 and 374 nm for samples h2 and h5, respectively.

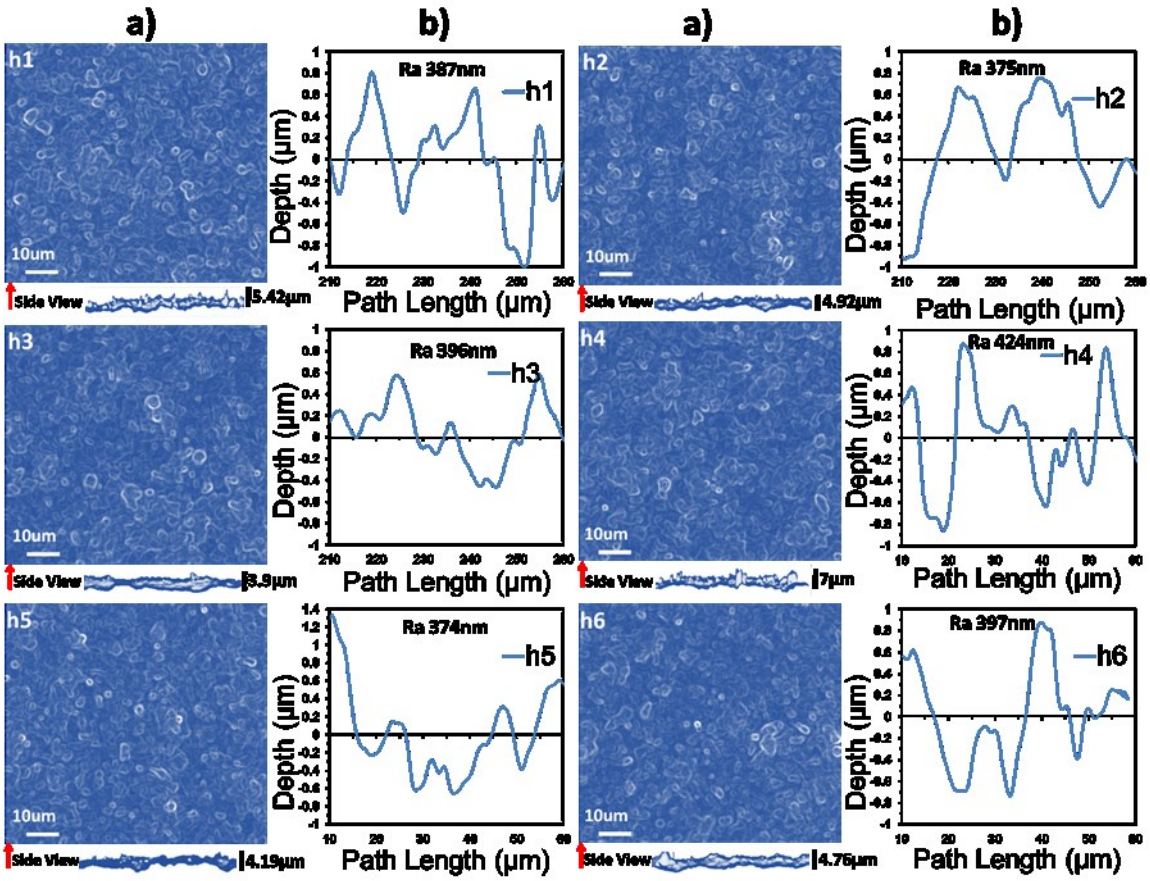

Figure 2. The samples h1 to h3 were textured by using circular polarization with three different hatch direction, e.g., horizontal, vertical and at 45˚, while the polarization was changed to linear for the samples h4 to h6. (a) Microscopic images from the top and side view of the microstructured ripples and (b) corresponding average roughness.

Additionally, the fabricated micro and nanostructures were scanned by using scanning electron microscope (SEM). Glass samples were coated with an ultrathin gold layer to avoid electronic charging and to clearly observe the surface features. The SEM imaging was done normally on the textured surface using a field emission gun (FEG)

at 10 kV. The SEM images are shown in Figure 3. The micro and nanoripples were fabricated by overlapping and multiple laser passes. The arrangements of structures produced is highly dependent on the hatch direction as shown Figure 3 (h4-h6). The high magnification images (Figure 3 a and b) reveal that the fabricated process produced nanoparticles on ripples in range of few hundred nanometres and comparable to the wavelength of light. These features produce the surface roughness, as measured in Figure 2. These rough structures enabled the light to be scattered based on Rayleigh scattering [83].

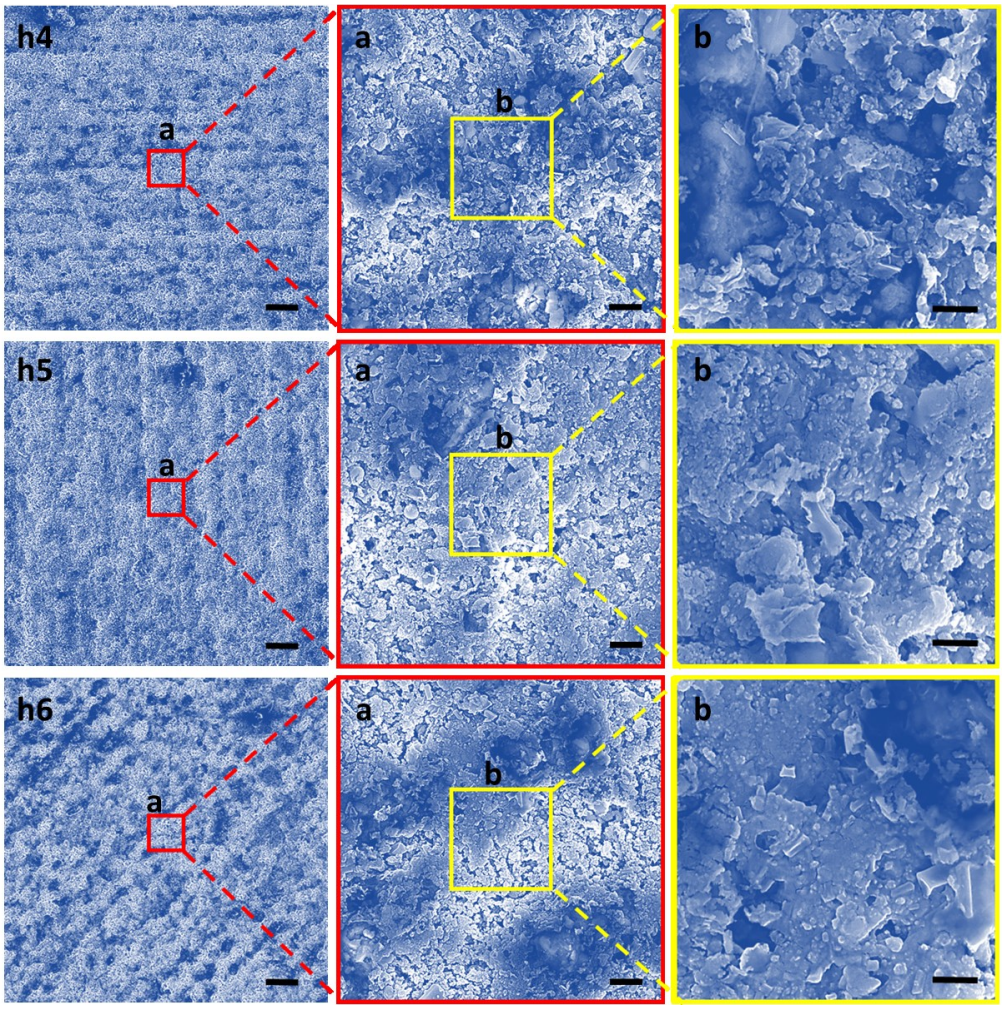

Figure 3. The samples h4 to h6 were scanned with SEM at 1000 magnification (Scale bar=25μm) and this magnification had been increased to 10,000 and 35,000 magnification in a and b, respectively. (scale bar in a = 2.5μm and scale bar in b = 1μm).

Characterization of Optical Diffusers

The samples were examined by angle-resolved optical power intensity measurements and spectroscopy analysis. The angular measurement setup consists of a rotational stage controlled by a computer, laser sources (wavelengths of 633, 533 and 450 nm), and an optical power meter (Figure 4(a-b)). The diffuser samples were rotated with 1° increments. To reduce the stray light effect, a cylindrical tube was placed in front of the power meter detector. The distances between the laser source-sample and sample-detector were 3 and 13 cm, respectively. The sample was rotated from -90° to +90° from the normal incident (Figure 4(b)). The motorised stage was controlled by software which recorded the power meter readings at each angle simultaneously.

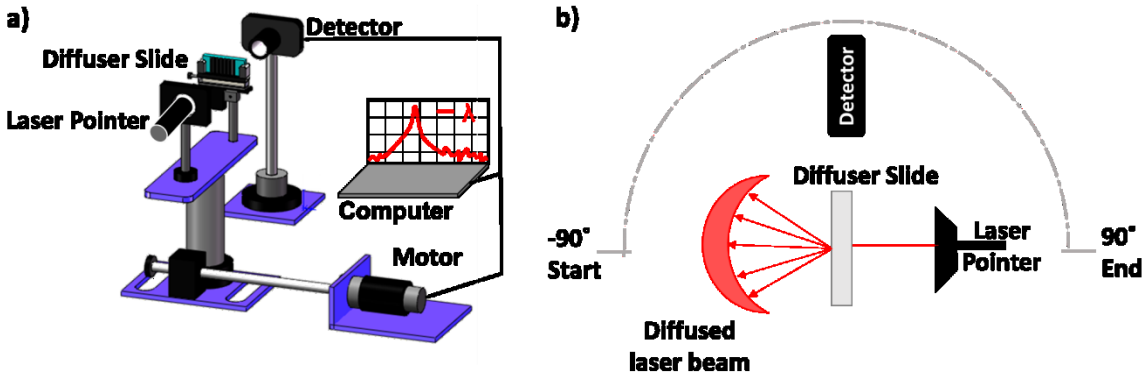

Figure 4. Angular spectral measurement setup for the analysis of diffusers. (a) Schematic of the experimental setup. (b) Top view of the experimental setup.

Figure 5(a-d) show the angle-resolved measurements of transmitted diffused light. In figure 5(a) and 5(b) measurements were performed on samples with circular and vertical polarization using a red laser source. Figure 5(c-d) shows the diffusion measurements using green and blue laser sources. The surface features produced on glass surfaces were randomly distributed causing the diffusion of light in wide angles.

According to Bragg law the large diffusion angles suggest that the structures are of the same scale as the wavelength of light (few hundred nanometres). Due to the random distribution of surface structures, the mean surface roughness measurements revealed that the surface features were overlapping and formed on each other, which affected the properties of the diffusion angles. The measured diffusion angle varied from 152° to 172°. Figure 5(a-b) shows wide diffusion angle (~172°) with peak transmission intensity (~1.1%) at zero degrees. Figure 5(a) shows that the normal transmission intensities for h1-3 were 0.5, 0.85 and 0.8% and the diffusion angles were 154°, 170° and 166°, respectively. The samples made with linear polarization (h4-6) displayed slightly higher transmission intensities (on average ~0.054%). Meanwhile, the diffusion angle was decreased by ~8˚ for samples h4 and h5. This signifies that the structures produced with linear polarization have larger lateral dimensions and lower spatial density, which leads to narrower diffusion field of view and more light being focused near zero degrees (zero order of diffraction), the diffusion properties of the samples were also analyzed using 405 and 533 nm laser diode sources. The samples displayed higher optical transmission for these two wavelengths but the light distributed at higher angles was lower.

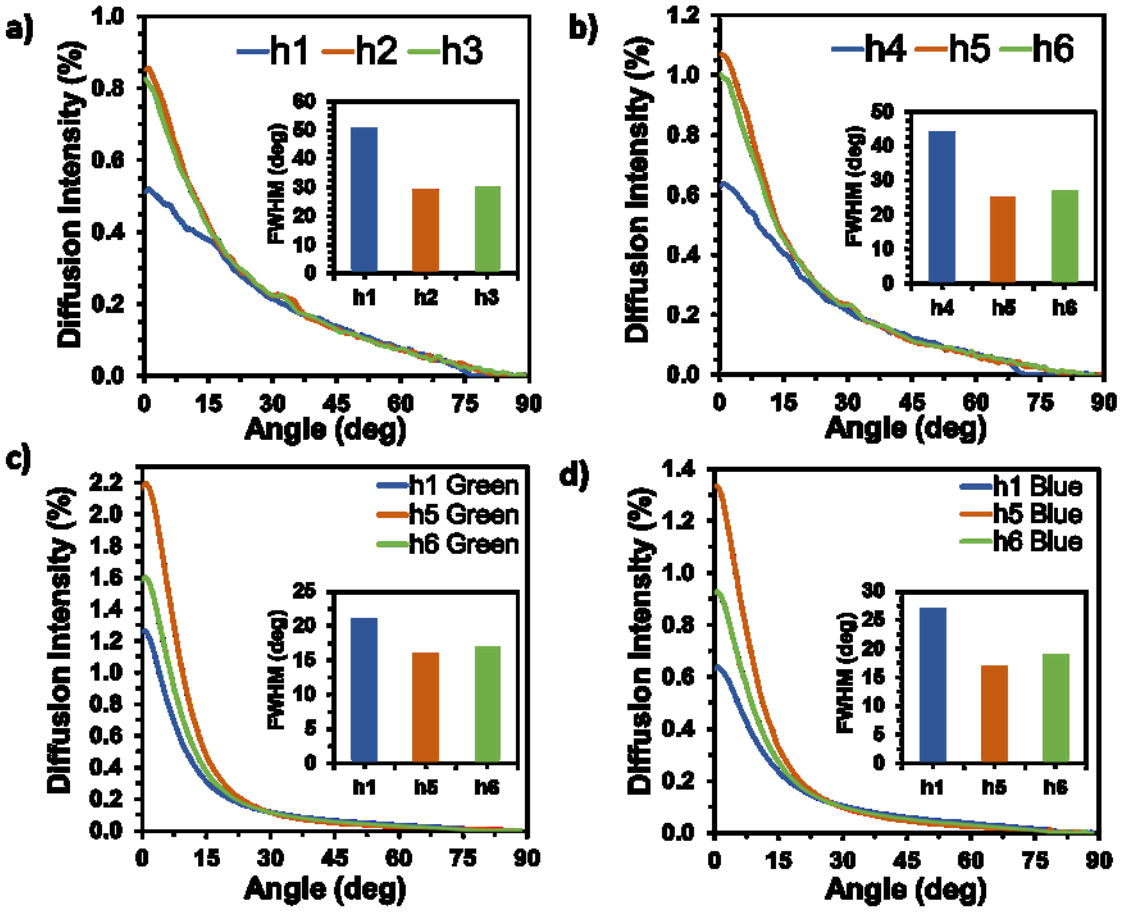

Figure 5. Angular diffusion characterization of the diffusers. (a-b) Angle resolved optical diffusion from h1-6 samples, in response to red laser. The insets show the full width half maxima. The diffusion in response to (c) green and (d) blue lasers.

Figure 5a-d also show the full width at half maximum (FWHM) for the diffusion plots. The highest FWHM were recorded in response to the red laser however, the intensity peak was at the lowest compared to other wavelengths. The reason being that the light was three dimensionally diffused at larger angles, hence reducing the light focused near zero degrees.

In practical applications diffusers are generally used for diffusing white light. Hence, optical reflection and transmission measurements were also conducted using broadband white light. These measurements were performed by using a spectrometer (2 nm resolution), which was connected to an optical microscope through an optical

fibre. Figure 6 shows the measured average reflection and transmission spectrums. In general, the surface features reduced most of the light transmittance with haze boosting effects [84]. The results show that ~40% of the light was transmitted through the diffuser at a wavelength of 400 nm, and it sharply reduced to near 20% at the wavelength of 475 nm (Figure 6a-b). However, the transmission intensities were gradually increased from 20% to 30% between the wavelengths of 500 nm to 700 nm. The reflection measurements showed that ~55% of the light was reflected from the textured surfaces near the wavelength of 400 nm and it reduced to 10% at a wavelength of 500 nm (Figure 6c-d). For larger wavelengths, the transmission remained stable until it reached 670 nm and then increased to 27% at a wavelength of 700 nm. In general, the transmission and reflection measurements through the microscope had higher efficiency values as compared to the angle-resolved measurements. This was due to the fact that the microscope objectives (due to high numerical aperture) received and focussed much more light (including the diffused light) coming from the samples.

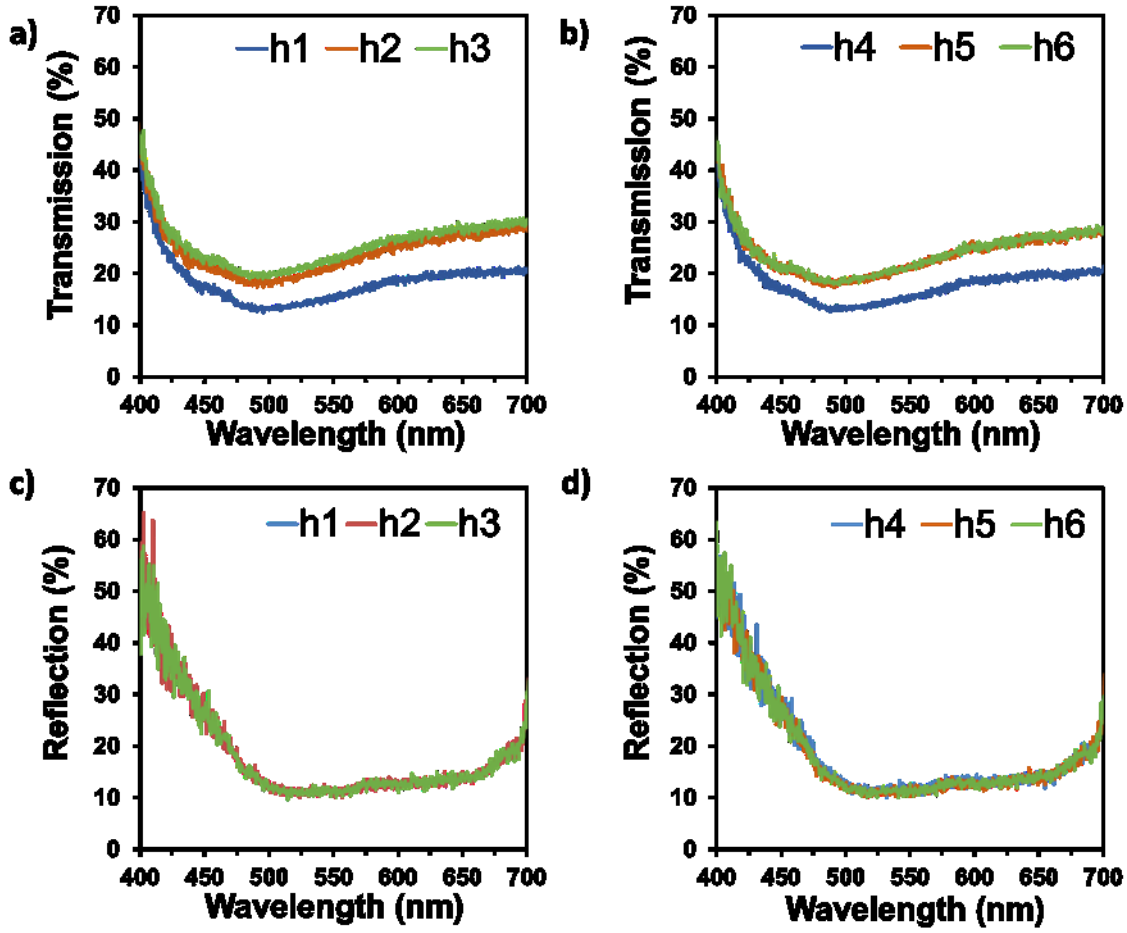

Figure 6. Optical spectroscopy of the diffusers using broadband light. Spectroscopic measurements in (a-b) transmission mode (c-d) reflection mode.

To visualize the three dimensional distribution of the diffused light, the diffusers were located at the centre of a white globe and the laser source was positioned below it (Figure 7a-b). Figure 7c shows photographs of the laser lights at 450, 533 and 633 nm without a diffuser. When the laser beams were transmitted through the diffusers, the light was diffused at large angles (Figure 7d). It can be observed that the field of view of optical diffusion increased from blue to red laser. This is in agreement with the Bragg law, [85, 86] which states that the diffraction angles increase with respect to incident wavelength. In some figures in Figure 7d, a red spot was noticed; this was not thought to be due to the diffuser itself but rather an artefact of the measurement setup.

The spot is seen to have a fixed position in the images, and although it appears that it is not present in the green h5 and h6 images, this is in fact not the case. The brightness of the diffraction is higher for the green light as compared to the blue and red, and so the intensity adjustment of the camera means the spot is not visible in those brighter green images. Looking at the images in figure 7c , where the laser is shone without the diffuser, it is seen that the spot is present in the green image as well. The most likely explanation for the red spot is a back reflection off the glass globe of the Infrared (IR) beam from the digital cameras autofocus function. The IR LED is offset from the lens on the front of the camera and so results in a spot that is reflecting from a point offset from the centre of the globe. The IR LED turns on when the picture is taken, as the camera is autofocusing. As the camera and globe positioning are fixed in the experimental setup the spot appears at the same place in all the images. The other possible explanation for the red spot would be for there to be a problem with the imaging sensor of the digital camera, where there was a damaged pixel area creating a bright spot on the image. This would also result in the spot appearing at the same position in all images. From the images it is clear that the spot is not the brightest part of the images seen and so would not be responsible for setting the intensity level of the camera, which is also another important fact. Hence, either way the spot is considered an artefact that has no bearing on the visualisation results of the 3D optical diffusion and so can be overlooked. However further work could be carried out to ascertain the exact cause of the spot if required - An imaging sensor problem with the camera could be ruled out by taking an image of a plain non-reflecting background; and the back reflection confirmed by either blocking the IR LED or changing the orientation of the camera which should result in the spot moving positon. Additionally using another camera without an IR autofocus function would be a possibility.

Our approach showed higher diffusion angles as compared to the commercial polished and sand-blasted diffusers, where the glass diffuser achieves light scattering up to 40°. In addition, our fabrication is very economical to scale up the manufacturing, due to fast laser writing speeds, flexible and tailored pattering of glass substrates.[10, 61, 87]

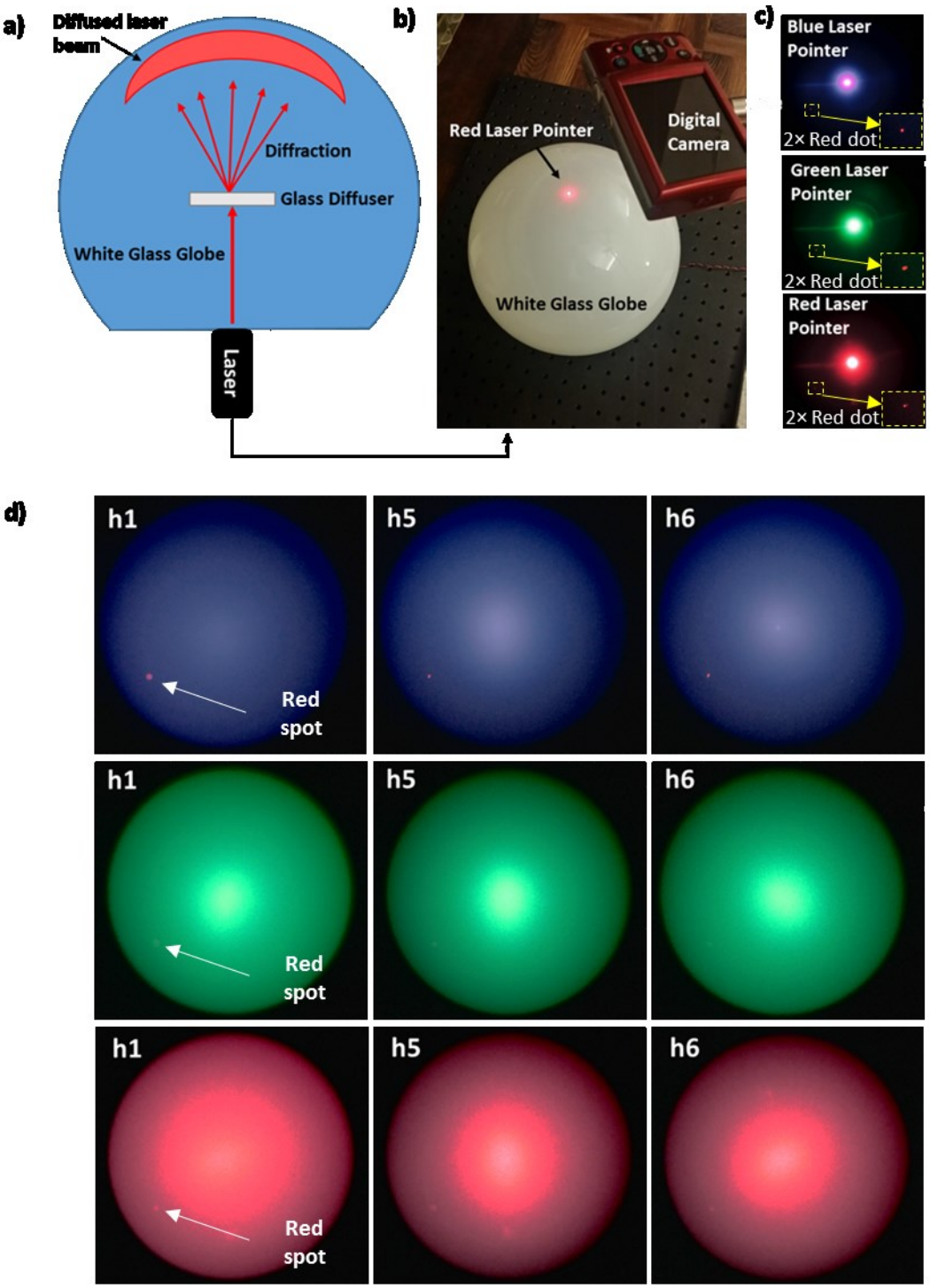

Figure 7. Visualization of the three dimensional optical diffusion under a white glass globe. (a) Schematic of experimental setup used to capture the speckle patterns from the diffusers. (b) A photograph of experimental setup. Scale bar=0.12 m (c) Three lasers of wavelengths 450, 550 and 700 nm illuminating the glass globe without a diffuser. Scale bar=0.12 m (d) Different laser beams were passed through the diffusers, producing different speckle patterns and intensities. Scale bar=0.06 m.

2.4 **Conclusion**

In conclusion, we developed a cost effective method for fabricating optical diffusers by using a FS laser. The laser machining micro and nano-scale surface structures on the float glass increased the diffusion angle to ~172° and reduced light normal transmittance with haze boosting effects. The effect of hatch direction and laser polarization on transmission characteristics of the diffusers was also investigated. It was found that the maximum and minimum transmissions were at the wavelengths of 400 and 475 nm, respectively. The relatively low processing time and flexibility of the fabrication process enables optical diffusers to have a variety of applications in optical industries such as photonic communication systems, displays and LEDs.

ASSOCIATED CONTENT

Author Contributions

H.B. conceived the idea, deigned the optical experimental setups and provided research direction. T.A., A.S and P.P performed the experiments and R.A performed SEM images. T.A. wrote the first draft of the paper. All authors proof read and contributed to the writing of the paper.

Conflict of Interest

The Authors declare no competing financial interests.

Acknowledgements

H.B. thanks the Leverhulme Trust for the research funding.

2.5 **Supporting Information**

Femtosecond Laser Directed Fabrication of Optical Diffusers

Published Supplementary information

Tawfiq Alqurashi[1,2,†], Pavel Penchev[1], Ali K. Yetisen[3], Aydin Sabouri, [1]Rayan M. Ameen[4], Stefan Dimov[1], and Haider Butt[1,]*

RSC Advances, 2017. **7**(29): p. 18019-18023.

[1]*School of Engineering, University of Birmingham, Birmingham, B15 2TT, UK*

[2]*Department of Mechanical Engineering, School of Engineering, Shaqra University, Dawadmi, Saudi Arabia*

[3]*Harvard-MIT Division of Health Sciences and Technology, Massachusetts Institute of Technology, Cambridge, Massachusetts 02139, USA*

[4]*School of Metallurgy and Materials, University of Birmingham, Birmingham, B15 2TT, UK*

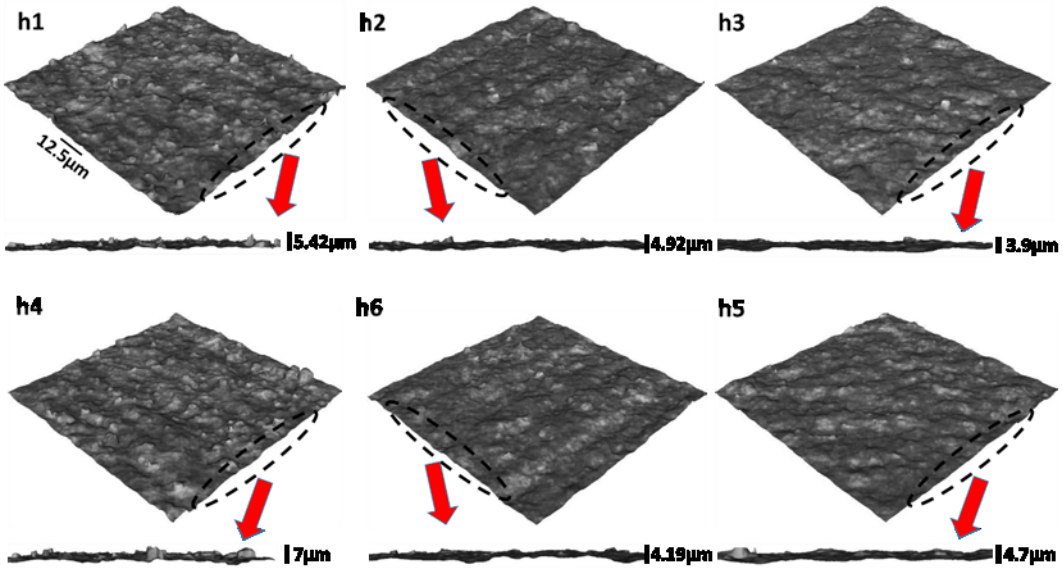

Figure S1. *3D view images of resulting surface topographies were captured by Alicona system.*

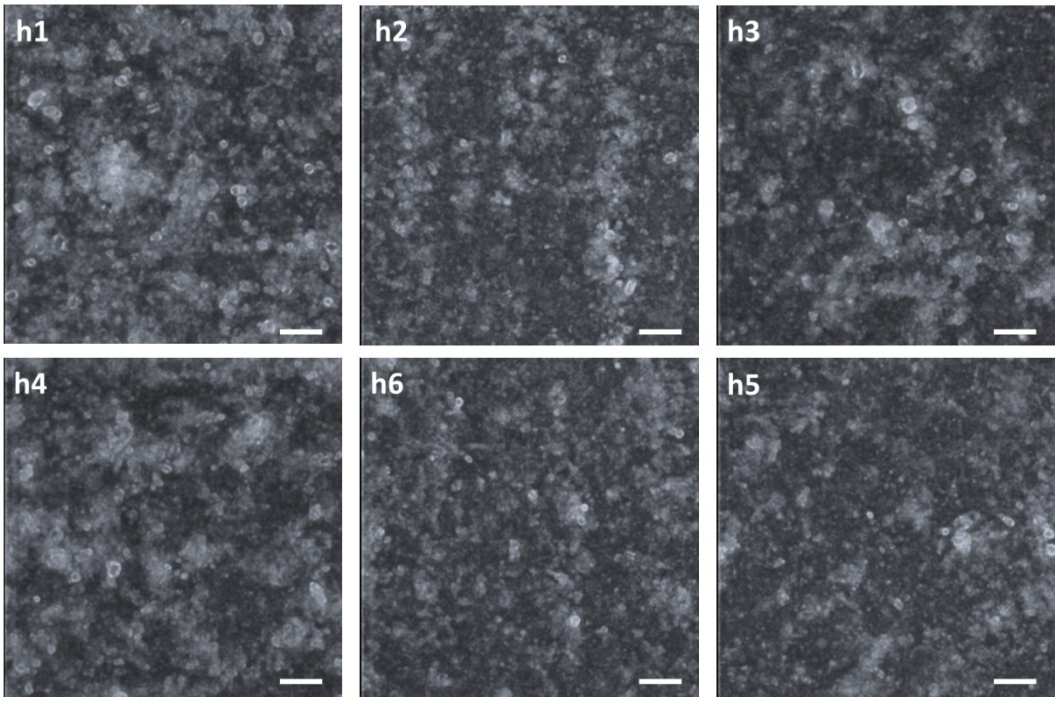

Figure S2. Normal view images of microstructure of ripples from rough surfaces were captured by Alicona system. Scale bar= 10 µm.

Chapter 3: Femtosecond Laser Ablation of Transparent Microphotonic Devices and Computer-Generated Holograms

Published article

Tawfiq Alqurashi, Yunuen Montelongo, Pavel Penchev, Ali K. Yetisen, Stefan Dimov, and Haider Butt

Nanoscale, 2017. 9: p. 13808-13819.

In the previous chapter, the fabrication of optical diffusers on a float glass surface was performed by using femtosecond (FS) laser machining. The optical diffusers fabricated were successfully produced on the float glass having a high diffusion angle of 172˚ with a low transmission efficiency of average 30%. This chapter introduces the fabrication of diffractive optical devices using FS laser machining directly on a transparent polycarbonate (PC) substrate which has a high light transmission efficiency and a high wettability resistance compared to float glass. The importance of the use of Polycarbonate is due to it providing a self-cleaning surface which results from the hydrophobic nature of the polycarbonate. This is important as it significantly reduces the light scattering from unwanted particles at the optic's surface.

Author Contributions

TA conceived the idea, deigned the optical experimental setups and provided research direction. Y.M simulated computer generated hologram and PP did laser writing onto the samples for one hour. T.A. wrote the first draft of the paper. All authors proofread the writing of the manuscript.

3.1 **Abstract**

Femtosecond laser ablation allows direct patterning of engineering materials in industrial settings without requiring multistage processes such as photolithography or electron beam lithography. However, femtosecond lasers have not been widely used to construct volumetric microphotonic devices and holograms with high reliability and cost efficiency. Here, a direct femtosecond laser writing process is developed which rapidly produces transmission 1D/2D gratings, Fresnel Zone Plate lenses, and computer-generated holograms on polycarbonate (PC) substrates. The optical properties including light transmission, angle-dependent resolution and light polarization effects for the microphotonic devices have been characterized. Varying the depth of the microgratings from 400 nm to 1.5 μm allowed the control over their transmission intensity profile. The optical properties of the 1D/2D gratings were validated by a geometrical theory of diffraction model involving 2D phase modulation. The Fresnel lenses produced had transmission efficiency of ~60% at normal incidence and they preserved the polarization of incident light. The computer-generated holograms had an average transmission efficiency of 35% over the visible spectrum. These microphotonic devices had wettability resistance exhibiting a contact angle ranging from 44° to 125°. These devices can be used in a variety of applications including wavelength-selective filters, dynamic displays, fiber optics, and biomedical devices.

3.2 **Introduction**

Femtosecond (FS) lasers have been widely used for the processing of polymers [88], metals [89, 90], and biological tissues [91]. Their applications also span across the machining of submicrometer sized features on silica and silver substrates [92, 93], along with a myriad of large-area industrial applications [71, 94, 95]. The unique advantage of FS laser ablation of transparent materials is that they have a nonlinear nature of light absorption due to the lack of electronic transitions at the energy of the incident photon [96, 97]. This nonlinear absorption confines any induced change to the focal volume, allowing the fabrication of complex structures [98, 99]. Additionally, FS laser processing is a deterministic process [100, 101]. First, it has no thermal effect because the laser pulse ends before the electrons thermally excite any ion and the heat diffusion outside the focal area is minimized. This FS machining process reduces heating caused by expansion effects, leading to an increase in its patterning precision as compared to other laser patterning processes [81, 102, 103]. Hence, FS lasers have the potential to rapidly produce tailored and accurate nano- and microstructures in automated manufacturing systems [74, 104].

FS lasers have been utilized to pattern transparent materials for the fabrication of 1D gratings [105-108], 2D devices [109], and Fresnel zone plate (FZP) lenses [15, 110]. These approaches have utilized either amplified Ti:Sapphire systems or long-cavity oscillators, which have relatively low powers and low pulse operating frequencies. Therefore, their fabrication speeds in patterning transparent materials are lower as compared to FS ytterbium-based laser sources, commonly used in optical device fabrication [111]. Here, the novelty was to integrate computer-generated holography (CGH) during the laser fabrication process to predict its optical characteristics. Rapid direct FS laser writing of optical devices through holographic

patterning on transparent polycarbonate (PC) substrates has not been reported before. Hence, the development of a patterning approach employing highly dynamic FS laser sources can enable the cost-effective production of microphotonic devices on polymeric substrates.

Here, a FS ytterbium-based laser microstructuring method is demonstrated to produce microphotonic devices, 1/2D transmission gratings, Fresnel lenses and holograms in the visible spectrum range directly on a transparent PC substrate. PC has a high light transmission efficiency, high-impact resistance, it is lightweight, and effective wettability resistant due to a low surface tension [20, 21, 112]. This will provide such a self-cleaning surface which reduces the concentrated light. It has also been reported to have high thermal stability (thermo-optic coefficient of -1.06×10^{-4} $^{\circ}C^{-1}$ at 1550 nm), ease of processability, high adhesion, and low propagation losses in the visible spectrum (0.197 dB cm^{-1} at 632.8 nm) [113]. It is also well-known as a retardation film which produces high contrast and wide viewing-angle properties [114] and is needed for electroluminescence displays to prevent the reflection of ambient light [115].The microphotonic devices were fabricated by using a FS ytterbium-based laser. This approach allowed the patterning of large areas of microstructures with a depth of few hundred nanometers to rapidly produce rigid and mechanically strong microphotonic devices and holograms as compared to other microfabrication techniques which require phase masks or photosensitive materials. In addition, a FS ytterbium-based laser has a higher fabrication speed as compared to other laser sources due to its high pulse repetition frequency (2 MHz). Optical characteristics of the fabricated microphotonic structures with different depths were studied through periodic structure visualization; diffraction intensity profiling, angle-resolved measurements, and light output shape symmetry analysis. The groove depths can be used to control the phase modulation of light and for producing wavelength selective

diffractive devices. Additionally, FFT has been utilized to write computer-generated holograms. Such microphotonic structures produce interference in the visible spectrum of light to create a desired light shape output. This fabrication approach combined with FFT simulations enables creating rationally-designed complex geometries that can produce any predicted shape, transmission intensity profile with precise diffraction angle and the geometry of output. These microphotonic devices can be used in a wide variety of industrial applications including laser patterning, dynamic displays, sensors, fiber optics and photomedicine [85].

3.3 **FFT-based Design and Fabrication of Microphotonic Devices**

The first step in the FS laser fabrication of the microphotonic devices was to rationally design microstructures using computational modelling (Figure 1a-c). 1/2D transmission gratings, a Fresnel Zone Plate (FZP) lens and a hologram pattern were designed to provide predefined photonic characteristics. These designs were micropatterned using a FS laser on a large surface area of 2 mm thick PC substrates.

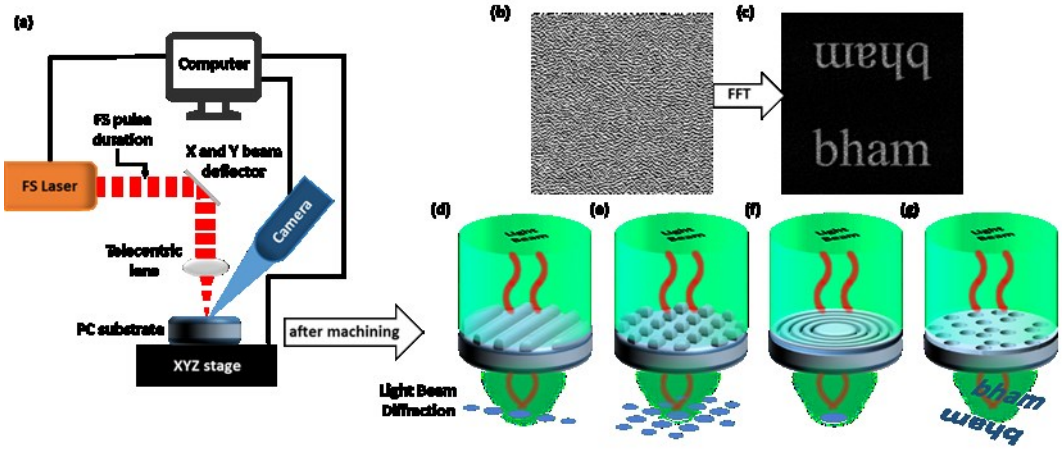

Figure 1. FS laser patterning of microphotonic devices. (a) A schematic of the FS laser microprocessing system. (b) Image of a 2D computed hologram based on 200 × 200 square array of aligned microgrooves. (c) A 2D Fast Fourier Transform of an image producing a light scattering pattern showing the first order of ‘bham’ diffraction. The

zero order produced in the center of the image was reduced to view the pattern clearly. The schematics of optical devices: (d) 1D grating, (e) 2D grating, (f) FZP lens, and (g) hologram.

1/2D transmission gratings were designed to disperse incident light on to the opposite side of the grating at a specific angle and direction. The dispersion of light depends on the angle of incidence and groove spacing. As the angle of incidence increases or the groove spacing decreases, the dispersion of light increases. This is based on the grating equation when light is normally incident on the microphotonic structures; in $d \sin \theta m = n \lambda$, where d is the distance from the center of one groove to another adjacent groove, θ_m is the angle of diffraction measured from the normal, *n* is the order of diffraction, and λ is the diffracted wavelength [116]. For a 1D grating, the periodic grooves (d=25 μm) were designed to be parallel to each other (Figure 1d); while the periodic grooves (d=35 μm) were designed to be perpendicular to each other for the 2D grating (Figure 1e). These images show the incident light dispersion after passing through periodic grooves to produce a diffraction pattern. The profile of groove grating affects the profile of the transmitted light diffraction.

A FZP lens consists of a series of concentric annular grooves resembling rings ablated on a PC substrate (Figure 1d). This FZP lens reduces the amount of material required for its fabrication as compared to the conventional lens or blazed Fresnel lens production. The rings diffract light to create constructive interference based on alternating transparent and opaque zones. These zones on the lens have been designed to operate in the optical regime. Therefore, to pattern the alternating zones by FS laser ablation, it is necessary to study the limitation of the spot size of the laser beam (20 μm). This led to determine the radius (d) of rings and their numbers(n) with

the wavelength of incident light (λ) to measure the focal length, $\mathrm{f} = \mathrm{d}^2/\mathrm{n}\lambda$, $(\mathrm{n} = 1,2,3 \ldots)$ [117], where d is the radius and n is the number of rings, and λ is the wavelength of the incident light [118-120]. The focal length and optical wavelength were set to (f=39.5 cm for 633 nm, 47 cm for 533 nm, and 56 cm for 450 nm) with nine rings. Due to fabrication on a transparent PC substrate, the lens operates in the transmission mode. The key advance in the fabrication of the lenses is their thin, lightweight construction in a variety of sizes for light gathering for use in a wide range of research and industrial applications.

A computer-generated 2D hologram consists of an array of vertically aligned microgrooves in a PC substrate. The circular pixels produce binary phase pattern which provide broad viewing angles and high-resolution image quality [121]. This microgroove array was produced by a direct FS laser ablation process. The array of circular pixels diffract light to create constructive interference based on alternating transparent and “dispersive” pixels to form a diffraction pattern [17, 122]. The pixel size dictates the resolution and beam divergence [123]. Larger pixels allow the dispersion of light at a small angle but large viewing distance [124]. Here, we used a FS laser to directly create an array of vertically aligned microgrooves as diffractive patterns to produce a high resolution image in the far field. The design of the microgroove array was calculated based on Fourier optics [125], to produce a 2D ‘bham’ diffraction pattern. The array represented a transparent and diffractive circular pixel mask that would create a pattern in the far field similar to a Fraunhofer hologram. The PC hologram was designed as a square array of 200×200 intensity delta spaced by a lattice constant of 40 μm and a groove diameter of 20 μm. A binary amplitude array was optimized by using the Gerchberg-Saxton algorithm [126]. Figure 1b shows the optimized solution for the microgroove array based hologram. Figure 1c illustrates the 2D Fast Fourier Transform (FFT) array of the microgroove hologram. This

computational approach allowed predicting the order of ‘bham’ diffraction for the hologram.

To fabricate optical devices, Figure 1a shows a schematic of the multiaxis laser micromachining that was utilized. FS pulses of an ultra-short ytterbium-based laser (λ=1030 nm, 310 fs) have a maximum pulse energy (10 μJ), repetition rate of 500 kHz and an average power of 5 W. The FS laser system integrates a 100 mm f-theta telecentric lens to provide a focused laser beam spot diameter of 30 μm and machining field of view of 35×35 mm. This system also integrates a high dynamic scan head that is computer controlled to produce with high speed micro patterns. The optimized laser parameters for the micromachining of the Fresnel lens, the hologram and the gratings are provided in Table 1. Furthermore, to ensure a machining accuracy of ±10 μm, a customized software was used to minimize the dynamic effects of the beam delivery subsystem on machining results during the fabrication process [15, 36, 37]. The profile of grooves was measured by a G5 Alicona Infinite system by using a 50× objective. This magnification allowed a lateral resolution of 1-2 μm to be achieved and thus to image and identify the edges of microgrooves (20 μm).

Table 1. Parameters used in FS laser patterning process of optical devices

Laser parameter	Units	Fresnel Lens	Hologram	Grating (1D)	Grating (2D)
Power	W	3.5	3.5	2.2	2.2
Repetition rate	kHz	500	125	125	125
Scanning speed	m/s	2	0.5	0.5	0.5
Pulse duration	fs	310	310	310	310
Beam diameter	μm	30	30	30	30
Hatch style	-	Horizontal	Outlines	Horizontal	Horizontal & Vertical
Hatch pitch	μm	7	-	15	15
Layers	-	1	1	1	3

3.4 Optical Characterization of Microphotonic Structures

1D and 2D Transmission Gratings

Transmission gratings were designed to disperse incident light at specific angles. Angular dispersion is a function of the angle of incidence and groove spacing. The grooves were designed either to be parallel (1D grating) or perpendicular (2D grating) to each other (Figure 2d, g). The samples were studied using an optical microscope (Alicona Infinite) with 20× magnification. During the laser ablation process, some amount of the PC evaporated from the groove zone (black) and then redeposited near the groove edges. Optical microscopy measurements revealed the surface profile of these gratings showing that the width and depth of grooves were in the range of micrometer except one sample has the depth of 1D grating grooves around 550 nm.

The laser-written gratings were characterized optically, where light transmission measurements were conducted using broadband light. These measurements were performed using a spectrophotometer (2 nm resolution), which was connected to a microscope by an optical fiber. The light transmissions of the gratings were measured, where a plane PC surface was used as a reference. Figure 2a shows the average transmission spectra of 1D and 2D gratings at a normal angle of incidence. An increase in the patterned area of the grooves reduced the light transmission because of the grooves that behaved as opaque zones. The 1D and 2D gratings had ~70% and ~60% total transmission efficiencies in all orders across the visible spectrum. Similarly, the light transmission through an analyzer was utilized to test the polarization of light and its effects on the diffraction in far field [127]. Both gratings preserved polarization, with less than 0.6% light transmission intensity. For angular dispersion, the angle-resolved measurements were performed at a normal angle of incidence with two laser beams (455 and 533 nm) (Figure 2c). The sample was placed on a rotary stage and a detector was located 2.0 m away from the sample to obtain far field viewing distances. The

stage was rotated to measure each order individually (Figure 2 f, i). Figure 2f shows the angle of diffraction pattern measured for a 1D grating illuminated at λ=450 nm and 533 nm with periodic grooves (d=25 μm). Well-ordered 1D diffraction patterns were observed but a lower intensity was noticed for the zero order in transmission mode at λ=450 nm and the zero order had a comparable light intensity to the second order. This is due to the effect of two dimensional phase modulation produced by changing the depth of grooves. Additionally, light diffraction patterns were captured using a digital camera. Figure 2b shows a schematic of the experimental setup to capture this pattern. The sample was placed on a rotational stage and a semi-transparent glass globe was positioned 0.55 m away parallel to the sample surface plane. This setup is suitable for light interference measurements as it has a far reaching view of the grating diffraction. The diffraction grating captured by the digital camera was in agreement with the simulated results. The fifth order diffraction pattern, for green and the third order diffraction pattern for blue consisted of two symmetrically conjugate spot diffractions located on the opposite sides of the semitransparent global screen. The diffraction results were consistent with Bragg's law, where the diffraction spot dispersed at a larger angle producing larger diffraction as the wavelength of the laser beam increased. The image of the 1D grating showed well-ordered bright spots on a large scale with a longer viewing distance as compared to 1D holographic gratings [30, 128]. Using the same interrogation setup, the 2D grating was analyzed. In the 2D grating, the diffraction was split into multiple spots on the horizontal and vertical planes. Figure 2g shows that the width and depth of the grooves increased when they crossed each other because laser ablation was duplicated at the cross point. This process changed the structure from a square to a squircle and the diffraction pattern showed this geometry (Figure 2h). In general, although both gratings produced less diffraction

orders once the wavelength of the incident light decreased, they maintained a high diffraction order as compared to the 2D holographic gratings [30, 128].

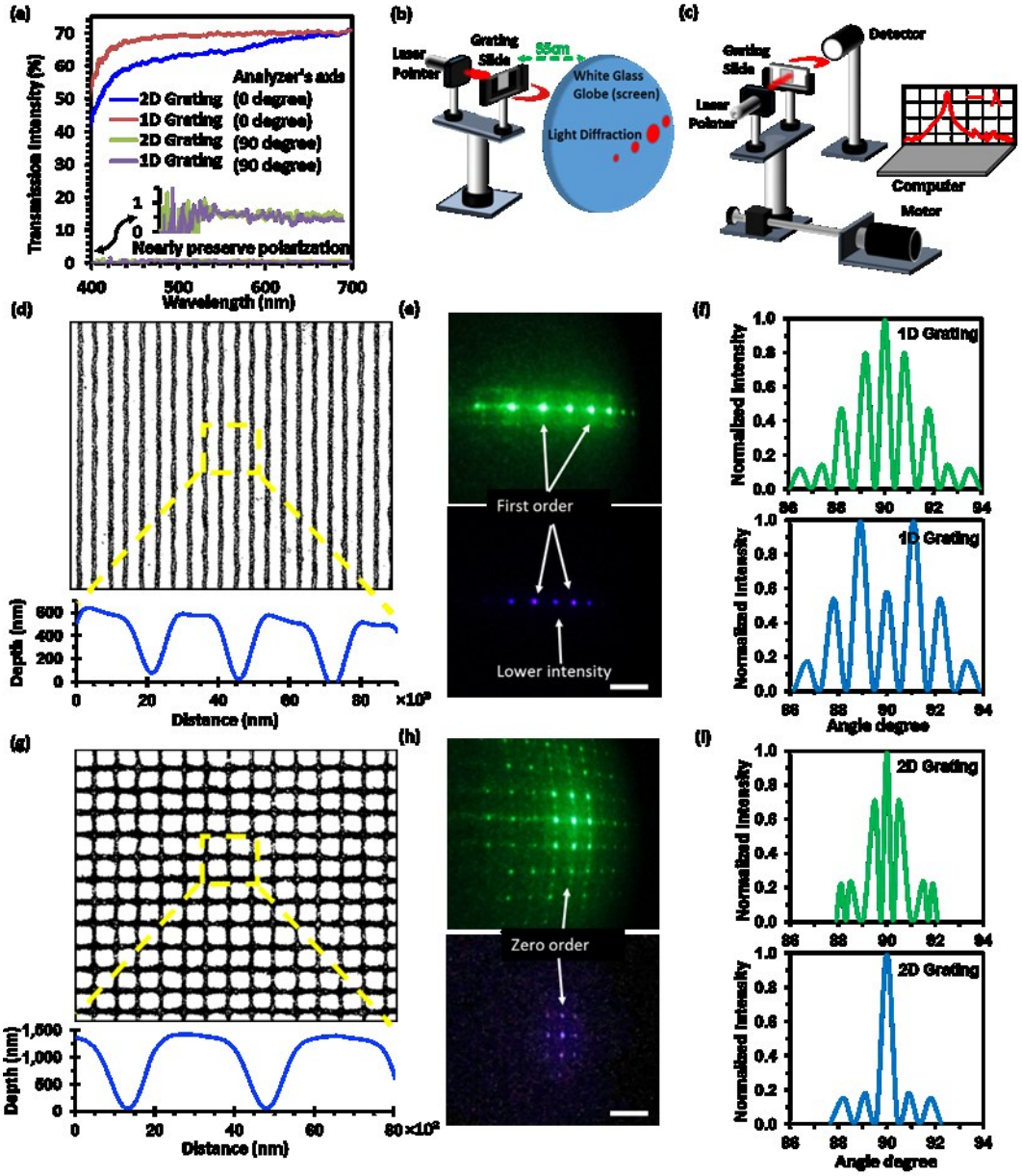

Figure 2. FS laser processing of PC 1D and 2D gratings and analyses of their optical characteristics. (a) Spectroscopic transmission measurements of the 1D and 2D gratings using broadband light at normal incidence. (b) Schematic of the experimental setup used to capture the 2D pattern from 1D and 2D gratings as seen in (e and h). (c) Schematic of the experimental setup of angle-resolved spectral measurements in (f and i). (d- f) Spectrum analysis of the 1D grating. (g-i) Optical

measurements of 2D grating. (d, g) Optical microscope images of the groove surfaces at normal incidence and their corresponding surface profiles. (e, h) 2D views of grating diffraction in a semi-transparent globe using 533 and 450 nm beams at normal incidence illumination (scale bar= 0.2 m). (f, i) The angle of diffraction pattern from the grating illuminated normally at λ=450 and 533 nm.

To simulate the diffraction effect, the Geometrical Theory of Diffraction GTD was used [129]. The effect of the two-dimensional groove was modeled with a two-dimensional phase modulation in a plane. The phase modulation was produced because of the difference in the path of the light beam at different depths of the grooves. The phase difference θ at different depths of the groove z(x,y) in the plane x-y is:

$$\theta(x,y) = z(x,y)k_1 + \left(z_{max} - z(x,y)\right)k_0 \qquad \text{(Equation 1)}$$

Where k_1 and k_0 are the wavevectors of the PC substrate and vacuum respectively and z_{max} is the maxima. The phase difference reduces to:

$$\theta(x,y) = z(x,y)(k_1 - k_0) + \phi \qquad \text{(Equation 2)}$$

Where ϕ is an arbitrary phase constant. Thus, the modulated complex-valued 2D wave is:

$$I(x,y) = I_0(x,y)\ e^{i\,\theta(x,y)} \qquad \text{(Equation 3)}$$

Where I_0 represents the intensity profile of the laser beam (Gaussian beam illumination). Finally, the Fourier transform of I(x,y) was applied to obtain the diffraction pattern observed at the far-field.

The characteristics of the groove were measured to simulate the depth profile in z(x,y). In the present case, the groove was observed with an inverted Gaussian shape. This Gaussian distribution was repeated periodically in the vertical axis, or in

both the vertical and horizontal axes. The full width at half maximum utilized was 8 μm which corresponded to the size of the laser beam writing spot. The maximum height of the Gaussian distribution was selected according to the measurements. The 1D grating was simulated to have a profile depth (950 nm), refractive index (1.53), grating pitch (25.5 μm), groove width (10 μm) and analyzed at various spectrum ranges (633, 533 and 450 nm). The 2D grating was simulated similarly, except profile depth (1450 nm) and grating pitch (35.2 μm) were varied. Figure 3 shows that the simulation results of the diffraction pattern observed at various wavelengths for 1D (Figure 3a) and 2D gratings (Figure 3c) and their intensity profiles of each diffraction order (b and d), respectively. Variation in the wavelength and groove depth changed the intensity profiles of each diffraction order. Furthermore, the intensity profile of each order for 1D grating were analyzed across various groove depths (200 to 2000 nm). Controlling the depth of the groove grating allowed modulation of the profile of the transmitted light diffraction.

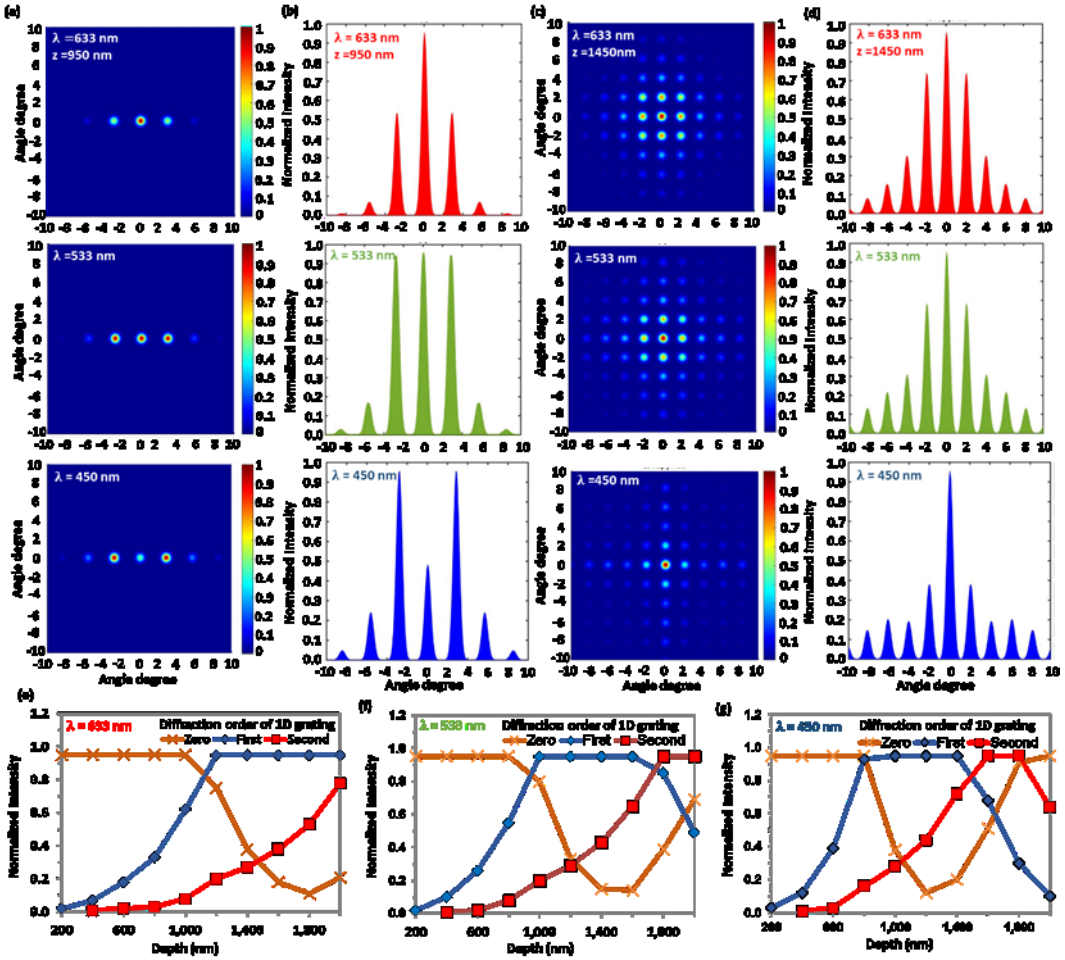

Figure 3. S Simulation results of radiant intensity profile diffracted by the phase modulation from a 2D groove. (a) Diffraction pattern for 1D grating at 633 nm, 533 nm and 450 nm (top, middle and bottom panels, respectively). (b) Radiant intensity profile normal to the vertical axis for the 1D grating. (c) Diffraction pattern for a 2D grating at three different wavelengths (633, 533 and 450 nm) and their radiant intensity diffraction. (d) Radiant intensity profile normal to the vertical axis for the 2D grating. (e-g) Intensity of each diffraction order (1D grating) across the groove depth change for various incident light wavelengths (633, 533 and 450 nm).

Fresnel zone plate (FZP) lens

A FZP lens was designed to focus incident light into a bright spot at the center within a focal length range. The fabricated PC FZP lens was characterized under an

optical microscope (Alicona G5 Infinite Focus) at 5× magnification to allow the imaging of the whole lens. Figure 4a illustrates the microscopic image of the FZP lens showing contrast between the series of concentric annular grooves (black zones) and the non-ablated PC substrate (white zones). The profile of FZP lens grooves were measured to understand the laser patterning process (Figure 4d). The laser patterning process redeposited the ablated material toward the edges, and the bottom of the grooves had a rough surface. Such rough surfaces consisting of nano- and microparticles have been reported in other materials such as buckypaper and float glass substrate [15, 130, 131]. Such artefacts in the optical device causes electron-phonon scattering, which is the main factor in the loss of energy.

The optical characteristics of the FZP lens fabricated on the PC substrate were analyzed using a spectroscopy setup and an optical microscope. An optical beam profile was conducted using three different laser wavelengths (633, 533 and 450 nm) on an interrogation setup (Figure 4b). A high order diffraction from the ablated Fresnel zones showed that most of the grooves were successfully created and behaved as opaque zones. Figure 4e illustrates that incident light from a series of non-ablated zones were focused into a bright spot in the center with a focal length (f) dependent upon the incident wavelength (f=39 cm in 633 nm, 47 cm in 533 nm and 56 cm in 450 nm). Light focusing at focal points were observed in the long-distance far field. Figure 4f shows the 2.5D beam profile intensity of images illustrated in Figure 4e. The three different laser beams focused higher intensity spots by bending parallel light to a common focal length. Therefore, the FZP lens works sufficiently within the visible spectrum and the light focusing effect results were in agreement with the analytical solution and simulated FFT model (Figure 4h,i). The light transmission efficiency of the FZP lens was measured to be ~55% across the visible spectrum and the polarization analyzer was oriented from 0° to 90°, where a non-patterned PC substrate was the

reference. This setup was used to analyze the linear polarization of light, which can affect the light focusing of a lens. In the present work, lenses nearly preserved the polarization (0.9%) in transmission mode (Figure 4c). Furthermore, the light transmission efficiency of the lens could be improved by increasing the contrast between the transparent and opaque zones; thus, reducing the roughness on the side and bottom of the grooves during laser ablation processes can improve the lens focusing efficiency.

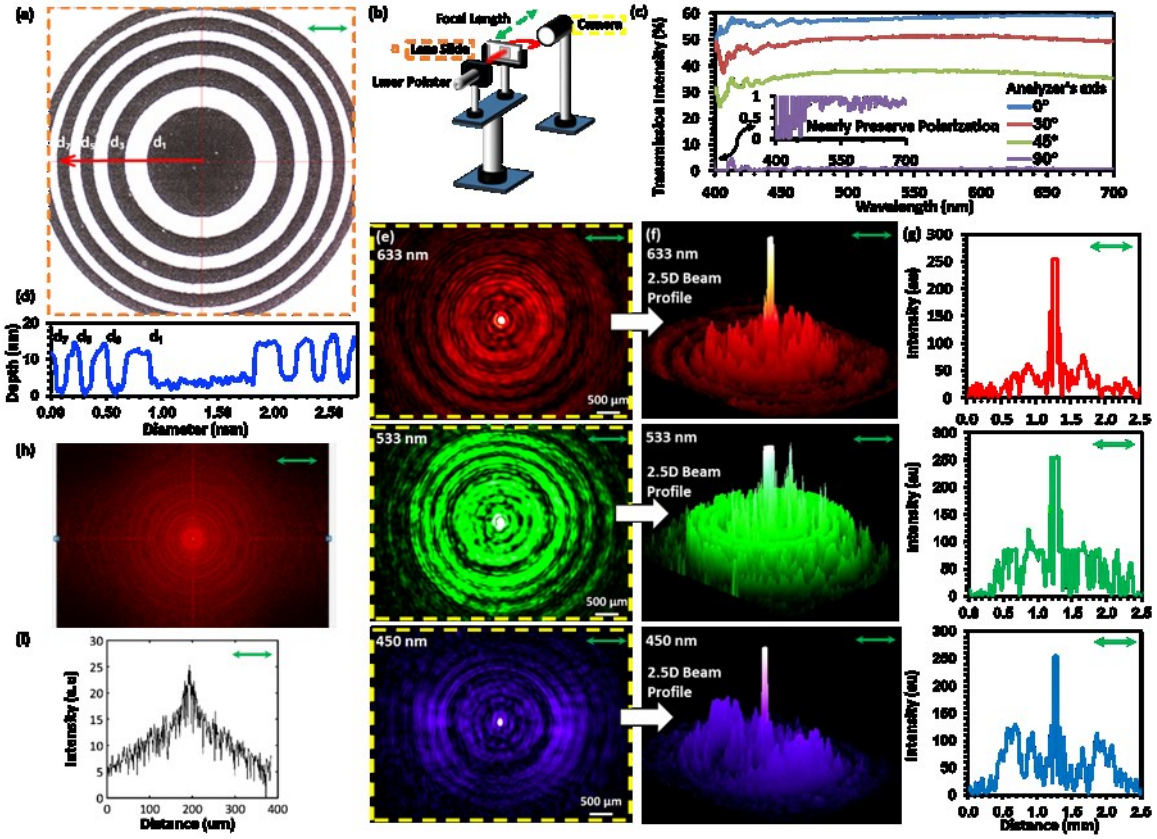

Figure 4. FS laser writing of PC FZP lenses and analyses of their surface topography and optical characteristics. (a) Optical microscope image of concentric annular grooves in the FZP lenses fabricated using FS laser ablation and their corresponding groove profile in (d). (b) Schematic of experimental setup to capture the bright spot in the center of the image. (c) Transmission measurement through lens and analyser axis (0°, 30°, 45°, and 90°) was changed to study the polarization of light. (d) Depth profile of the grooves. (e) 633, 533 and 450 nm beams illuminated through the

lens in transmission mode. The observed patterns from the lens were recorded by a high-resolution camera and their corresponding 2.5D profile images are shown in (f). (g) The intensity profile of 633, 533 and 450 nm beams at certain focal length points. (h) FFT simulated model of FZP lens and (i) its intensity profile.

Computer-generated 2D transmission hologram

A 2D array of circular pixels was designed to produce a holographic projection image. The fabricated array of vertically aligned microgrooves as circular pixels were characterized using an optical microscope at normal incidence (Figure 5b). Figure 5f shows a magnified view of the microgrooves. These microscopic images showed the contrast between the ablated circular pixels (black) and the non-ablated pixels (white). Some amount of PC evaporated from groove zones (black) and then redeposited near the groove edges during the laser ablation process. A FFT simulation was carried out using the designed pattern and displayed ‘bham’ diffraction symmetrically located around the center of zero order in transmission mode (Figure 5a). The highly-intense zero order of the non-diffracted light was reduced from FFT image to clarify the ‘bham’ diffraction. Additionally, the optical behavior of the hologram based on the microgroove array was experimentally characterized. The PC hologram was mounted onto a slide holder with a white screen located 2.5 m away to capture the diffraction pattern in the long-distance far field. The white screen was aligned parallel to the surface plane of the hologram substrate and a digital camera was placed in front of the screen. Laser beams (633, 532 and 450 nm) were normally positioned behind the hologram incident to the substrate. A transmission diffraction pattern was produced when the PC hologram was illuminated with the laser beams. Figure 5c shows captured diffraction pattern images, which were consistent with the computed FFT diffraction pattern (Figure 5a). The first order diffraction pattern consisted of two symmetrically conjugate

‘bham’ diffraction patterns located on the opposite sides of the white screen. A clear and intense ‘bham’ diffraction was produced at a long viewing distance with a wide field of view. Furthermore, the wavelength dependence of the diffraction from the PC hologram was also studied. The microscale dimensions of the 2D holographic array produced diffraction at a long viewing distance. According to Bragg’s law, the diffraction angle depends on illumination wavelength. The diffraction pattern from the PC hologram was studied under red (633 nm), green (533 nm) and blue (450 nm) laser beams. The ‘bham’ diffraction pattern was projected at the long-distance far field producing larger images as the laser wavelength increased (Figure 5c). The diffraction results were consistent with Bragg’s law [10]. The images for the blue laser had low quality as the diffraction angles were close to the zero order making it hard to image the hologram. The intensity profile of “bham” diffraction and their sizes along the x-axis were measured (Figure 5d), showing that the diffraction images with the green and blue laser were reduced by 1.5 and 2.5 cm from an original size of 6.0 cm, respectively. However, the efficiency of the PC hologram can be improved by increasing the transmission contrast between the transparent pixels and dispersive pixels. Thus, reducing the evaporation and redeposition of PC from pixel edges during laser ablation processing can improve the resolution of the hologram in the long-distance far field.

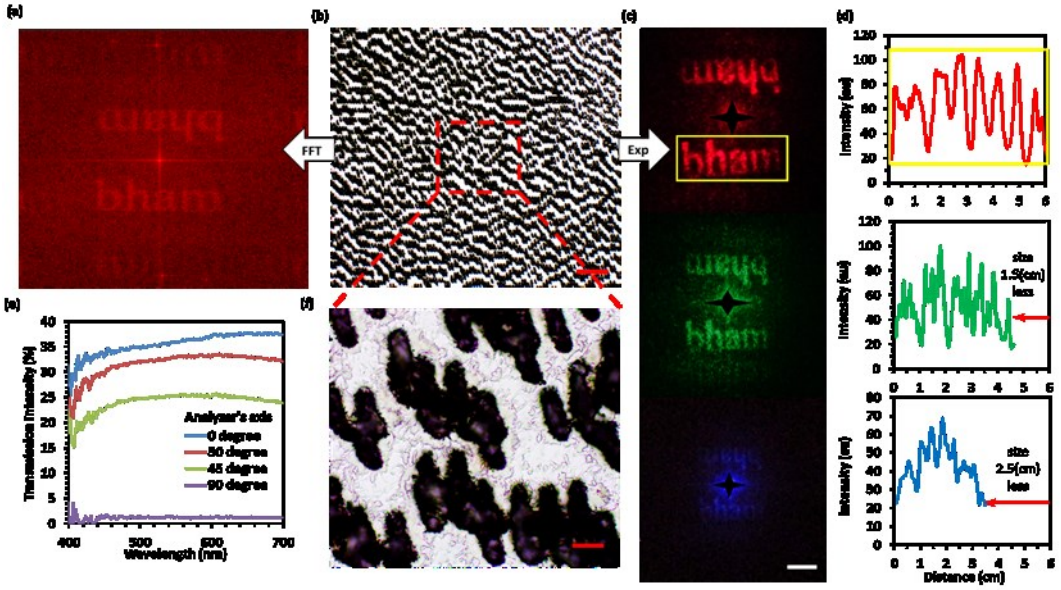

Figure 5. FS laser writing of a PC computer-generated 2D hologram. (a) Fourier transform displaying ‘bham’ diffraction symmetrically located around the zero order. A highly intense of zero order was excluded to clarify the first order diffraction. (b) An optical microscope image of the fabricated hologram pattern (scale bar= 200 μm). (c) The ‘bham’ diffraction pattern of the holographic array produced on a screen with 633, 533 and 450 nm beam illumination. Scale bar=2 cm. (d) The intensity profiles of the “bham” diffraction pattern in response to 633, 533 and 450 nm wavelength beams. (e) Light transmission intensity of the holographic pattern with different probe orientations using broadband light at normal incidence. (f) A magnified view of the holographic array. Scale bar= 20 μm.

Optical Wettability Resistance of Microphotonic Structures

Transparent devices which have a predefined affinity to water is highly desirable in optical and electronic devices. These hydrophilic devices may spread water across their surface to maximize contact based on the Wenzel model ($\theta < 90°$) while hydrophobic devices that naturally repel water and form droplets are defined by the

Cassie-Baxter model (90° > θ < 150°) [132]. The hydrophilicity of transparent devices can have a significant impact on the optical and electrical performance in a wide range of applications including self-cleaning [133, 134], anti-fouling [135], anti-corrosion [136], anti-fogging [137], icephobicity [138], and drag reduction properties [139, 140]. FS lasers can be employed not only to fabricate microphotonic devices but also modify the surface wettability resistance simultaneously, while this device will require multistep processes in other fabrication techniques [36].

Due to the effective wettability resistance of PC, the fabricated microphotonic devices were analyzed and tested for their surface wettability resistance. In practical applications, water contact angles (CAs) of the optical devices were measured with a deionized water droplet (5 μL) 30 days after fabrication to determine surface morphology changes over time [141]. In the present work, a water droplet from a pipette was deposited vertically along the microphotonic surface at 24 °C. A digital microscope was utilized to visualize the side profile of each deposited drop on microphotonic surfaces. The captured images were obtained after the droplet had formed its final shape to analyze the interface between the liquids and the surface of the microphotonic device. As a result, various shapes were obtained from different optical devices affecting the contact angle. Therefore, image processing was utilized to measure the contact angle of each shape. Surface wettability characterization showed that water droplets changed their contact angle from one device to another due to various groove depths, across groove widths and the space between them (Figure 6). PC substrate (the non-ablated area) had a contact angle of 72°, while the contact angle of water droplet on 1D and 2D gratings (periodicity d=25 and 35 μm) was reduced to 52° and 44° (achieving hydrophilicity), respectively. This hydrophilic surface reduces distorted light or vision in optics during condensation by spreading water uniformly over the surface [142]. However, the contact angle for the hologram and FZP

lens increased to as much as 92° and 125°, achieving hydrophobicity. Accordingly, the energy barriers associated with the local contact line depended upon the spacing between the microgrooves and resulted in the loss of circular symmetry in the contact line on the surface [143]. These microphotonic devices with hydrophilic and hydrophobic surfaces can be used in various optical applications such as outdoor surveillance cameras, and dynamic displays in extreme environments, biomedical optics, and endoscopy.

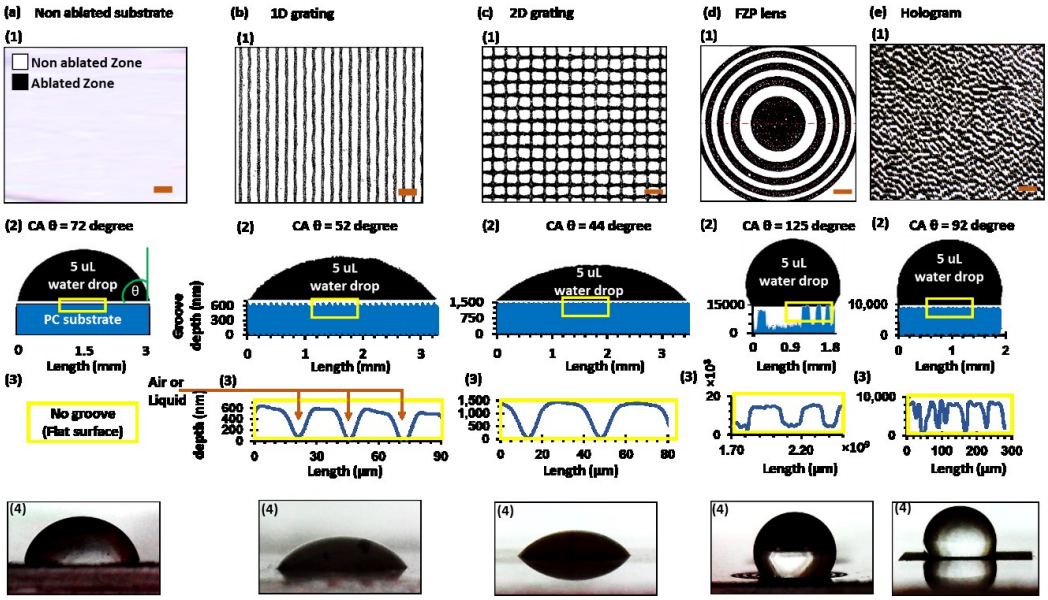

Figure 6. Water droplet contact angle for hydrophilic and hydrophobic microphotonic devices after the droplet had formed its final shape to analyze the interface between the liquids and the surfaces of the microphotonic devices. Water droplets were deposited on (a) the PC substrate with non-ablated zone, (b) 1D grating, (c) 2D grating, (d) FZP lens, and (e) hologram. Each device has been illustrated with (1) optical microscope images of the fabricated devices at normal incident, Scale bars=50, 50, 50, 400 and 400 μm respectively, (2) droplet profiles on the grooves, (3) the magnified views of groove profile, and (4) microscopic images of water droplets on optical devices.

3.5 **Conclusion**

The fabrication of 1D/2D gratings, a FZP lens and a 2D hologram on PC substrates was demonstrated by using direct FS laser writing. This microphotonic device fabrication approach allows the production of microphotonic devices with nanoscale depth. This technique is applicable for producing 3D microphotonic devices in various polymeric and glass materials, where a few hundred nanometers in depth of 3D grooves can change the 2D phase modulation and diffraction efficiency. These structures produced affected the wettability resistance. The major challenge in using this route for fabricating such microphotonic devices is the control and reproducibility of the 2D grooves whilst also minimizing the unwanted burrs on groove edges and bottom. The FS direct laser patterning technique presented in this work can enable rapid, accurate, and cost-efficient production of displays, optical filters, sensors, and fibre optic devices.

Chapter 4: Nanosecond pulsed laser texturing of optical diffusers

Published article

Tawfiq Alqurashi, Aydin Sabouri, Ali K. Yetisen, *and* Haider Butt

AIP Advances, 2017. **7**(2): p. 025313.

In chapter 3, the fabrication of diffractive optical devices using FS laser machining were produced on a transparent polycarbonate (PC) substrates. It was found that the areas treated with the laser become opaque surfaces; these surfaces do not allow light to be scattered thoroughly. Also the FS laser machining in chapter 2 and 3 has high-cost and low throughput pulsed laser system compared to nanosecond laser. This chapter introduces the fabrication of optical diffusers on float glass by using nanosecond laser machining.

Author Contributions

T.A. conceived the idea, deigned the optical experimental setups and provided research direction. RP did laser writing onto the samples for a half hour. T.A. wrote the first draft of the paper. All authors proofread the writing of the paper.

4.1 **Abstract**

High-quality optical glass diffusers have applications in aerospace, displays, imaging systems, medical devices, and optical sensors. The development of rapid and accurate fabrication techniques is highly desirable for their production. Here, a micropatterning method for the fast fabrication of optical diffusers by means of nanosecond pulsed laser ablation is demonstrated (λ=1064 nm, power=7.02, 9.36 and 11.7 W and scanning speed=200 and 800 mm s^{-1}). The experiments were carried out by point-to-point texturing of a glass surface in a spiral shape. The laser machining parameters, the number of pulses and their average power had significant effect on surface features. The optical characteristics of the diffusers were characterized at different scattering angles. The features of the microscale structures influenced average roughness from 0.8 μm to 1.97 μm. The glass diffusers scattered light at angles up to 20° and their transmission efficiency were measured up to ~97% across the visible spectrum. The optical devices produced diffuse light less but do so with less scattering and energy losses as compared to opal diffusing glass. The presented fabrication method can be applied to any other transparent material to create optical diffusers. It is anticipated that the optical diffusers presented in this work will have applications in the production of LED spotlights and imaging devices.

4.2 **Introduction**

Optical diffusers are widely used to distribute the light intensity from a focused light source to expand the beam [144, 145]. Optical diffusers are categorized according to their ability to distribute radiant energy effectively from an incident source in the far field [146]. Their applications range from photovoltaic devices, optical imaging, photolithography to photodynamic therapy [147]. Moreover, optical diffusers are one of the essential components in liquid crystal displays (LCDs) [14, 148, 149]. The diffusion of light can be achieved either from a surface or through the volume of an optical element. It may comprise of incorporated micro- and nanoparticles or structured patterns [147, 150]. Most diffusers consist of surface-relief structures including microlenses, pyramids, and textured surfaces due to the simplicity and time required for their fabrication [10, 66, 151-153]. Optical diffusers have been fabricated employing a range of coating processes [14, 25]. However, nanosecond pulsed laser patterning of an optical diffusers have not been studied. This technique can enable the fabrication of optical diffuser by direct material structuring or texturing without any coating processes.

However, the fabrication of optical diffusers by nanosecond laser sources has not been exploited as it has challenges compared to conventional continuous wave (CW) lasers [154].The demand for laser manufacturing methods has increased as a result of the fast growing optoelectronics market [155]. Direct laser manufacturing: (i) enables the flexible production of complex geometries [156]; (ii) offers a fast fabrication route compared to conventional techniques, (iii) is more environmentally friendly compared with coating processes; and (iv) provides precise control over the size and shape of the microstructures [157]. At the same time, the engineering applications of optical diffusers depend on their homogenization, performance, and efficiency [158]. Optical

diffusers can spread light in one or two dimensions depending up on their application [159].

In this research, we report the fabrication of optical diffusers by using nanosecond laser induced surface texturing. This method differs from other techniques used for producing holographic diffusers, where a pulsed laser is used for patterning a photopolymer layer coated onto a plastic or glass substrate [30, 160]. In contrast to this, we perform direct laser ablation of float glass substrates (without any polymer coating) for the production of tailored surface textures and roughness. The proposed new fabrication approach allows functional microstructures (topographies) to be created on float glass substrates to distribute light efficiently. The optical diffusers produced were characterised by using angle-resolved optical power intensity and spectroscopy analysis to assess the light scattering and transmission efficiency. In addition, the diffusers' three-dimensional light distribution was captured *via* a digital camera to analyse their light transmission properties. Additionally, an Alicona G5 Infinite Focus (IF) system was employed to analyze the surface topographies (roughness) of the optical diffusers.

4.3 **Optical Device Fabrication**

To fabricate diffusers, a float glass slide (1 mm thickness) was used as a substrate to create the surface micro structures. The surface patterning was performed using a master oscillator power amplifier (MOPA) based Yb fiber laser (λ=1064 nm). The micro groove structures on the glass substrate were produced, point-to-point texturing a glass surface in a spiral pattern, using three different power levels, i.e. 11.7 W, 9.3 W, and 7.02 W. A scan head and 100 mm telecentric focusing lens were included in the beam delivery system to focus the beam and two different scanning speeds, i.e. 200 $mm.s^{-1}$ and 800 $mm.s^{-1}$, were used in this feasibility study.

After the laser texturing operation the micro surface structures on the glass slides were analysed by employing the Alicona G5 InfiniteFocus (IF) system, to measure the average roughness (Ra). Table 1 shows the effects of varying laser power and scanning speeds on the resulting surface roughness. Increased pulse energy led to an increase in groove depth, therefore increasing the average roughness. Higher pulse energy resulted in material splashes over the edge of the grooves. The micro surface structures of glass substrates produced using the laser power levels and scanning speeds investigated are shown in Figure 1. Depending on the laser power and scanning speed, the depth and distance of the grooves can be controlled to achieve accurate spiral shapes. However, exceeding 11.7 W at a scanning speed of 200 $mm.s^{-1}$ may destroy the substrate (Figure 1a). Hence, the experimental parameters were optimized not to pass this average power threshold to avoid the cracks induced. These results provide some insight into the laser settings required to create optical diffusers as the roughness of the textured surfaces affects their performance [161, 162]. The interaction of the fabricated grooves with a beam of light diffuses the photons and expands the focused beam.

Table 1. Average roughness for the spiral pattern diffusers with various average powers and scanning speeds.

Machining Power (W)	**Scanning speed ($mm.s^{-1}$)**	**Average roughness (µm)**
11.7	200	1.97
11.7	800	1.64
9.36	200	1.66
9.36	800	1.61
7.02	200	1.16
7.02	800	0.8

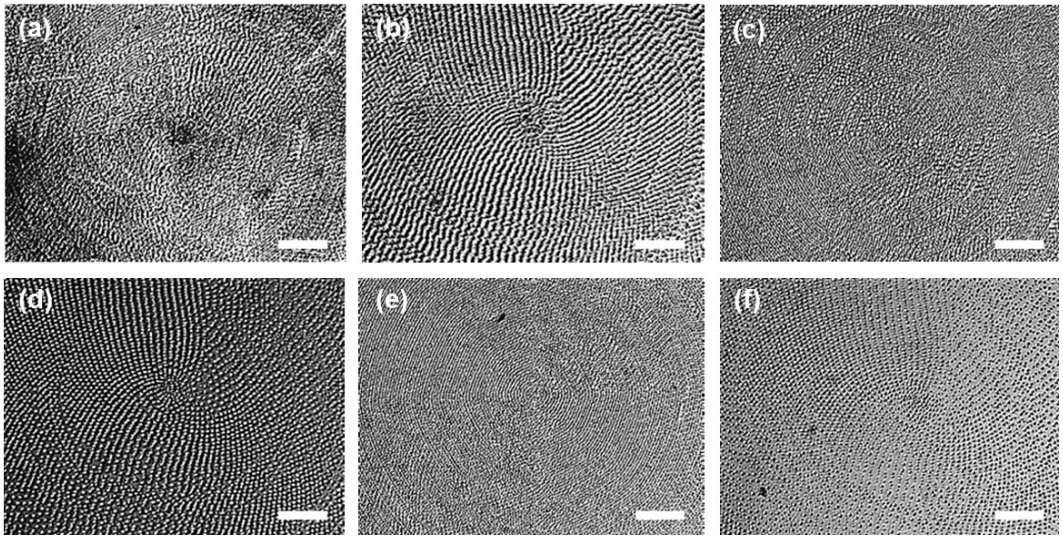

Figure 1. The micrographs of textured glass substrates with different laser powers and machining speeds: (a) 11.7 W, 200 mm.s^{-1}, (b) 11.7 W, 800 mm.s^{-1}, (c) 9.36 W, 200 mm.s^{-1}, (d) 9.36 W, 800 mm.s^{-1}, (e) 7.02 W, 200 mm.s^{-1}, and (f) 7.02 W, 800 mm.s^{-1}. Scale bar= 200 μm.

4.4 **Optical Characterization**

To characterize the optical performance, micropatterned glass samples were cleaned with isopropyl alcohol and dried before characterization. The light diffusion from the samples was characterized by two sets of experiments. The diffusers were placed onto a post with a semi-transparent hemispherical screen set above it. The radius of the hemispherical screen was 0.15 m. This setup allowed for the capture of the diffraction pattern in the far field because of there being sufficient distance from the sample to the hemispherical screen surface [146]. The plane of the sample was placed so as to be parallel to the base of the screen (Figure 2a). The laser was placed below the sample, the laser beam was set to be 1 mm wide and normally incident to the

sample. The laser light was transmitted vertically toward the hemispherical screen. A digital camera was used to capture the diffraction patterns produced.

Angle-resolved measurements were performed to characterize the angular distribution of diffused light (Figure 2b). The setup consisted of three laser sources (λ=450, 533 and 633 nm), diffuser sample, an optical power meter to detect the intensity of the scattered light at different angles and a servo motor to rotate the sample. The light source and the sample rotated together on the same base so the incident light remained normal to the sample. The rotations were performed in 1° increments, to allow that the intensity of light to be measured at every single angle.

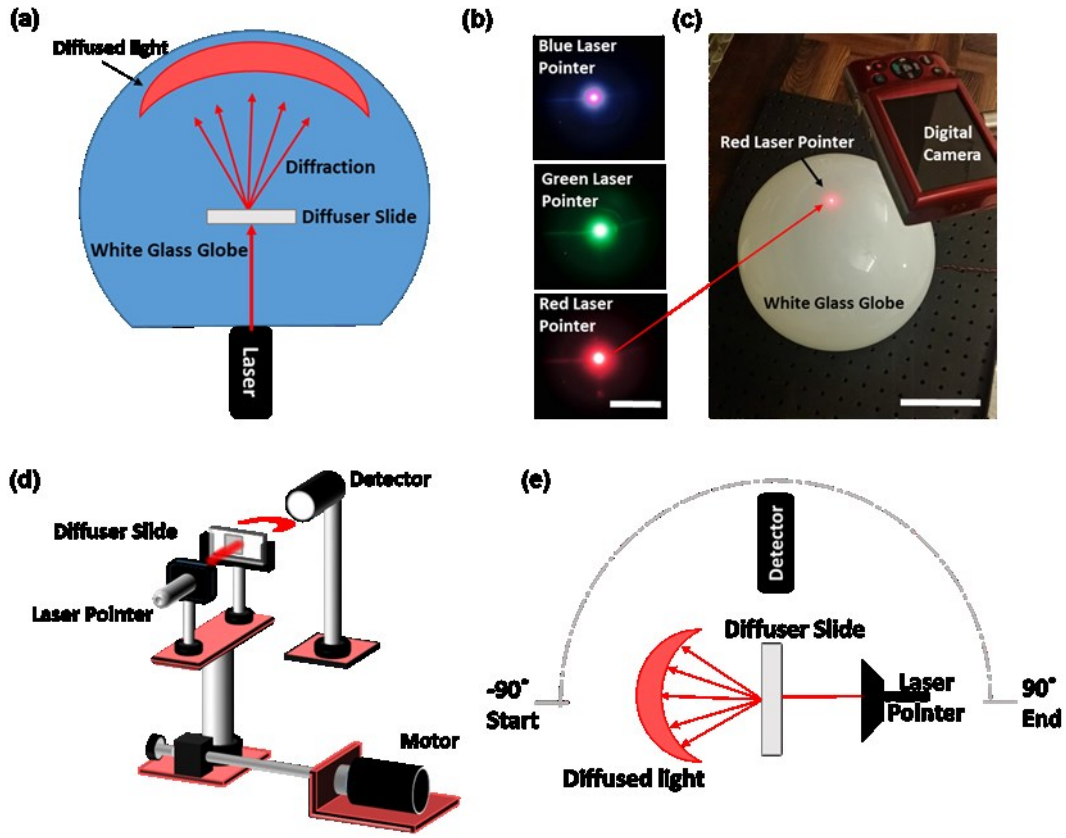

Figure 2. Optical characterization of the diffusers using angle-resolved measurements. (a) Schematic of globe diffusion measurements. (b) The output of three laser beams projected on the screen (Scale bar= 0.01 m). (c) The image of the

globe setup (Scale bar= 0.12 m) (d). The schematic of the angle-resolved diffusion measurements. (e) The top view of angle-resolved light transmission setup.

Figure 3a-c shows the diffusion efficiency of the textured surfaces on glass substrates. The diffusers textured with lower energies had higher intensity values at central peaks. Slower scanning speed resulted in lower peak intensities in the central region and consequently provided wider light transmission. The depth of grooves changed the transmission intensity from 35 to 65%, a deeper groove resulted in intensity decrease. Generally, the diffusers had scattering angles in range of 14° to 20° and their intensities had been in the range of 35 to 85%. Once the light wavelength was reduced, both the scattering and their intensities were reduced, respectively. Additionally, Figure 3d shows that the lowest transmission was recorded for the highest scanning speed with lowest power, while the highest transmission was recorded for the lowest scanning speed with highest power. They diffuse light less but do so with less scattering losses which result in less energy losses as compared to opal diffusing glass (Figure 3e). This is due to changing the roughness of the surface and the number of grooves per unit area, where lowest roughness and fewer grooves on the surface have higher light transmission intensities.

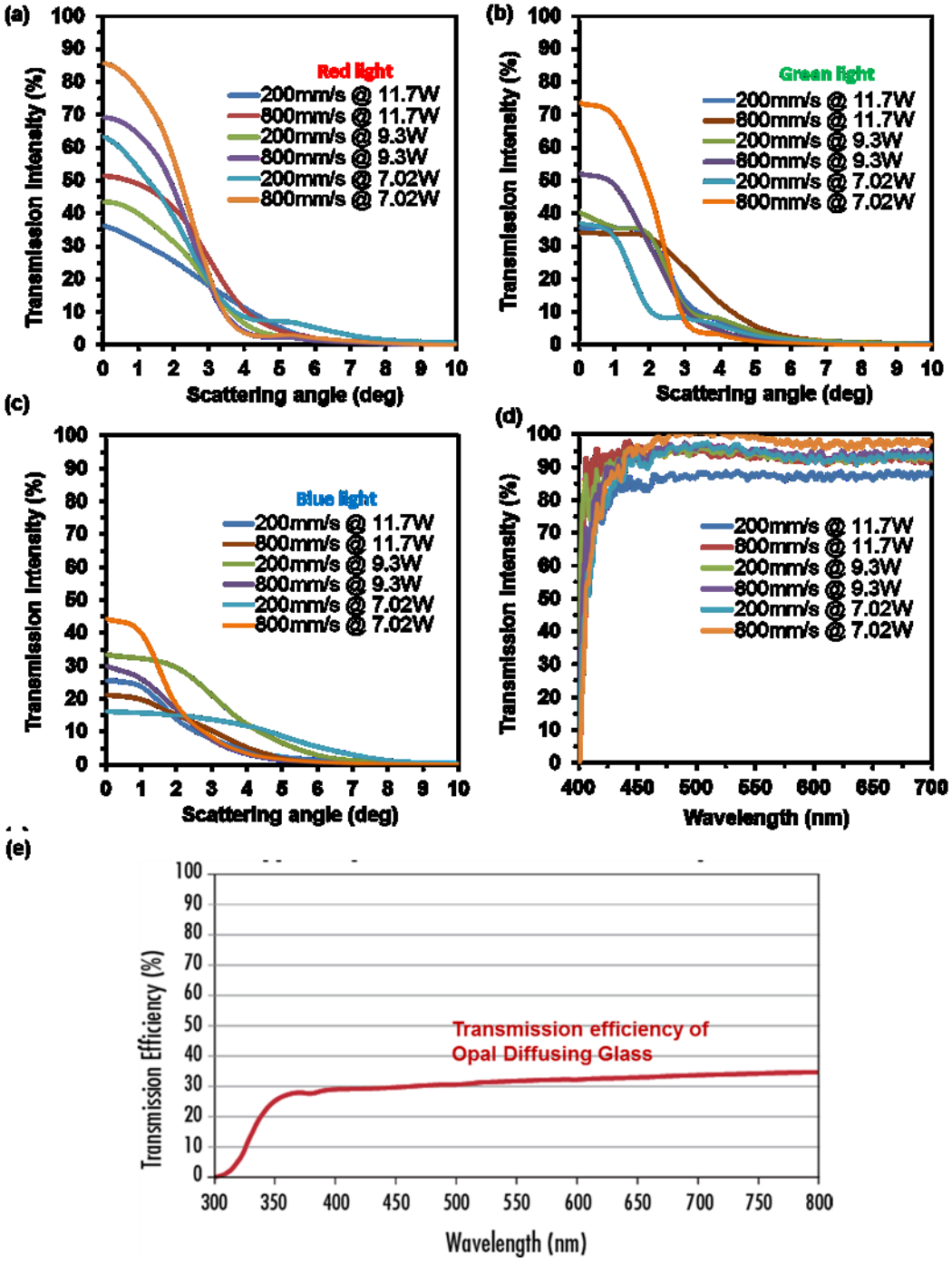

Figure 3. Transmission spectrum of various diffusers machined by a nanosecond laser. (a-c) Angle-resolved measurements of the optical diffusers by using different laser beams (633 nm, 533 nm, and 450 nm). (d) Spectroscopic measurements of the optical diffusers using a broadband light and the light intensities in transmission mode. (e) Transmission efficiency of opal diffusing glass made by Edmond optics Ltd [25].

Furthermore, the polarization dependence of the diffusers were also tested. A polarized optical microscope was used to carry out cross polarized transmission measurements on the diffuser samples. The diffuser samples were placed between the analyzer and polarizer and the corresponding transmission spectra were measured using an integrated spectrophotometer (2 nm resolution). The measurements were performed at analyzer/polarizer orientation angles of 15°, 45° and 90°. Over 90% transmission was observed at an orientation angle of 15° (Figure 4a-b). The transmission reduced to near 50% and 0% for the orientation angles of 45° and 90°. This signified the diffused light had the same polarization as the incident light, hence the polarization was preserved.

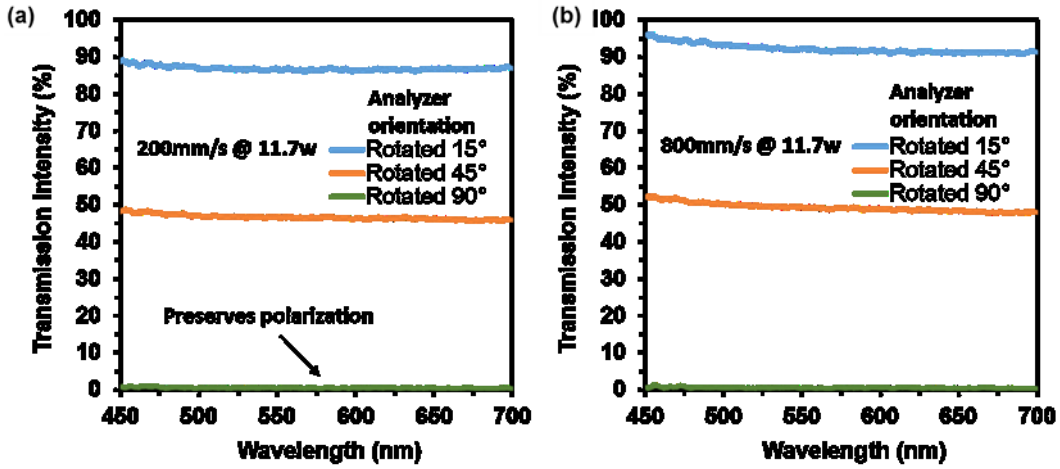

Figure 4. (a and b) Polarised spectroscopic measurement of the optical diffusers using analyser and polarizer oriented at 15°, 45° and 90°.

To compare the transmission efficiency of diffusers with various machining parameters, the total number of transmitted photons was calculated. Figure 4 shows the efficiency of fabricated diffusers which were achieved by the integration of transmission spectra. By increasing the laser power for material ablation, the transmission efficiency of the diffusers decreased (Figure 5a). This was due to an increase in material removal rate producing the rougher surfaces, which was

consistent with the roughness measurements performed. Similarly, faster texturing produced smoother surfaces, which resulted in less light scattering and consequently increased the transmission efficiency (Figure 5b).

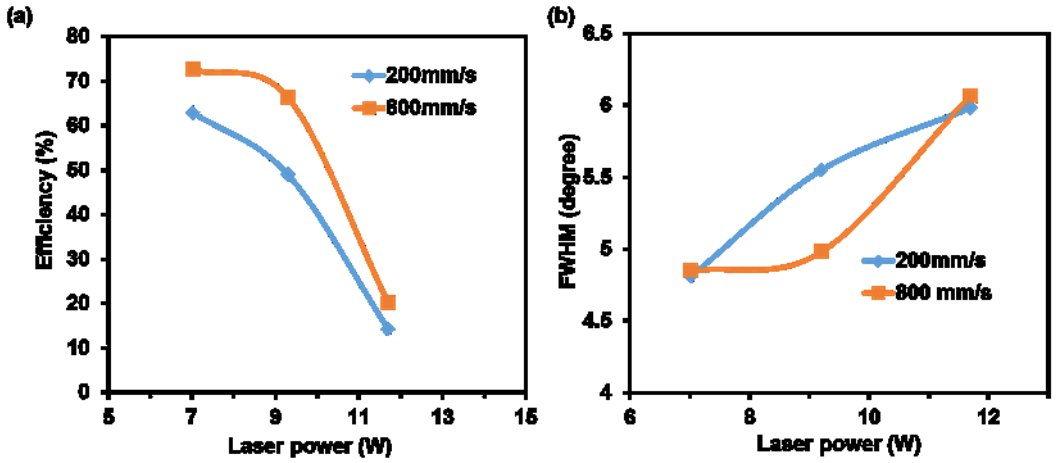

Figure 5. *The effect of laser light power and scanning speed on light transmission intensity of machined optical diffusers. (a) Light transmission efficiency of the optical diffusers. (b) The full width at half maximum of the diffracted spectrum from the optical diffusers.*

Figure 6 shows the three-dimensional distribution of the diffused light for laser wavelengths of 450, 533 and 633 nm. When the laser beams were transmitted through the glass diffuser, the light scattered at small angles, but with high transmission of light. Increasing the laser beam wavelength increased the angle of light diffusion (as also shown in figure 3a to c). The results show that such optical diffusers can be used in LED screens and spotlights for producing soft light. Although, in this research, we studied circular surface patterns produced on glass substrates, the laser processing unit is capable of 5 axis motorized motion and can produce a variety of sophisticated one/two dimensional surface patterns. By producing custom-designed surface

patterns, diffusers can be produced, which will enable high performance and tailored light distribution and intensity profiles.

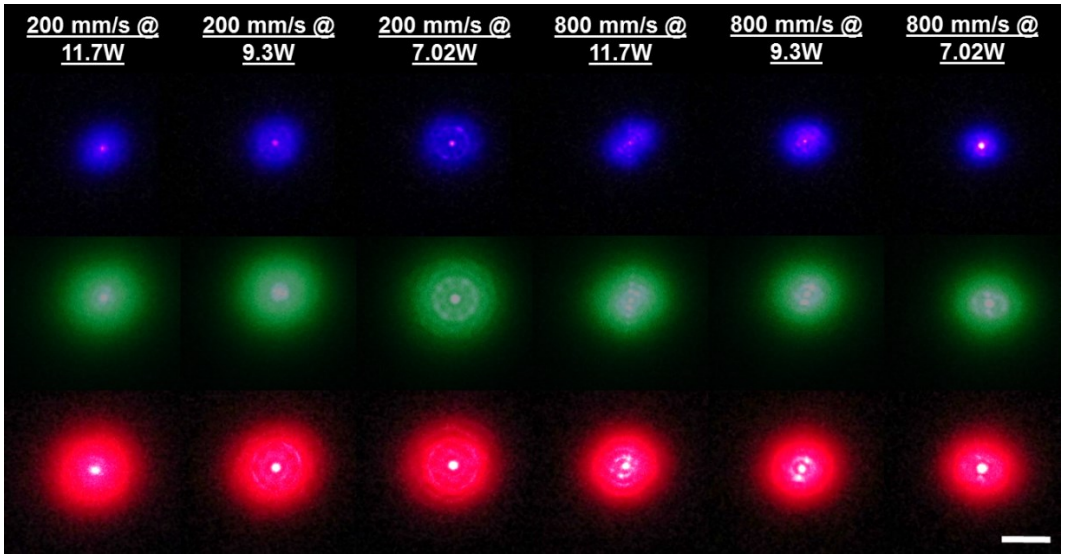

Figure 6. Different laser beams (450, 532, and 635 nm) were transmitted through the optical diffusers, producing circular diffusion patterns. The nanosecond laser parameters used for producing the diffusers are listed. Scale bar=1.5 cm.

4.5 **Conclusion**

The micro surface features of the textured glass slides were investigated using an Alicona microscope system showing that there is a direct relationship between the average roughness and power while there is an inverse relationship between the average roughness and the scanning speed. The characteristics of the optical diffusers patterned by this method can be altered by changing the laser machining parameters. The faster laser machining along with lower ablation energies produced the diffusers with higher transmission efficiency and wider scattering patterns. By increasing the roughness area of the surface, the distribution of light can be precisely controlled in wide ranges. The study conducted showed quick and efficient fabrication of spiral textured patterns as optical diffusers using a nanosecond laser by inscribing the

surface of glass. Such glass diffusers may be utilized in headlights. Producing thin optical diffusers using nanosecond laser ablation reduced the time of fabrication compared to femtosecond laser processing which it may achieve high light transmission and less energy consumption in consumer electronics.

4.6 **Supporting Information**

Nanosecond pulsed laser texturing of optical diffusers

Published Supplementary information

Tawfiq Alqurashi[1,2,a], Aydin Sabouri[1], Ali K. Yetisen[3], *and* Haider Butt[1,b]

AIP Advances, 2017. **7**(2): p. 025313.

[1]School of Mechanical Engineering, University of Birmingham, Birmingham, B15 2TT, UK

[2]Department of Mechanical Engineering, School of Engineering, Shaqra University, Dawadmi, P.O. Box 90 Zip Code 11921, Saudi Arabia

[3]*Harvard-MIT Division of Health Sciences and Technology, Harvard University and Massachusetts Institute of Technology, Cambridge, MA, 02139, USA*

The optical image of all the produced diffusers

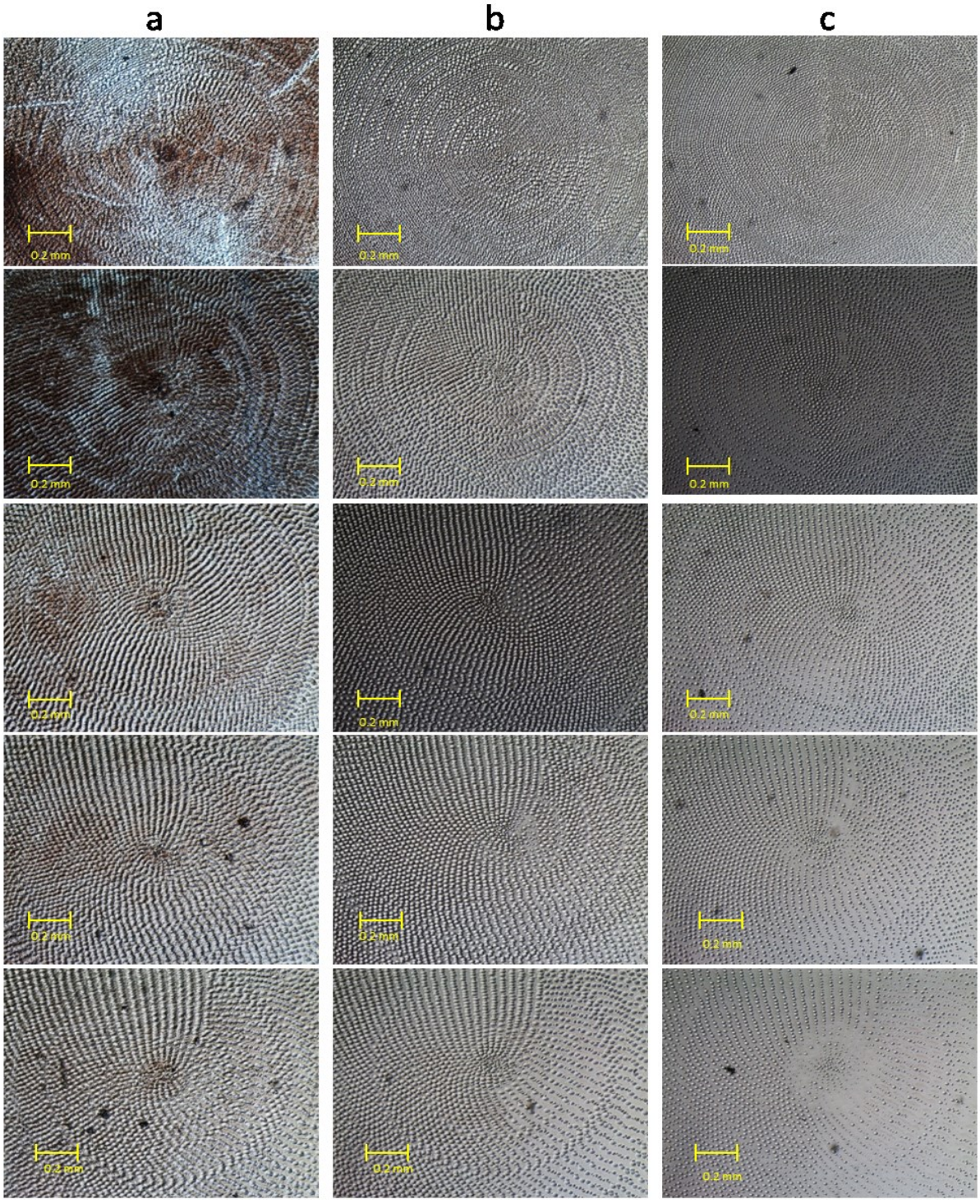

Figure S1. Diffusers under the microscope with different scanning speed. Column (a) shows diffusers with 100% power, (b) diffusers with 80% power and (c) diffusers with 60% power.

Simulated far field diffusion pattern and power meter measurements

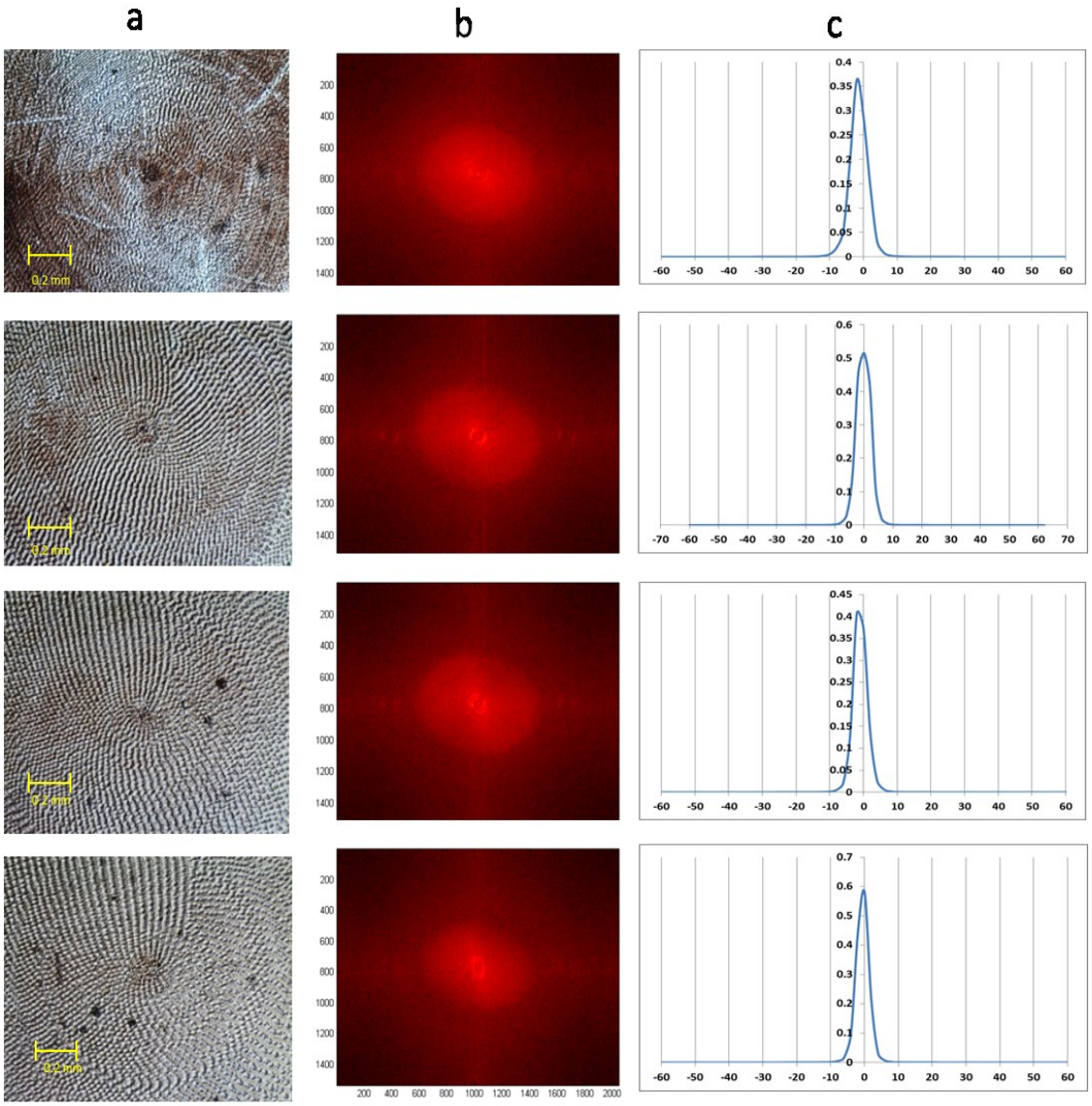

Figure S2. Column (a) shows microscope pictures for the diffusers manufactured with 100% power, (b) shows the simulated far-field diffusion patterns and (c) shows the power rate and the diffraction angle for the same diffusers.

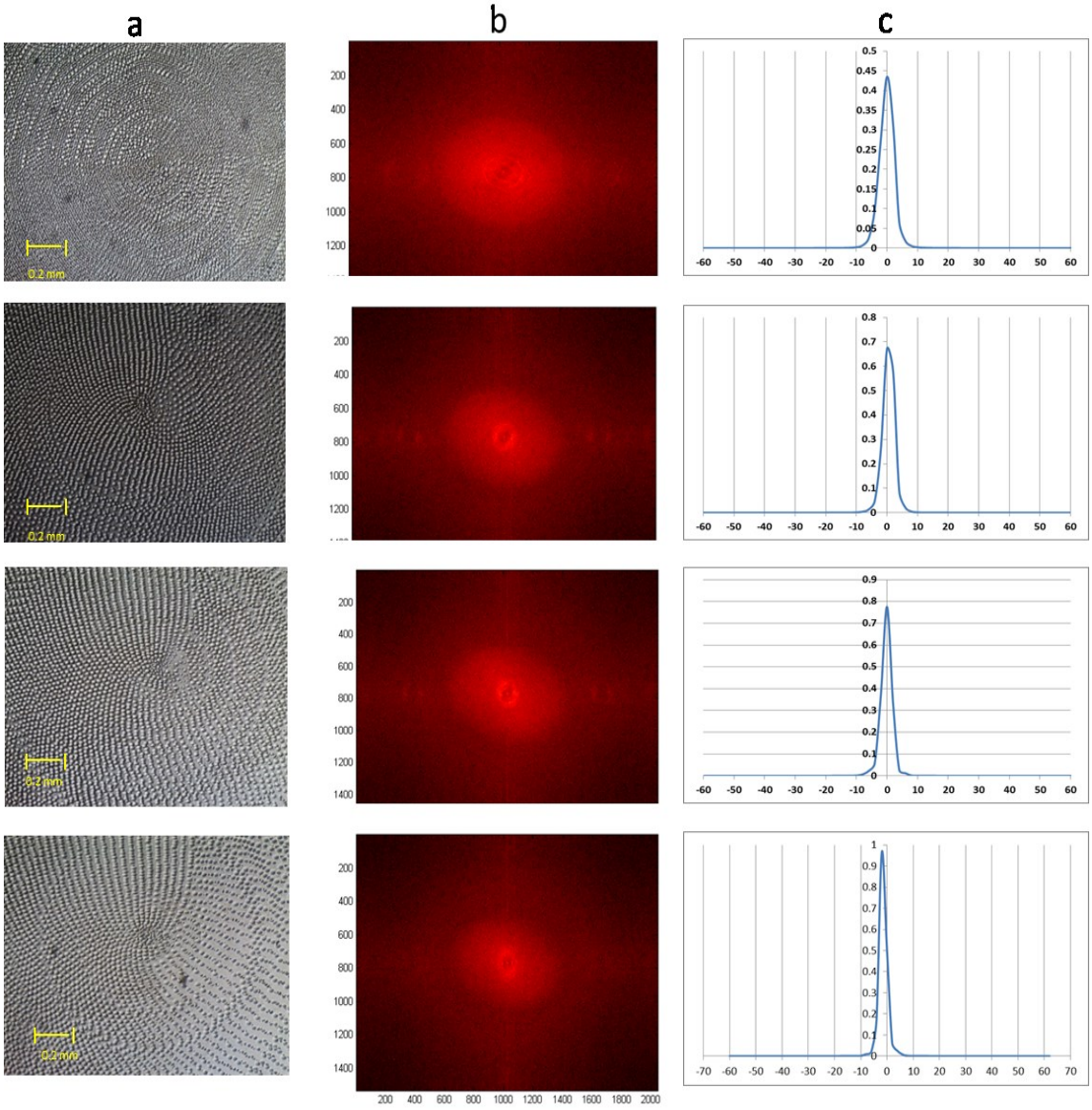

Figure S3. Column (a) shows microscope pictures for the diffusers manufactured with 80% power, (b) shows the simulated far-field diffusion patterns and (c) shows the power rate and the diffraction angle for the same diffusers.

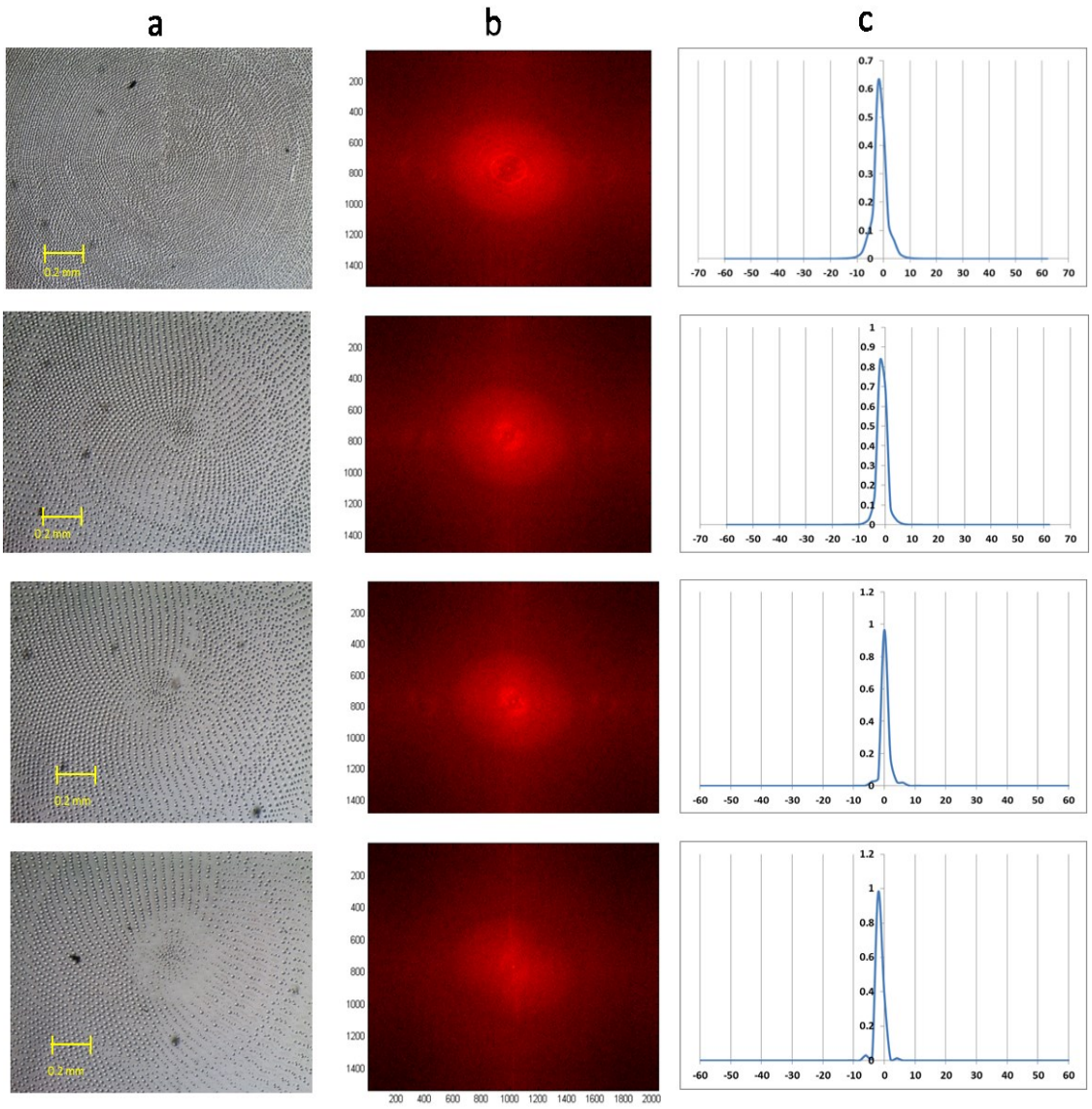

FigureS4. Column (a) shows microscope pictures for the diffusers manufactured with 60% power, (b) shows the simulated far-field diffusion patterns and (c) shows the power rate and the diffraction angle for the same diffusers.

Roughness measurements for all the samples

Table S1. *Average roughness for the circular pattern diffusers with various powers and scanning speeds.*

Sample power (%)	Sample scanning speed (mm/s)	Average roughness (µm)
100	200	1.976
100	800	1.64
100	1000	1.59
100	1400	1.546
80	200	1.659
80	800	1.614
80	1000	1.469
80	1400	1.412
60	200	1.156
60	800	0.805
60	1000	0.975
60	1400	-

Power measurements of all the samples

The first number represents the power used for producing the diffusers as number 1, 2 and 3 represent 100%, 80% and 60% respectively. However, the second number represents the scanning speed used for producing each diffuser as the numbers 1, 2, 3…. 7 represent 200, 400, 600 ….. 1400 (mm/s) scanning speed for manufacturing of the diffusers respectively.

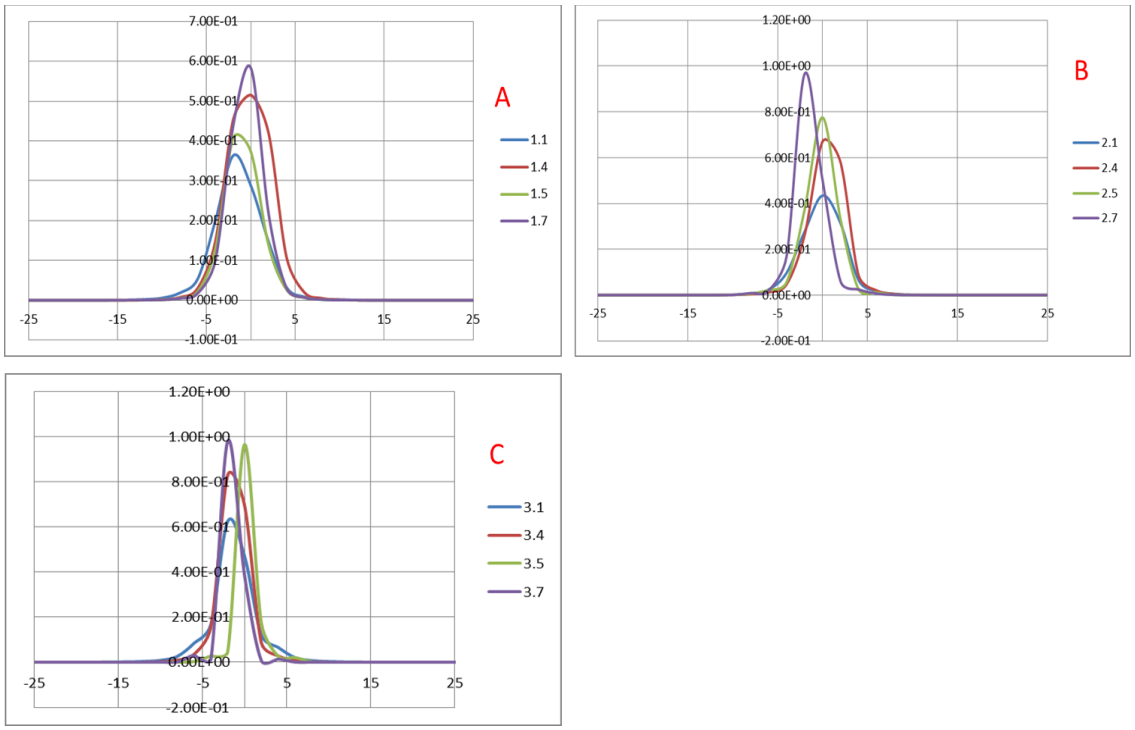

Figure S5. Comparison between the diffusers with different scanning speeds for the circular pattern diffusers, (a) 100% power, (b) 80% power and (c) 60% power.

Chapter 5: Laser Inscription of Pseudorandom Structures for Microphotonic Diffuser Applications

Published article

Tawfiq Alqurashi, Abdulla Alhosani, Mahmoud Dauleh, Ali K. Yetisen, and Haider Butt

Nanoscale, 2018,10, 7095-7107

In the previous chapters, the optical diffusers were fabricated by using femtosecond and nanosecond laser micromachining systems on a float glass. These machining systems have expensive laser sources; thus making a high production cost of optical diffusers compared to continuous wave CO_2 laser. Also, FS and ns laser micromachining produced different types of surface-relief microstructures due to the pulse duration changes and these fabricating surface microstructures have a direct influence on enhancing the optical performance of glass diffusers. Therefore, this chapter introduces the fabrication of optical diffusers on float glass by using CW CO2 laser which is highly economical laser system as compared to pulsed laser machining.

Author Contributions

T.A. conceived the experimental idea for fabrication of optical diffuser using CO_2 laser and T.A deigned the optical experimental setups and provided research direction under the supervision of H.B. A.A did FEM simulation and T.A fabricated the samples. T.A. wrote the first draft of the paper. All authors proofread the writing of the paper.

5.1 **Abstract**

Optical diffusers provide a solution for a variety of applications requiring a Gaussian intensity distribution including imaging systems, biomedical optics, and aerospace. Advances in laser ablation processes have allowed rapid production of efficient optical diffusers. Here, we demonstrate a novel technique to fabricate high-quality glass optical diffusers with cost-efficiency using a continuous CO_2 laser. Surface relief pseudorandom microstructures were patterned on both sides of the glass substrates. A numerical simulation of the temperature distribution showed that the CO_2 laser drills a 137 μm of deep hole in the glass for every 2 ms of processing time. The FFT simulation was utilized to design predictable optical diffusers. The pseudorandom microstructures were characterized with optical microscopy, Raman spectroscopy, and angle-resolved spectroscopy were used to assess the chemical properties, optical scattering, transmittance, and polarization response of the surface machined.

Increasing laser exposures and the number of diffusing surfaces enhanced the diffusion and homogenized the incident light. The resulting speckle pattern showed high contrast with a sharp bright spot free diffusion at the far field view range (250 mm). A model of glass surface peeling was also developed to prevent its occurrence during the fabrication process. The demonstrated method provides an economical approach in fabricating optical glass diffusers in a controlled and predictable manner. The optical diffusers produced have applications in fibre optics, LED systems, and spotlights.

5.2 **Introduction**

Optical diffusers are wavefront processors used to alter the intensity distribution of an incident light beam into a specified pattern [163, 164]. They are widely used in imaging systems, LED displays, and barcode scanners to provide a uniform light exposure and eliminate high-intensity spots [14, 61, 165-167]. Depending on the incorporated light scattering method, optical diffusers are classified as the volumetric or surface relief types [131]. Volumetric diffusers scatter the light *via* transparent microscopic beads and/or fillers trapped inside the surface that cause the light to diverge as it is transmitted through the material [10, 149]. However, this article focuses on the surface-relief type, which utilizes unique nano and microstructures on the diffuser surface to scatter light. The fabrication of these nano and microscale surface relief structures (*e.g.* pyramids, microlens arrays and textured rough surfaces) is a rapidly growing area of interest [32, 168, 169]. Surface relief structures are the most common diffusers due to simplicity and reliable processing time during fabrication as compared to volumetric diffusers.

Over the past decades, various fabrication methods including holographic recording [29], replica molding [169], ink printing [30], and surface texturing [131, 133] were utilized to produce microstructured diffuser surfaces. Advanced continuous wave (CW) CO_2 laser based systems rival the lasers used traditionally (e.g. Nd: YAG and femtosecond lasers) in the fabrication of optical diffusers [170]. Moreover, due to their relatively high efficiency compared to fiber laser, high average power [171], and low capital cost [39], CO_2 laser based systems are more economical in the fabrication of optical diffusers via laser inscription processes. In particular, CW CO_2 lasers are widely used in micromachining soda-lime silicate glasses due to the high radiation absorption of silicate glasses at a wavelength of 10.6 μm [172]. Additionally, the low thermal conductivity, heat treatability and relatively low cost makes soda-lime glasses the

common material for CO_2 laser processing [173]. Machining glass substrates using laser inscription processes can alter their physical properties [174], which may result in a modified surface wettability, conductivity, and optical properties [175-177].

Surface relief diffusers diverge the light emulating a negative lens; thus, their performance is usually characterized by the intensity of the light transmitted and its diffusion angle (α) [178]. The diffusion angle (α) is defined as the maximum exit angle of the light when it is passed through a diffusing material and it is determined by the Full Width at Half Maximum (FWHM) of the light intensity diffusion profile [131]. The optical performance, light homogenization level and efficiency of an engineering optical diffuser can vary depending on its diffusion angle [158]. Typical diffusion angles of glass-based optical diffusers range from 0.2° to 100° depending up on the required application [179]. Low diffusion angles (5°-25°) are particularly desirable in filament lamps and fluorescent lamps [22], where homogenizing the light without excessively diverging the beam is necessary to remove the hot spots and provide an even light distribution. On the other hand, optical diffusers with wider angles are already used to disperse light evenly across the screens of laptops, smartphones, and instrument panels [180, 181].

This research reports a novel technique in fabricating surface relief optical glass diffusers using a CW CO_2 laser. The fabrication method differs from the established conventional techniques, by coating the glass surface [30, 79, 128] as direct laser inscription of the glass substrates was performed without surface coating in the present work. Additionally, other polished optical diffusers had shown low FWHM scattering (20°). The presented technique provides a fast and economically viable approach in fabricating glass optical diffusers compare to femtosecond laser [182]. A numerical model was developed to simulate the laser ablation process on the soda-lime glass substrates. This study examines the effect of implementing different surface relief

micro structures and increasing the diffusing surfaces on the optical performance. The fabricated surface was characterized using optical microscopy and Raman spectroscopy to examine its structural morphology and chemical properties. The optical scattering and transmission efficiency of the produced diffusers were assessed using an angle-resolved intensity measurement setup and spectroscopic analysis. The glass surface peeling phenomenon [183, 184] was also examined and a prediction model was constructed.

5.3 **FEM Simulations of Laser Ablation on Glass Substrates**

To investigate surface morphologies produced on the soda-lime glass substrates due to CO_2 laser ablation processing, a numerical model was developed. Multiple studies have been conducted to simulate laser ablation processes; however, most of which focused mainly on simulating pulsed lasers. A 3D model has been developed to predict temperature distribution and material removal during nanosecond laser ablation of various materials [185]. Therefore, an analogous approach was adopted in this study for a continuous CO_2 laser. The Finite Element Analysis (FEA) method was utilized to simulate the model. This simulation demonstrates the effect of the laser intensity profile on the temperature distribution and the shape of the irradiated region. Given the increased complexity in modelling real life laser ablation problems, some assumptions were made to produce a feasible simulation without affecting the primary outcome of the study. These assumptions were: (i) The maximum temperature is developed on the surface of the model and there is no internal heating that could lead to an internal gas-filled void within the solid material. This limits the sublimation process to occur on the exposed layer of the material only. (ii) Once the material transitions into the gas

phase, its thermal significance vanishes. This excludes the necessity to model the thermal properties of the vaporized material around the heated surface.

Theoretical Model

Modelling the ablation process involved creating a model that governed temperature variations with time. Therefore, the conduction of transient energy-transport equation was used as the primary in domain heat transfer mode:

$$\rho C_p \frac{\partial T}{\partial t} + \nabla \cdot (-k\nabla T) = Q \qquad \text{(Equation 1)}$$

Where ρ is density, C_p is specific heat capacity, T is the temperature, t is time, k is thermal conductivity, and Q is heat flux. When an absorbing material is irradiated with a laser beam, the laser beam intensity begins to attenuate and its energy is transferred to the incident surface. However, the amount of energy transferred to the material depends on the laser wavelength, laser energy distribution profile, absorption coefficient of the material and its reflectivity [75, 186, 187]. This was implemented into the model in the form of an inward heat flux (Equation 2). Moreover, a Gaussian beam profile was defined for the CO_2 laser intensity distribution and it was applied to the model heating source using Equation (3).

$$Q = I \times \alpha \times (1 - R) \qquad \text{(Equation 2)}$$

$$I = 8 \times \frac{P}{\pi \times D^2} \times \exp\left(-8 \times \left(\frac{r}{D}\right)^2 \times \text{rm2}\left(t\left[\frac{1}{s}\right]\right)\right) \qquad \text{(Equation 3)}$$

where I is a function of the laser beam energy distribution, α is the absorption coefficient of the material, R is the reflectivity of the material, P is the laser power, r is

the laser spot radius, D is the laser spot diameter, and rm2(t[1/s]) is a smooth ramp function to begin with 0 power inlet. As the high intensity laser beam hits the material surface, its temperature rises and eventually exceeds the ablation temperature. Once the ablation temperature is reached, the incident energy on the surface is no longer used to raise its temperature, instead it forces the material to undergo a phase change from solid to gaseous state [188]. This phase transition results in a mass loss from the surface, which is governed by the material density and the heat of sublimation[189]. To model this element, the ablative heat flux boundary condition in Eq. 4 was used to set the temperature limit, while the deformed geometry feature used Eq. 5 to model the material removal:

$$q_a = h_a\left((T_a - T) \times \left(\frac{1}{k}\right)\right) \qquad \text{(Equation 4)}$$

$$v_a = \frac{q_a}{\rho \times H_s} \qquad \text{(Equation 5)}$$

Where q_a is the heat flux due to material ablation, T_a is the ablation temperature, v_a is the material ablation velocity, H_s is the heat of sublimation, $h_a = h_a(T)$ is a temperature-dependent heat transfer coefficient that is zero for $T < T_a$ and increases linearly as $T > T_a$, and $\frac{1}{k}$ is a growing specific heat capacity for $T > T_a$, to ensure that the material absorbs more energy at high temperatures to sublimate.

FEM Modelling

To start the simulation process, a geometry with a radius of 3 mm and a height of 4 mm was created to model the glass substrate in finite element method simulations. Eq. 1-5 were applied to the created geometry in the form of boundary conditions to model the laser ablation process. The dimensions and boundary conditions are described in Figure 1a-b. The inward and ablative heat flux boundary conditions

applied to the top surface represent the heat transfer from the laser source, while the thermal insulation boundary condition was employed in the bottom and lateral surfaces to limit the heat loss from the material body.

The laser properties, material properties and the ambient conditions were defined, as shown in supporting information Table 1. A uniform triangular mesh with a minimum element size of 1.2 μm was generated for the domain. To increase the accuracy of the model, an additional 0.3 μm mesh was created using the sizing function and applied to the top surface and along the geometry center line to capture the deformation due to material removal efficiently. The meshed geometry is shown in Figure 1b. The laser processing time was set to 2 ms and the model was solved.

Simulation results

At the initial stage of the laser ablation process, microscopic particles begin to fracture from the glass surface allowing the post ablation effects to take place on the surface. During the ablation process of glass, a roll of solidified melt called recast forms at the edges of the ablated structure due to the material being melted and ejected out of the surface [188]. Additionally, a debris layer is deposited around the structure due to the precipitation of the vaporized material. However, the simulation assumes direct sublimation process of the material. Therefore, the melting and precipitation effects are not accounted for in the simulation.

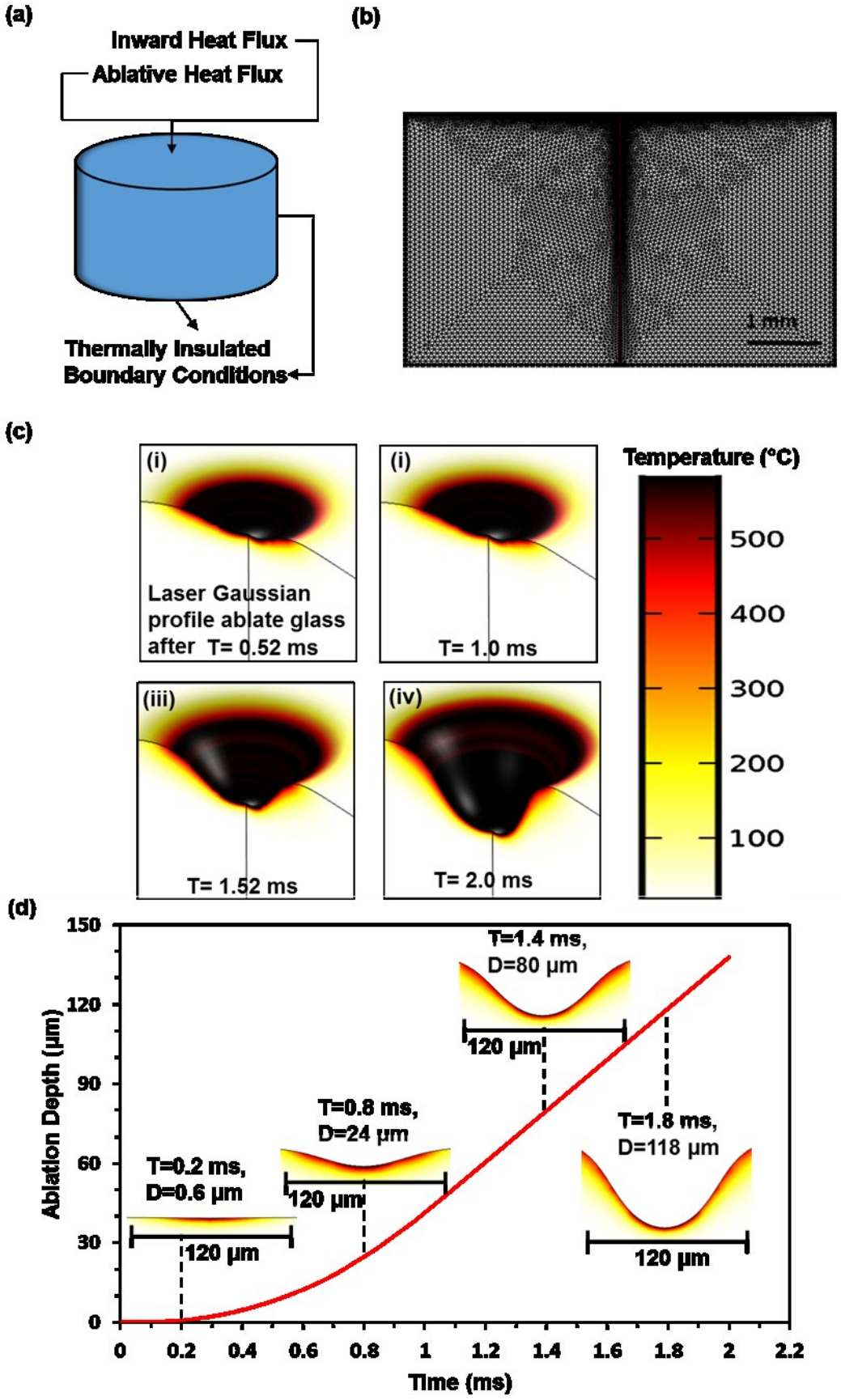

Figure 1. The simulated CO_2 laser ablation process of the soda lime glass. (a) The geometry created to simulate the glass substrate with the applied boundary conditions.

(b) The meshed geometry. (c) Temperature and 3D cavity profiles variations with time; (i) 0.52 ms, (ii) 1.0 ms, (iii) 1.52 ms, and (iv) 2.0 ms. (d) The ablation depth of the concavity as a function of the laser processing time.

Figure 1c shows the temperature distribution and the profile of the propagating concavity in the ablated region with time. The exposed glass layer experiences almost a constant temperature (590 ºC) at the point of laser beam focus, while the surface temperature cools down as the depth of the concavity increases. Figure 1(c-iv) shows the formed concavity profile when the material was ablated for 2 ms using a laser with a Gaussian intensity distribution. The Gaussian distribution intensity is concentrated in the center of the beam, thus, results in a non-uniform hole shape with the maximum depth in the center. Hence, CO_2 lasers are less efficient than pulsed laser at drilling holes of uniform sizes. Figure 1d shows the ablation depth against the laser exposure time. Increasing the laser processing time increased the material removal with a linear correlation. A concavity with a 137 μm depth formed on the glass surface after 0.2 ms processing time. Hence, laser ablation was a time dependent process, thus, by controlling the laser machining time, the depth and shape of the hole could be controlled.

5.4 **Experimental Section**

A CW CO_2 laser

The diffusers were fabricated by machining a surface relief pseudorandom microstructure on float glass slides (thickness ~1.1 mm). The patterns were implemented using a desktop laser setup (LS3040, HPC Laser Ltd, UK). The desktop setup utilizes a CW CO_2 laser as the heating source with a maximum power of 60 W and a wavelength (λ) of 10.6 μm. The laser features a adjustable optics head and

platform configuration, where the substrates are mounted on a z-axial translation stage and the laser head moves in the x-y horizontal axes. The laser operates at a maximum engraving speed of 1500 mm s^{-1} within a 420 × 300 mm work area. The laser beam focus on the glass surface is provided by a ZnSe lens (focal length ~28.1 mm and minimum spot diameter ~180 μm). Finally, the desired machining patterns can be imported from a computer-aided modelling software.

A high-resolution imaging camera

The speckle pattern was recorded using an AXIOCAM 105 color with a basic resolution of 5 megapixel and integrated with complementary metal-oxide-semiconductor (CMOS) sensor from Carl ZEISS Company. This camera was placed on holder and connected to an optical microscope and the microscope was connected to a computer to provide the speckled pattern image on screen.

5.5 Results and Discussion

Optical Diffuser Fabrication and Surface Characterization

Surface relief diffusers utilize a complex microstructure to perform their optical function. According to Huygens' principle [190], optical diffusers modify wavefronts by segmenting and redirecting the segments through the use of interference and phase control, which is mainly controlled by the microstructure on the surface. Hence, by controlling the microstructure, the angular distribution of the incident light in the far field can be controlled. Common surface relief diffusers have profiles with two or more surface levels. This can be achieved by overlapping laser exposures on the surface of the diffuser. Figure 2a shows a schematic of the CO_2 laser setup. In this experiment, three different surface patterns were employed during the fabrication stage to determine the effect of varying the microstructure on the optical characteristics. The

linear, gird and prismatic patterns are shown in Figure 2b. The grid structure incorporates overlapping laser exposures, where the surface was initially machined in the vertical direction, then left to cool down before machining it in the horizontal direction. The parallelogram pattern is similar to the grid pattern; however, the angle between the machining lines was reduced from 90° to 45°. Overlapping the laser inscription produced small pseudorandom, non-periodic microstructures superimposed on a large pseudorandom microstructure (Figure 2c). Figure 2d shows the profile of large microstructures; these have a large microstructure with a width of 35 μm and a depth of 20 μm. The large microstructure was superimposed with a small microstructure (Figure 2f) within a range of 1.5 to 2.5 μm in width and 50 to 200 nm in height (figure 2g, h). These large area (5×5 mm) non-periodic microstructures (figure 2i) cause the diffusion of light by randomizing the reflection of collimated incident laser beams [181].

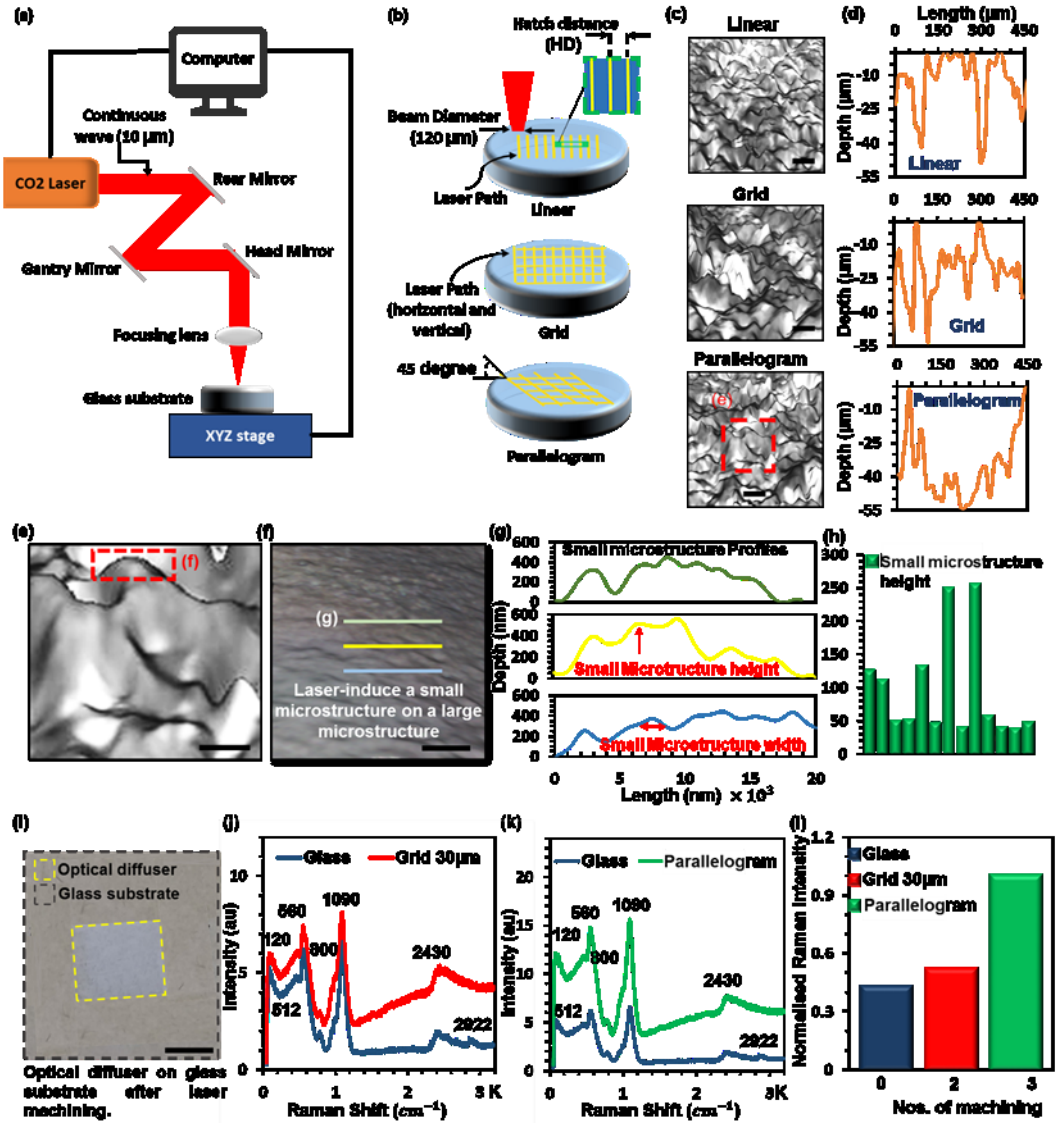

Figure 2. The CO2 laser inscription of optical diffusers. (a) A schematic of the CO_2 laser setup utilized to fabricate the glass diffusers. (b) A schematic of the different surface designs fabricated as linear, grid and parallelogram patterns. (c) The 3D optical microscope images of large pseudorandom microstructures on float glass substrate (Scale bar 100 μm) and (d) their profile. (e) Magnified image of the red square shown in (c). (f) A 3D optical microscope image of a small microstructure superimposed on a large microstructure. (g) The profile of a small microstructure from three different parallel linear positions. (h) The depth distribution of small microstructures. (i) Photograph of optical diffuser based on pseudorandom microstructure in a large area (Scale bar 2.5 mm). (j-l) The Raman spectra of soda lime glass; unmodified and CW

CO_2 laser patterned glass. (l) The normalized Raman intensity differences between unmodified and patterned glass.

Prior to implementing the surface micropatterns on the float glass substrates, optimal laser operating parameters were specified. The specification of the laser parameters were determined for achieving optimum optical performance: a beam power of 24 W, a scanning speed of 300 mm s^{-1} and a hatch distance of 10 μm (Supporting Information Figure S1). However, in the case of the surface relief profiles that require overlapping laser inscriptions, the hatch distance was doubled to prevent surface peeling of glass and heterogeneous surface morphology. Throughout the fabrication stage, the peeling of the glass surface was a limiting factor in employing the desired laser parameters and it was eliminated by using an experimental prediction model (Supporting Information Figure S2) machined by a CO_2 laser.

Initially, the optical diffusers were fabricated by machining the linear, grid and parallelogram microstructures on one side of the float glass substrate. Surface relief profiles were also produced on both sides of the diffuser slide samples. Incorporating two or more diffusing surfaces can alter the diffusion characteristics of the microphotonic devices. As the incident light hits the first diffuse surface, the collimated light beams are scattered off the surface at different angles. This leads to beam scattering with small angles to force and propagate light through the material. Thus, employing a second diffuser surface on the other side of the substrate, can further spread out the light beam propagating through the material; hence, altering the homogeneity and the diffusion efficiency of the glass substrates.

Here, CW CO_2 laser inscription was utilized to produce variety of optical diffusers by using different laser parameters (Table 1). After each process, the reflecting mirrors of the laser system were cleaned to maintain a high accuracy of the laser inscription.

The microstructures of the samples produced were imaged using optical microscopy (Supporting Information Figure S3). A maximum of 2 minute and 4 minute processing time was needed to produce the one-sided and double diffusers, respectively. Alternative fabrication methods (*e.g.* rolling) have higher production rates for fabricating polyester and polycarbonate diffuser sheets; however cannot be used to fabricate glass diffusers.

Table 1. List of the fabricated samples including the structure implemented on the surface of diffusers and the laser parameters in fabrication. Power was 24 W and beam speed was 300 mm.s^{-1}.

Sample	Pattern	Diffuser Surface side	HD (μm)
S1	Linear	Single	10
S2	Grid	Single	20
S3	Grid	Single	30
S4	Parallelogram	Single	20
S5	Linear	Double	10
S6	Grid	Double	20
S7	Grid	Double	30
S8	Parallelogram	Double	20

Furthermore, Raman spectra of laser modified soda lime glass slide (optical diffuser) alongside unmodified soda lime glass slide were recorded at a 50× objective with a 532 nm laser. Soda lime glass is a non-crystalline form of sodium oxide (soda) and calcium oxide (lime). The intense bands observed for modified and unmodified soda lime glass can be attributed to bending of silicone bridging oxygen at 480 cm, symmetric stretching of bridging oxygen at 630-740 cm, symmetric stretching with a different number of non-bridging oxygen at 850-1050 cm and symmetric stretching of bridging oxygen at 1100 cm. The weak band at 2350 cm has been attributed to Si-OH groups involved in intratetrahedral hydrogen bonding across an edge of the SiO_4 tetrahedron [191-193].

The Raman spectra measured in soda lime glass (unmodified surface), 30 μm grid and parallelogram optical diffuser (modified surface) have six bands at 120, 512, 560, 800, 1090 and 2430 cm^{-1} except the unmodified glass has one more band at 2922 cm^{-1} (Figure 1j,k). The Raman spectrum of the modified and unmodified glass slides recorded have prominent and intense bands around 120, 560, 1090 and 2430 cm^{-1} with weak shoulder bands at 512. Additionally, two weak intense bands appear at 512 and 800 cm^{-1} and a weak hump around 2922 cm^{-1}. The peak at 2922 cm^{-1} disappears on modified glass. However, the intensity of bands at 512 and 800 cm^{-1} are higher when compared with the Raman spectrum of unmodified soda lime glass and the intensity increased with repeated machining cycles. This is due to fundamental vibration of soda lime glass after laser processing. It has been reported that the Raman intensity was increased by either increasing the heat treatment temperature or achieved by huge pressure modelling in glass [194, 195].

Optical Characterization of Microphotonic Diffusers

The optical performance of the glass-based optical diffusers were determined using an angular light distribution measurement setup including a digital camera and a spectrophotometer. The angle-resolved measurement setup was used to determine the light diffusion intensity profiles of the glass diffusers. Figure 3a,b shows the setup consisting of a laser pointer, a microphotonic diffuser and an optical detector to measure scattered light intensity at various angles. The laser pointer and the diffuser were mounted on a 360° continuous rotation stage with a stepper motor actuator controlled by a computer. This setup allows operating parameters to be set. The confined rotation of the light source and the sample ensures that the incident light remains normal to the diffuser surface. The stage was rotated from (+90°) to the incident normal (0°) and the photometer recorded the intensity of the diffused light at

2° rotation increments to characterize the diffuser beam shape, including its diffusion angle, FWHM of diffusion angle and intensity profile. This setup was calibrated after every rotation to ensure the high reliability of the measurements.

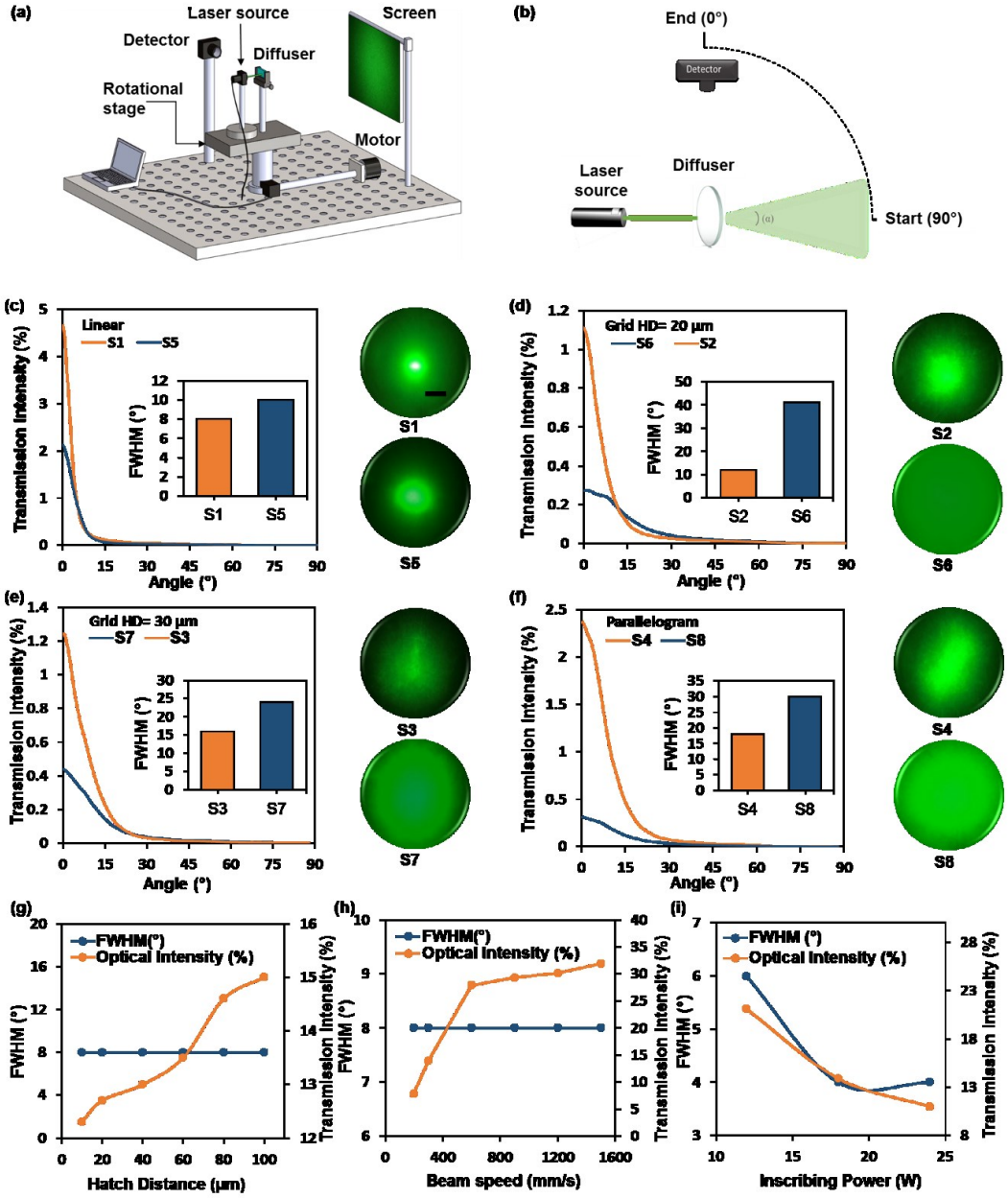

Figure 3. (a) A schematic of the angle-resolved measurement setup utilized to measure the diffusion angle of the fabricated device, (laser-to-diffuser=2 cm) and (laser-to-detector=19 cm). (b) A diagram showing the top view of the angle-resolved

measurement setup, indicating the start and end points of the measurement cycle. (c-i) The angular diffusion measurements of the fabricated samples with their diffusion patterns when illuminated with a green laser pointer (λ=532 nm). The comparison of the one sided and the double-sided diffusers for the each pattern is shown on (c) linear patterns, (d) grid patterns (HD=20 μm), (e) grid patterns (HD=30 μm), (f) parallelogram patterns. Scale bar= 3 cm. The distance from the digital camera to the projection screen was 16 cm. (g-i) The effect of changing the laser processing parameter on its FWHM of diffusion angles and transmission at normal incidence, (g) hatch distance, (h) laser speed and (i) power.

Figure 3c-f shows the light intensity profiles and the scattering patterns of the fabricated diffusers when illuminated with a green laser pointer (λ=532 nm). The diffused light profiles exhibited a Gaussian illumination distribution, which indicated that the light diffusion was caused by variations in surface topography features [31]. The diffusion characteristics were compared between one-sided and double-sided diffusers with the same patterns. As expected, two-sided diffusers displayed greater diffusion angles, their capabilities to diffuse light were almost twice that of those of the one-sided diffusers. The FWHM of diffusion angles ranged from 8° to 41°, where the smallest angles were recorded for the linear surface pattern while the grid and parallelogram patterns displayed higher diffusion angles. The highest diffusion angles obtained were 41°, 30° and 24° with peak transmission intensities of ~29%, ~39% and ~42% for samples S6, S8 and S7 respectively. The variations in the thickness of the glass layers caused the energy of the particles to be dependent on their in-plane location in the layer; thus, resulting in a roughness-dependent light scattering profile which shows the importance of the design of the structure embedded on the surface [196].

A collimated green laser beam was used to illuminate the diffuser surfaces and their scattering patterns in the far field were captured off a projection screen using a

digital camera. Figure 3c shows that the linear one-sided diffuser (S1) displayed higher intensity density at the 0^{th} order as compared to the double-sided diffuser (S5), which showed slightly wider diffusion in the center. However, the intensity at the 0^{th} order for the linear surface relief diffuser was high. On the other hand, the one-sided diffusers S2, S3 and S4 fabricated using the overlapping grid and parallelogram micropatterns displayed relatively high diffusion angles but with a non-homogenous illumination, resulting in different areas receiving more/less light intensity. Furthermore, the double-sided grid and parallelogram microstructures (S6, S7 and S8) showed the most efficient diffraction patterns with an even intensity distribution and high diffusion homogeneity across the illuminated surface. Light homogenization and high diffusion angles are critical factors in determining the efficiency of optical diffusers. Therefore, the proposed method of producing overlapping grid and parallelogram patterns on two sides of the glass substrates have potential in fabricating high-quality optical diffusers.

To visualize the effect of varying the wavelengths on the distribution of the diffused light, a setup (Figure 4a) was used to capture off the scattering image projected on screen. The diffusion profile depends strongly on the wavelength or frequency of the transmitted light. Therefore, samples S6, S7 and S8 that displayed the highest diffusion angles were analysed against varying laser sources (λ_1=450 nm, λ_2=533 nm, λ_3=633 nm). The diffusion plots of the samples with their respective diffusion patterns are shown in Figure 4b-d. The highest FWHM of diffusion angle was 40° in response to the blue laser for the grid micropattern S6, where the diffuser displayed a lower intensity (~16%) at the 0^{th} order (Figure 4b). Furthermore, the correlation between the diffusion angle and the transmitted light wavelengths was ambiguous as the optical diffusers showed higher diffusion angles at the shortest and longest wavelengths (λ_1=450 nm & λ_3=633 nm), while the moderate light wavelength (λ_2=532 nm) displayed the lowest diffusion angles.

The double sided grid and parallelogram micropatterns (S6, S7 and S8) were illuminated with three different collimated laser sources and the observed light scattering patterns were captured using a white globe. A semi-transparent spherical globe was utilized due to its capability to provide the visual representation of wide scattering patterns. Figure 4b-d shows the different diffusion patterns produced. Almost all the diffusers reacted to varying the wavelengths in a similar manner, thus, further comparisons were conducted on the patterns produced by the blue, green, and red laser beams. The optical diffusion field of view increased from ~172° for the green laser to ~177° for the blue and red lasers.

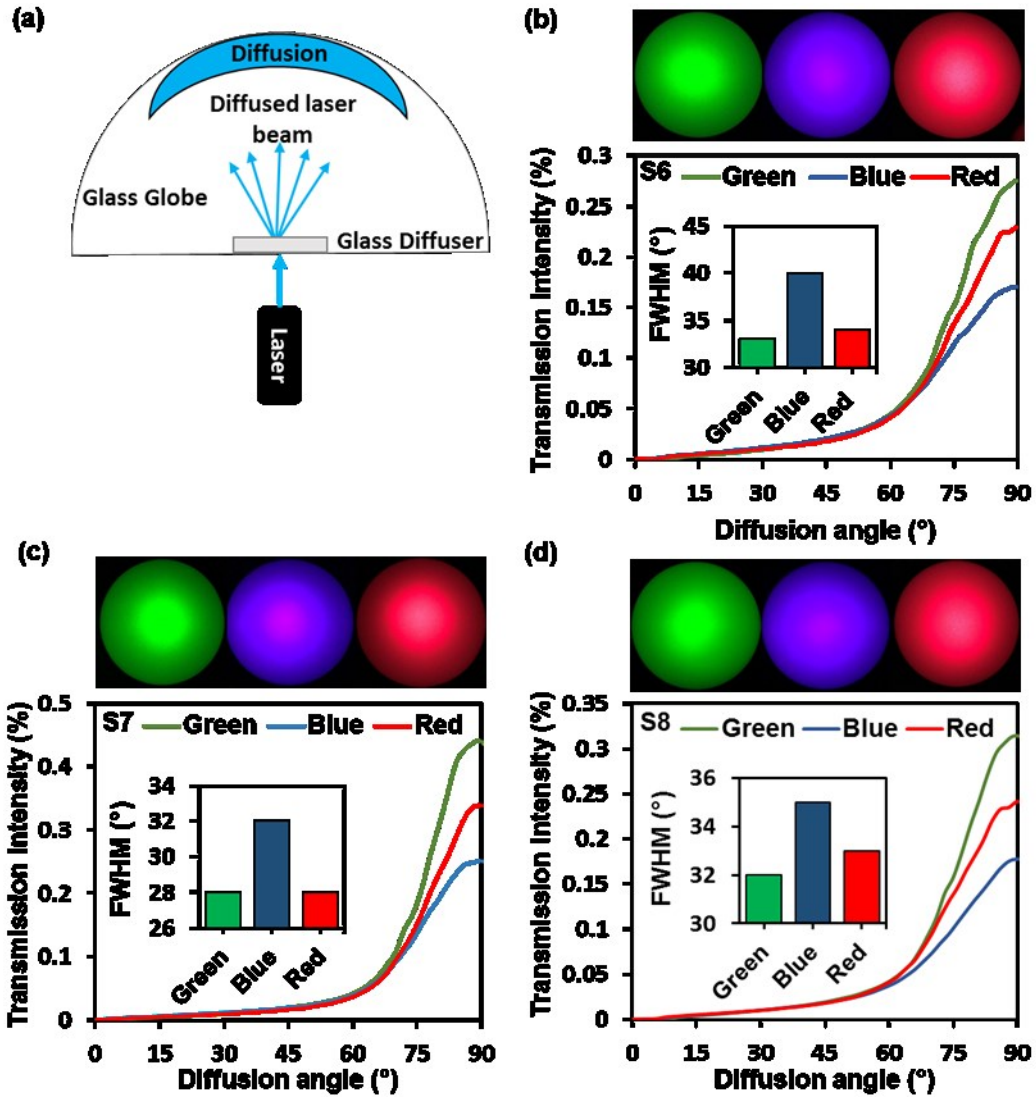

Figure 4. Light scattering from optical diffusers. (a) Schematic setup for recording 3D diffusion pattern. (b-d) Diffusion plots of the double-sided surface relief devices analyzed using different wavelengths (λ1= 450 nm, λ2=533 nm, λ3=633 nm), with their respective diffraction patterns captured using a circular semi-transparent white globe. (a) Grid (HD= 20 μm), (b) grid (HD= 30 μm), and (c) parallelogram patterns. Scale bar = 6 cm.

A Fast Fourier Transform (FFT) simulation [17, 197] and a 2D/2.5D speckle imaging experiment were performed to assess the relationship between the pseudorandom microstructures and light scattering from optical diffusers. The

difference between the simulation and the experimental results were used to determine the homogeneity of light diffusion. The FFT simulation was employed to predict the optical characteristics of the diffusers (Figure 5b, c). These simulations were analyzed based on optical images taken from normal incidence at transmission mode (Figure 5a). The simulated image produced speckles with a wide range of bright regions in the centre of image and the bright region reduced with increasing of the dark region toward to the edge. At the zero order, the light scattering area increased for the parallelogram pattern diffuser compared to the grid diffuser. The intensity profile revealed that the intensity profile of parallelogram pattern diffuser was a smooth as compared to the grid patterned diffuser.

The 2D/2.5D speckle imaging was conducted experimentally to analyze the speckle/diffusion pattern. In a polarization experiment, the sample was mounted on a holder and the diffuser was placed between linear polarizer and analyzer to make the laser linearly polarized and to adjust analyzer at 5°, 45° and 90° from the normal. Collimated laser sources (450, 533 and 633 nm) were located on one side and a high-resolution imaging camera with a complementary metal-oxide-semiconductor (CMOS) sensor was placed on the opposite side of the optical diffuser. This allowed photons to propagate through the diffuser to be captured as a 2D high-resolution image via the CMOS sensor. The 2D recorded image was used to reconstruct a 2.5D image (intensity profile) using optical image processing.

The diffuser (HD=30 μm) generated speckle patterns preserved the linear polarization of the laser beam incident normally to the plane of the horizontal polarizer (0°) but the image was recorded at an angle of 5° with respect to the surface plane due to low light intensity (Figure 5d). Thus, the diffusion pattern can be controlled by modifying the polarization orientation.

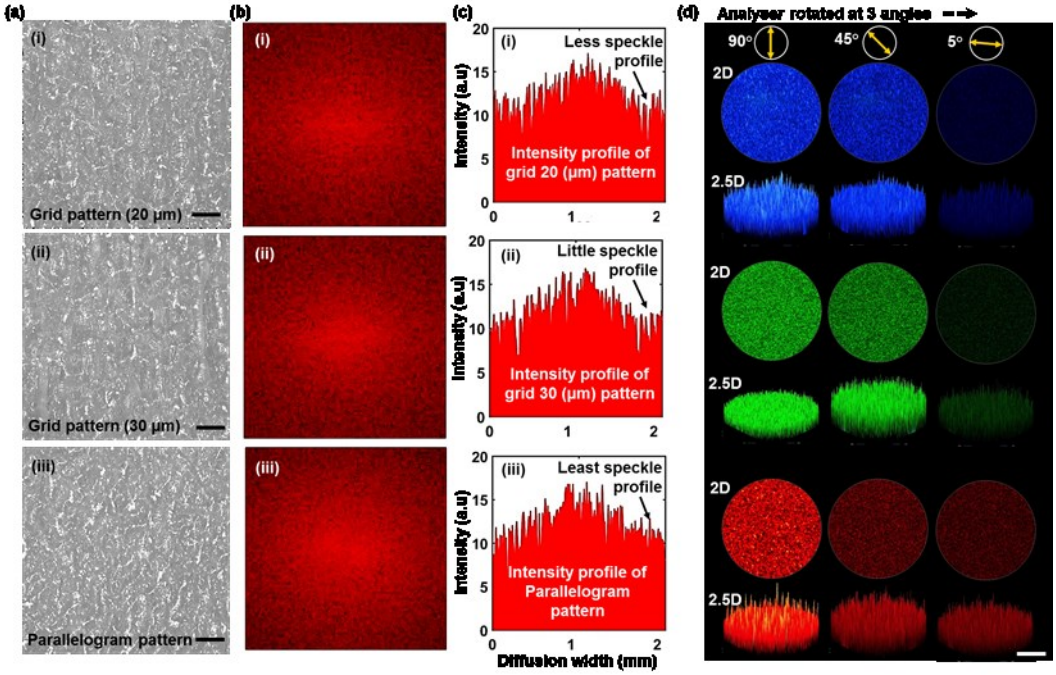

Figure 5. The FFT simulations and the recorded images of speckle patterns. (a) Optical microscope image of the 2D structure of diffuser. Scale bar = 20 μm. (b) The predicted FFT simulation image of diffusion or speckle pattern, and (c) their profile intensity for different optical diffusers; (i) grid pattern (HD= 20 μm), (ii) grid pattern (HD= 30 μm), and (iii) parallelogram pattern. (d-f) The laser illumination of the diffuser and speckle pattern of formation recorded with a digital camera integrated with a CMOS sensor. (d) The speckle patterns recorded at varying analyzer rotations (90°, 45° and 5°) for grid pattern (HD= 30 μm) diffuser at different spectrum ranges (450, 532 and 633 nm). Scale bar = 2 mm.

Three optical diffusers with different fabrication patterns produced speckle intensity distributions in the far field upon illumination with monochromatic light (Figure 6a). The speckled patterns consisted of highly-intense spots and bright and dark regions over an area with 5 mm in diameter. In general, the sharp bright spots increased slightly from the parallelogram diffuser to grid (HD=30 μm) diffuser. Additionally, the speckle pattern was studied at different projection lengths. Over 90%

of highly-intense spots were reduced by increasing the projection length from 15 to 25 cm. This provides sufficiently high contrast with sharp bright spot free condition at long far field view range. Supporting Information Figure S4 provides additional speckle pattern images of other diffusers. This optical diffuser can be utilized as part of an imaging device, in which scattered light can be used for image reconstruction [198, 199].

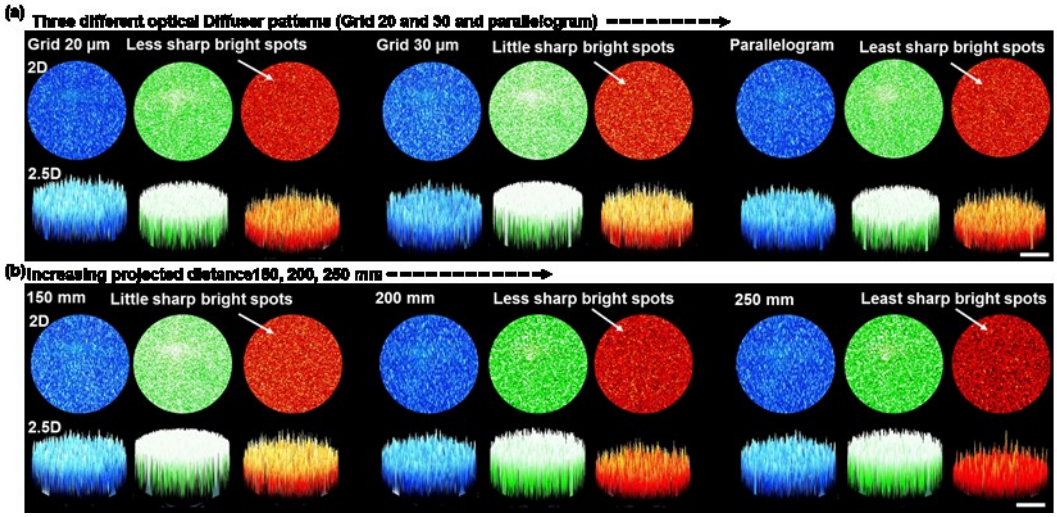

Figure 6. *(a) The speckle pattern imaged for the grid pattern (HD= 20 µm), grid pattern (HD= 30 µm), and (3) parallelogram pattern diffusers. Scale bar = 2 mm. (b) The projected pattern of the grid pattern (HD= 30 µm) diffuser recorded at varying lengths (15, 20 and 25 cm). Scale bar = 2 mm.*

Broadband light transmittance was utilized to assess the performance of the fabricated optical diffusers. A typical soda lime glass substrate with a thickness of 2 mm has a transmittance of ~90% across the visible spectrum. The spectral transmittance measurement setup consisted of a broadband light and a spectrometer (2 nm resolution) connected to an optical microscope via an optic fiber. For transmitted light polarization measurement, the experimental setup had a linear polarizer and

analyser, which were underneath and above the optical diffuser, respectively. This ensured a linearly polarized light before it passed through the diffuser and to control and modify the polarization direction and to measure its effect on transmittance measurement. Figure 6a shows a schematic of the spectral transmittance measurement setup integrated with two polarizers.

Figure 7b-i shows the transmittance of the fabricated diffusers as a function of the incident wavelength (450-700 nm). The results indicated that one-sided diffusers were more efficient in transmitting visible light than double sided diffusers. The parallelogram diffuser (S4) showed the highest transmission (~50%), thus, the parallelogram structure was considered to be the most efficient one-sided structure as it also revealed the highest diffusion angle (18°) for one-sided diffusers (Figure 3d). The spectral transmittance of diffusers S6, S7 and S8 showed the highest diffusion angles of ~25%, ~35% and ~28% respectively. Hence, it was observed from the grid samples S6 (HD= 20 μm) and S7 (HD= 30 μm) that increasing the hatch distance increases the transmittance of the diffuser but results in a lower diffusion angle. It can be deduced that the double-sided diffuser fabrication technique negatively influenced the transmittance of the optical diffuser. This is attributed to the increase in the number of diffusing surfaces, thus, having additional microsurface features that can further scatter the incident light. However, the use of an additional anti-reflective coating on the surface of the diffusers can improve the transmittance of the diffusers by reducing the reflection from the diffusion surfaces.

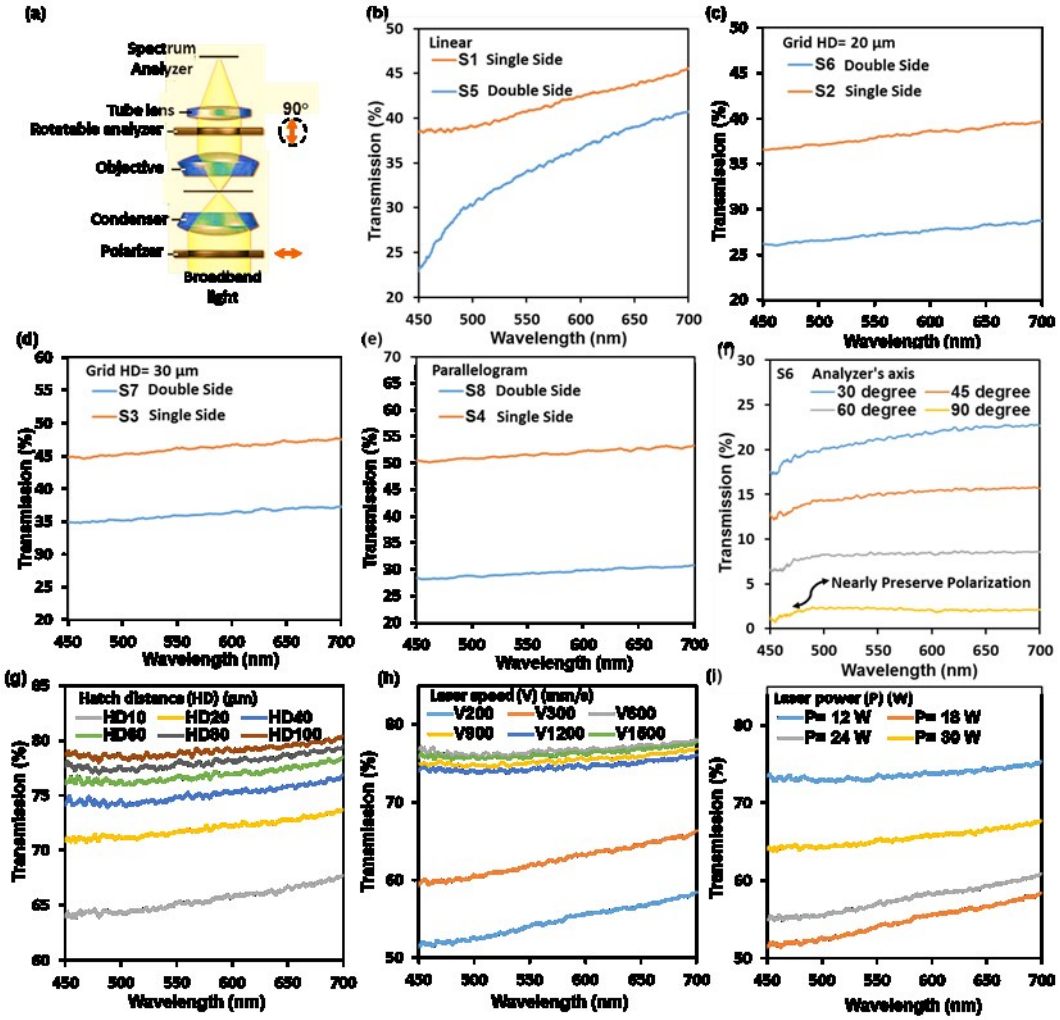

Figure 7. *Broadband light and polarization characterization of the optical diffusers. (a) A schematic of spectroscopy setup. Measurements of the optical diffusers using broadband light illumination at normal incidence with transmission mode for (b) linear patterns, (c) grid patterns (HD=20 µm), (d) grid patterns (HD=30 µm), (e) parallelogram patterns, and different laser parameters with varying (g) hatch distance (h) laser speed, and (i) laser power.*

Glass Surface Peeling

Surface peeling is defined as the continuous removal of a thin layer from the surface of an ablated material [183, 184]. The removed layer is usually of a constant thickness. Applications of glass surface peeling include improving the surface finish of

laser cut glass products and forming microchannels on glass substrates for optofluidic devices[200]. Laser cutting of glass substrates induces the formation of defects on the cutting edges which act as starting point for cracks to propagate through the material[184]. Thus, peeling off the cutting-edge layer that contains these defects can strengthen the material and create a defect free surface [36] causing nonhomogeneous scattering. For this reason, a model of glass surface peeling was developed to prevent its occurrence during the fabrication process. Glass surface peeling is a function of the energy deposition rate on the surface, which in turn depends on the input laser power and scanning speed [183]. When the ratio of the two parameters results in an energy deposition rate in the range of 3.0-6.0 $\times 10^4$ $W.m^{-2}$, the temperature inside the material exceeds the strain point and reaches the softening point of the glass, where a thin layer starts to separate from the surface. Figure 8a shows a glass substrate experiencing surface peeling. The formed microstructure on the surface of the glass due to surface peeling indicates that multiple microchannels with varying lengths are engraved on the substrate (Figure 8b). In Figure 8c, a strip was peeled off the diffuser surface, showing material removal from the surface of the diffuser in the peeled region.

Throughout the experiments, glass surface peeling was a key factor in determining the optimum laser operating parameters to avoid it during fabrication of optical diffusers. During the fabrication stage, the samples that experienced surface peeling were discarded from the experiment and considered to be in-viable optical diffusers. Therefore, it was essential to develop a glass surface peeling prediction model based on experimental data. Figure 8a shows a schematic of the surface peeling process with the adopted texturing pattern (linear pattern). A hatching distance of 10 μm was implemented within the texturing pattern to authenticate the prediction model with the parameters employed in the fabrication stage.

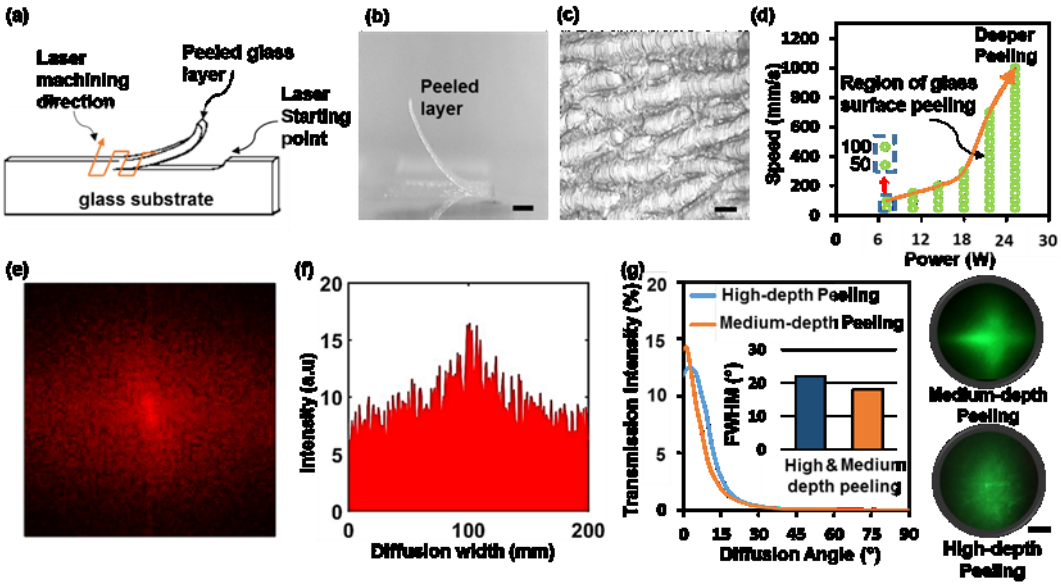

Figure 8. Glass surface peeling. (a) A schematic of the surface peeling process. (b) Image of a peeled glass surface layer produced at (P=30 W, V=200 mm s^{-1}, HD=10 µm). Scale bar= 100 µm (c) Microscopic image (5×) of the microstructure of the sample shown in (b). Scale bar= 200 µm. (d) A prediction model of CO_2 laser induced glass surface peeling. (e) FFT simulation of the peeled glass structure to reconstruct the intensity profile (f) and the diffusion pattern. (g) The diffusion properties of two surface peeled samples, high-depth peeling sample processed at (P=42 W, V=100 mm s^{-1}, HD=10 µm) and medium-depth peeling sample processed at (P=12 W, V=50 mm s^{-1}, HD=10 µm). Scale bar= 3 cm.

Figure 8d shows the experimental prediction model of glass surface peeling for a CW CO_2 laser. The graph indicates that the ratio of the laser power and speed must fall outside the arrow produced in Figure 6d to avoid glass surface peeling. At low laser powers (12-30 W), it is necessary to maintain a linear relationship between the two parameters to prevent the induction of glass layer peeling, while at higher laser powers (+30 W) the speed must be doubled. This is due to the high material removal rate from

the surface at high laser powers. Figure 8g shows the diffusion plots of two glass slides that exhibited surface peeling with their respective scattering patterns. The high-depth peeling sample (P=42 W, V=100 mm s-1, HD=10 µm) experienced material removal, which resulted in a thicker layer being peeled from the surface. The peeled layer was detached from the glass surface and its optical diffusion properties were measured. A diffusion angle of 22° was obtained for the high-depth peeling sample. The sample produced a heterogeneous diffusion pattern with reduced intensity at the 0^{th} order when the surface was illuminated with a green laser beam. By contrast, the medium-depth peeling sample (P=12 W, V=50 mm s-1, HD=10 µm) that exhibited a thin layer removal from the surface showed a lower diffusion angle (17°) with a defined transmission peak intensity ~1.4%. The sample also displayed a random cross shaped diffusion pattern. The obtained diffusion characteristics of the peeled samples indicate that they are in-viable to be used as efficient optical diffusers. Moreover, the most popular method is that of the holographic diffuser, which relies on surface structure of various shapes to spread out light. This method falls short due to the finer structures, which they are easier to be get damaged chemically or mechanically.

5.6 **Conclusion**

The work demonstrated the viability of producing glass based optical diffusers using direct CO_2 laser writing. The proposed approach of fabricating overlapping surface relief structures on both sides of the glass substrates was successful and its direct influence on enhancing the optical performance of glass diffusers was measured. The characteristics of diffusers fabricated using this method can be altered by changing the microstructures including linear, grid and parallelogram patterns. This novel technique provides a fast and economically viable approach in a massive

fabrication of the optical diffuser. The diffusion measurements showed that structures with overlapping laser exposures were efficient diffusers. Increasing the number of diffuser surfaces resulted in wider scattering patterns and increased homogeneity. The highest diffusion angles were recorded for the two-sided grid diffuser with (HD=20 μm) to be 40°, 33° and 34° in response to wavelengths of 450, 633 and 532 nm, respectively. The broadband light transmission of the fabricated samples decreased when the structures were patterned on both sides. The parallelogram structure displayed the highest (~50%) broadband light transmission across the visible range. A prediction model of glass surface peeling induced by CW CO_2 laser was constructed to see how it affected the diffusion of light. The diffusion characteristics of the peeled samples were determined and its negative impact on the diffuser performance was determined. The laser ablation process on the glass substrates was simulated to create a model, which displayed the temperature variations on the ablated region together with the material removal rate. The Gaussian profile of the laser intensity distribution resulted in a non-uniform concavity forming on the surface of the material with a maximum depth of 0.5 mm in the center, after 2 ms ablation time. The conducted experiments demonstrated a rapid and accurate fabrication method of high-quality glass diffusers that can serve multiple optical functions. Future studies to enhance the optical performance of the fabricated diffusers can involve additive surface coatings or implementing this approach in materials with higher light transmittance capabilities.

5.7 **Supporting Information**

Laser inscription of pseudorandom Microstructures for Microphotonic Diffuser Applications

*Tawfiq Alqurashi[a, b, *], Abdullah Alhosani[a], Mahmoud Dauleh[a], Ali K. Yetisen[c], and Haider Butt[a,*]*

[a]School of Mechanical Engineering, University of Birmingham, Birmingham, B15 2TT, UK

[b]Department of Mechanical Engineering, School of Engineering, Shaqra University, Dawadmi, P.O. Box 90 Zip Code 11921, Saudi Arabia

[c]Harvard-MIT Division of Health Sciences and Technology, Harvard University and Massachusetts Institute of Technology, Cambridge, MA, 02139, USA

Optical diffuser fabricated with continues CO2 laser, differ from other texture sources [131, 133], has provided more data on this supplementary.

Table S1. The global parameters used in FEM to carry out the CO2 laser simulation with their respective values.

Parameter	Value
Radius of the substrate	0.003 m
Height of the substrate	0.004 m
Total time of simulation	0.002 s
Ablation temperature	837.15 K
Density	2530 kg/m³
Specific heat	750 J/(kg·K)
Thermal conductivity	1.12 W/(m·K)
Power of beam	24 W
Laser beam spot	2E−4 m

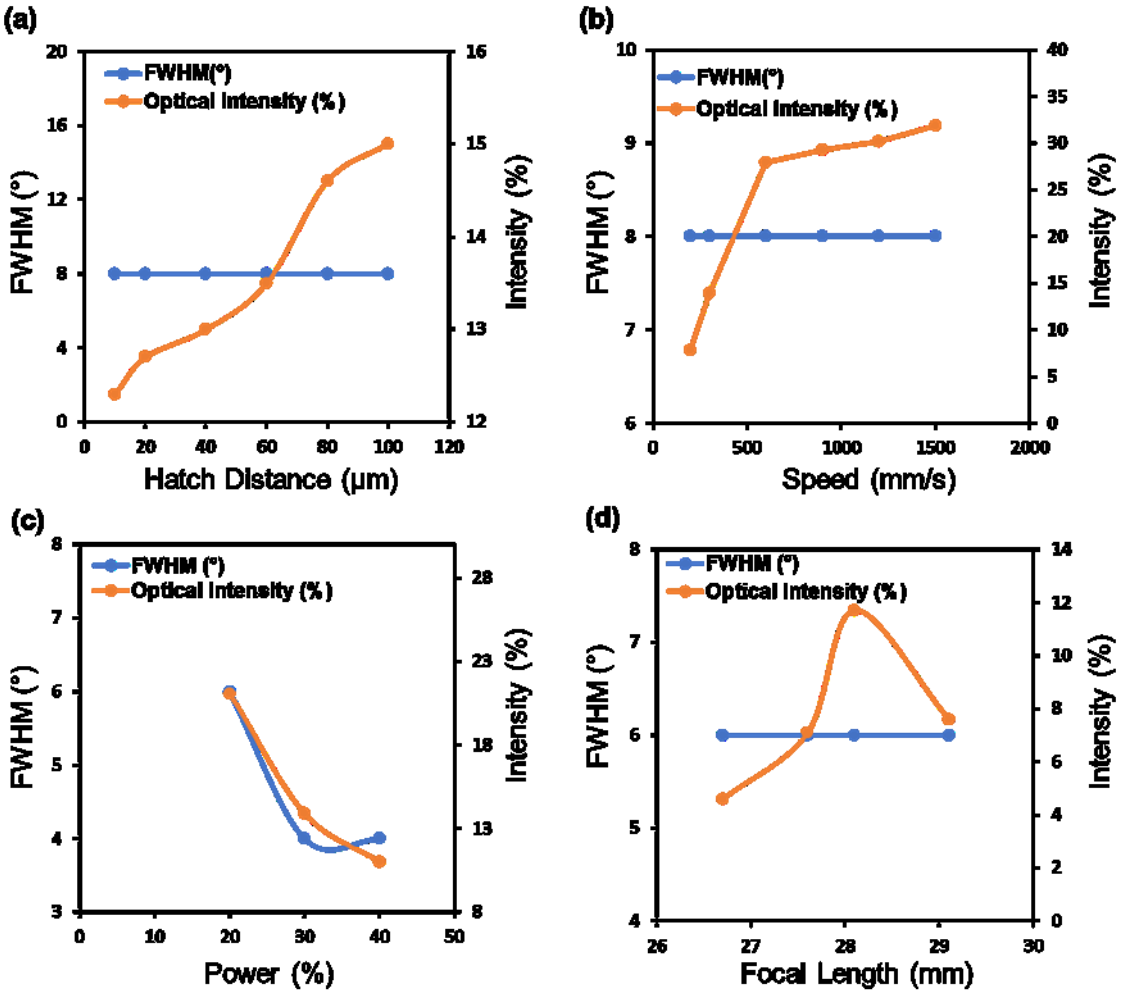

Figure S1. *Graphs showing the effect of changing the different laser parameters on the diffusion angle (FWHM) and the optical intensity of the transmitted light, one parameter was altered while fixing the other parameters for each experiment. (a) Hatch Distance (μm). (b) Scanning speed (mm/s). (c) Laser power (% of 60 W). (d) Focal length (mm), the minimum laser spot diameter is provided at 0.281 m.*

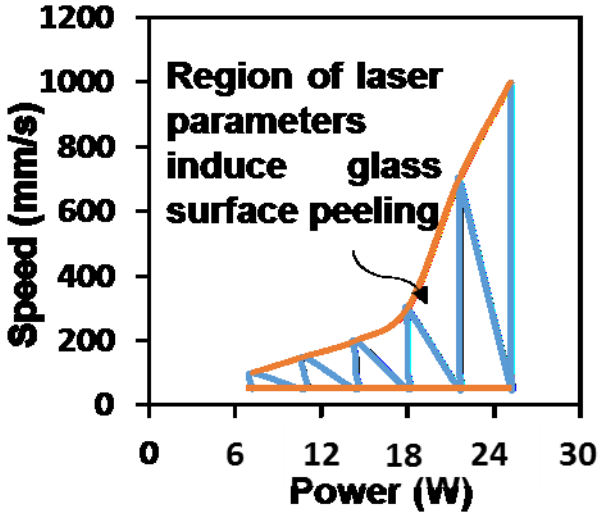

Figure S2. A prediction model of CO2 laser induced glass surface peeling.

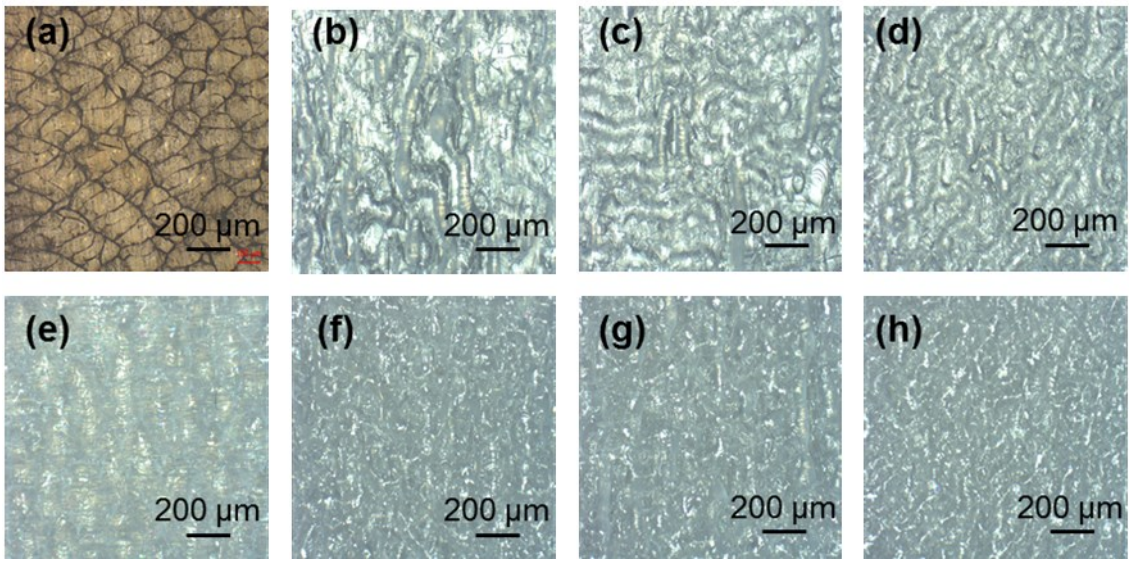

Figure S3. Microscopic images (x5) of the fabricated diffusers using different surface relief structures, the specifications of the laser fabrication parameters and number of diffuser surfaces are detailed in Table 1. (a) Sample (S1), (b) Sample (S2, (c) Sample (S3), (d) Sample (S4), (e) Sample (S5), (f) Sample (S6), (g) Sample (S7), (h) Sample (S8).

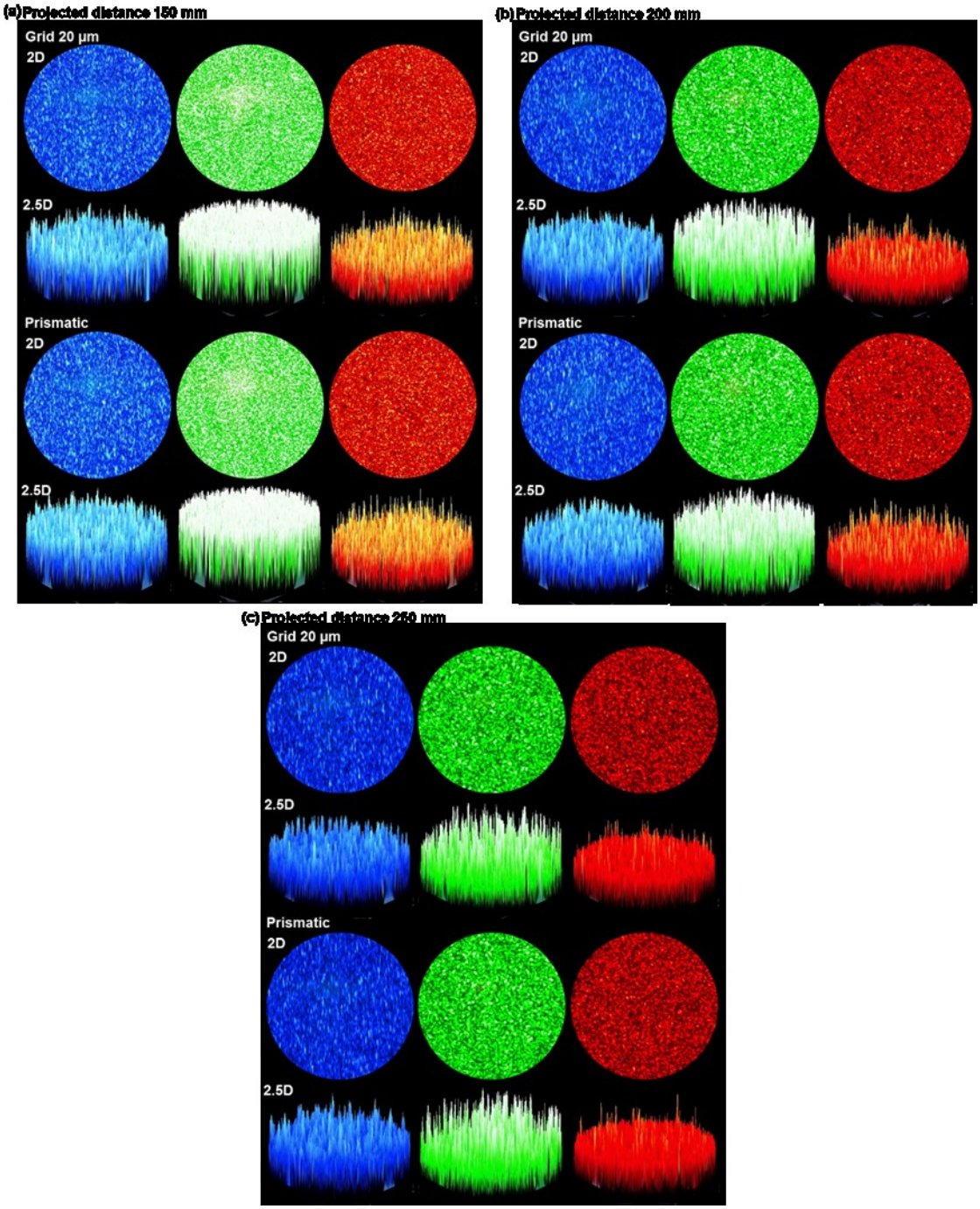

Figure S4. The recorded image of speckle pattern at different projected distance (a) 150mm, (b) 200mm and (c) 250 mm for Grid 20 µm and prismatic diffuser with varying laser wavelength (450, 533 and 633 nm).

Chapter 6: Highly Flexible, Stretchable, Superhydrophobic and Tunable Optical Diffusers

Published article

Tawfiq Alqurashi and Haider Butt

ACS Central Science 2019 5 (6), 1002-1009

In the previous chapters, optical diffusers were produced on a solid materials by using three different laser machining systems whilst the continuous CO_2 laser has cost-efficiency. Therefore, this chapter continues the fabrication of optical diffusers by using a CW CO_2 laser but on a flexible material, PDMS elastomer. This allows the design and experimental realization of the pioneering, mechanically stretchable and tunable optical diffusers compared to all previous chapters. Also the elastomer material provides a good self-cleaning surfaces which repels liquids, and offers the possible uses of materials in electronic devices and biomedical applications.

Author Contributions

T.A. conceived the idea for fabrication of flexible and stretchable optical diffuser. T.A deigned the optical experimental setups, interpreted the data and provided research direction under supervision of H.B. T.A. wrote the first draft of the paper and H.B proofread the writing of the paper.

6.1 **Abstract**

Highly stretchable and superhydrophobic photonics provide a new geometric degree of freedom for photonic system design and self-cleaning applications. Here, we describe the design and experimental realization of mechanically stretchable and tunable photonic diffusers. These intrinsically designed diffusers (based on cylindrical lenslet and micro tip arrays) were made directly on elastomer material using laser ablation. The dimensions of both the tips and the lenslet arrays play a critical role in the distribution of illumination and wettability resistance. By stretching the diffusers mechanically along the lenslet arrays, diffusion angle tuning was achieved and also a reversible change between hydrophilic to superhydrophobic states. These multifunctional diffusers constitute an important step towards integration with flexible materials or devices such as stretchable organic light-emitting diodes (OLEDs) and polymer light-emitting diodes (PLEDs).

6.2 **Introduction**

Stretchable photonics and optoelectronics have been perceived over the past decade as an alternative technology for the realization of the next generation of optoelectronics and optomechanics applications. The use of advanced materials for adaptable photonic devices is of great significance across a wide range of sciences and technologies including material chemistry, soft matter physics, optics, electronics and engineering.[201, 202] Considering the mechanical flexibility in a photonic device, the technology has potentially enormous applications for optical imaging[203], epidermal sensing[204, 205], light-emitting diodes (LEDs)[206, 207], wearable strain sensor[208, 209] and bio-inspired photonics[210, 211]. Consequently, increasing the development of stretchable LEDs or OLEDs that are suitable for integration with electronic tattoos or displays is of great interest, because such OLEDs can potentially lead to an increase in demand for stretchable optical components, such as optical diffusers. These diffusers would be useful, for example, in allowing the light to mix before entering the visible part of the display, resulting in a more uniform and brighter displays without increasing the number of OLED lights.

Photonic diffusers are one of the most promising optical elements that can continuously process light beams directly, and convey a diffraction of light for wearable biosensors[212], intraluminal photodynamic therapy, LEDs and a wide variety of medical and electronic applications.[213] Photonic diffusers made from glass, plastic or fibre are not flexible, stretchable, soft or superhydrophobic devices[10, 214] and have therefore governed significant attention. In contrast, the recent development of an optical diffuser based on a hydrogel film has provided the possibility of meeting these requirements for a stretchable element. However, its working principle is only based on a swelling behaviour of hydrogel from chemicals with a substantial limitation

in properties, such as stiffness and physical contact.[213] This is because hydrogel photonic elements are relatively fragile against external stress and strain.[209] To date, there is a lack of research into how photonic diffusers respond to mechanical deformations. This is an issue because photonic devices need to be adapted for stretchable and flexible optoelectronic and optomechanical devices, which are becoming significantly more important.

Mechanical deformations are useful characteristics, particularly when employing thin photonic devices in advanced applications such as biorobotics and lab-on-chips. The majority of photonic devices are fabricated from rigid or soft material in rigid substrate, and cause an inherent mismatch for application that should be stretchable like human skin[205], or flexible like OLEDs[215]. The transparency of rigid material, such as glass, in a visible spectrum, tend to be slightly less than an elastomer material, thus, affecting the light efficiency[216]. On the other hand, elastomer materials achieve four typical aspects of the wettability: superhydrophobicity, controllable water adhesion, anisotropic sliding, and anisotropic wetting when it has been structured with periodic line-patterned surfaces[217]. A practical approach is to fabricate photonic diffusers directly on the stretched elastomer substrates and release it later to reduce the dimensions of the formed structures. There have been several reports where surface wrinkles were induced on elastomer materiels in response to applied-mechanical compression beyond certain critical strains.[218-220] Even in some cases when mechanically stretched, a small residual strain led to the formation of wrinkles[221]. These structures on the elastomer materials created a waved pattern across a stretched axis. For this reason, many optimisations are required to make reusable and strain resistant optical diffusers.

Here, we demonstrate a new route for the fabrication of photonic diffusers from stretchable elastomeric materials which present mechanical stretchability, superhydrophobicity and tunable optical properties while maintaining its desirable optical property. The development process pursued a range of initial designs and fabricating final applications. The surface structures were directly fabricated using laser ablation on stretched planar elastomer substrate, to enable the relative reduction the in feature size once the substrate had been released. These high-relief structures responded to the mechanical strain by tuning the photonic and wettability properties. Also, the elastomeric material allows fabricating thin devices with high-strain response. Finally, the relations of the droplet contact angles and the diffusion angle of illuminated light, with the stretchability characteristic were systematically investigated along the applied strain.

6.3 **Material and Methods**

Elastomer fabrication

The polydimethylsiloxane (PDMS) elastomer was prepared from solidifying a Dow silicone 10: 1 encapsulant (Sylgard 184, Dow and Corning, USA). The 10 to 1 ratio of resin as base and curing agent were processed into a disposable glass container. When liquid components were thoroughly mixed, they were poured directly into petri dishes, 5 cm in diameter (Thermo Scientific). The pouring mixture had to be de-aired using a vacuum pump (Island Scientific Ltd., UK) for two hours, to minimize air entrapment. After that, the mixture cured at a room temperature for around of 48 hours achieving a substrate of the cross-linked polydimethylsiloxane (PDMS). The thickness of the PDMS substrate was about 1 mm. The substrate was initially positioned on a custom-designed strain stage and subsequently stretched uniaxial to the strain of 66%.

Stretchable device fabrication

Device fabrication was performed at Nanotechnology laboratory at UOB using a rapid and direct desktop laser ablation system (Rayjet, Trotec Laser Inc., UK) with a CO_2 laser in an air atmosphere. The diffuser to be ablated was designed on a square-sized shape (5 × 5 mm) using the CorelDraw design suite. The design of the diffuser has a combination of identical tips and cylindrical lenslet arrays which were achieved by altering the dot-per-inch (dpi) parameter. The ablation was directly carried out on the stretched elastomer substrate, with 66% applied strain where the substrate is placed on a honeycomb table. This kind of structure table provides a reduced contact surface for the material, in order to reduce beam reflection. The dpi parameter was pre-set to 333 and 500 and for each dpi parameter, the substrate was fabricated with various laser powers (4.5, 4.8, 5.1, 5.4, 5.7 and 6 W) at an ablation speed of 750 $mm.s^{-1}$ The customized laser power was identified between 4.5 W to 6 W as no ablation was produced under 4.5 W and substrate damage occurred over 6.5 W. During fabrication, air extractor continuously blew clean air onto the substrate being ablated to avoid dust being burnt into the fabricated substrate by the laser beam.

Surface characteristics

The topography of fabricated diffusers was studied in the Laser Micro Processing (LMP) group at UOB. It is equipped with an Alicona G5 InfiniteFocous (IF) system for conducting high-resolution 3D surface measurements. The optical diffuser was placed onto a working stage of the IF system using 10× magnification, and the lateral solution was manipulated to reduce the measurement error. To run the measurement, the lowest and highest focal plane was selected between -100 and 100 μm and the measurement was processed to extract the topographical features. The extracted

result was provided 3D topography of the diffuser surface and enabled measurements to be carried out to find the surface depth and roughness (Ra). Both measurements were carried out across the combined of tips and cylindrical lenses with the selection of profile length and width of 1.57 mm and 0.2 mm, respectively.

Wettability characteristics

Wettability measurement was carried out by the Nanotechnology Group at UOB using a simple contact-angle system consisting of a microscope camera (USB Microscope, Plugable, Washington USA) with a 60×-250× magnification, a working stage with the custom-designed strain stage, a LED light source and a micropipette (SP0020-Auto, SciQuip, Shropshire). Contact angle (α) was measured for all modified surfaces by applying 2.00 ± 0.06 µl drops at 24 °C at a relative humidity level of 23-25%. The aqueous drop was imaged. The image was processed using ImageJ software (Wayne Rasband, National Institute of Health, USA) which uses Laplace equations to determine the contact angle based on the shape of the drop captured. The average CA values were obtained by measuring the device three times at various strain of 0%, 33% and 66% - three sets of readings, where the droplet acting on a flat, inverted and a vertical orientation, were obtained.

Optical characteristics

Optical transmission measurements of optical diffusers across the visible spectrum range of 450-700 nm were performed using the spectral transmittance measurement setup. It consisted of a broadband light and a spectrophotometer with 2 nm resolution (USB2000+, Ocean Optics, Oxford, UK) integrated with an optical microscope (Axio Scope.A1) via an optic fibre. The sample was vertically orientated between the spectrometer and the broadband light source at the normal incident.

For diffraction analysis, an angular spectral measurement setup was used to capture the diffracted light. The setup consisted of a rotational stage with the custom-designed strain stage, a collimated laser diode with a wavelength of 633 nm (Thorlabs) and a screen, instead of optical power meter. The optical diffuser was mounted onto the custom-designed strain stage, between the laser source and screen. The distance between the released sample-screen and stretched sample-screen were 30.5 and 47 cm, respectively. The laser light was pointed through a sample from the normal incident while a digital camera, on another side, captured the diffracted pattern on the screen. After capturing diffracted patterns, an Image Intensity Process was utilized to produce the angle of diffraction and its intensity by processing the captured image. The angle of diffraction was calculated based on the measurement from the diffracted pattern on the screen. This measurement allows to adjust and obtains the result for light intensity vs diffraction angle.

6.4 **Result and Discussion**

Device design and fabrication

Silicone encapsulants including two liquids were selected to provide highly stretchable PDMS elastomer substrate. When liquids are thoroughly mixed and poured into a petri dish (Figure 1a,i), the mixture subsequently cured to a flexible elastomer substrate, which is suited for fabrication of photonic devices. The chemical structure of the elastomer is represented in Figure 1a,ii using the structural formula and molecular graphic. This material is highly transparent, elastic and a thermal insulator. The elastomer substrate was stretched under a mechanical strain of about 66% and the laser ablation was utilized to fabricate the diffuser structures (Figure 1a,iii). These high relief structures were fabricated in the form of an array of cylindrical lenses separated

with tips, to produce more scattering. To understand the structure formed on the stretched elastomer, the design model was prepared and calculated based on strain law: $\varepsilon = \delta/\mathrm{D}$ where ε is a nominal strain, δ is a change in lens diameter and D is lens diameter after being released. Because the fabrication was produced on the stretched substrate and due to elastomer instability, low strain deformation was selected. Figure 1a,v shows the stretched lens diameter (D_T) at an applied strain of 66%, which is similar to a laser ablation spot size (70 μm). Based on calculation, if the sample was engraved at different applied strain, the diameter of lens will be varied (Figure 1b). This allows the production of a smaller fabricated feature once the strain is released and thus reduces the ablated feature diameter (D) to 43 μm (Figure 1a,vi). So, changing the applied strain could directly produce various lens diameters without requiring an extra optical lens to change the ablation focal spot sizes (Figure 1c).

A series of diffuser elements were fabricated on stretched elastomer substrate using a rapid and direct desktop of a CO_2 laser ablation system. To optimize the laser ablation process, three parameters are of fundamental importance: laser beam spot size, laser power, and dots-per-inch (number of laser scans per inch upon one axis). The beam size and power have a direct relationship with the cylindrical lens's diameter and its depth, while the dpi affects the periodicity of the cylindrical lenses and the tip width. This is usually the longest part of the process with the laser speed was maintained as a constant at 750 $mm.s^{-1}$, to ensure consistency of ablation in all the samples. Therefore, the fabricated diffusers were intended to have a similar cylindrical lens diameter with two different identical microtip widths (4.5 and 2 μm) on a pattern area of 5 × 5 mm, achieving functionalities of optical diffusion. These identical microtips were produced using 333 and 500 dots-per-inch (dpi), respectively. Furthermore, the depth of cylindrical lenses was controlled using laser power (4.5 to 6 W). As the power increased, the depth greatly increased and produced a parabolic shape. After the

diffuser fabricated was released (unstretched), the structured surface shrank producing smaller surface features.

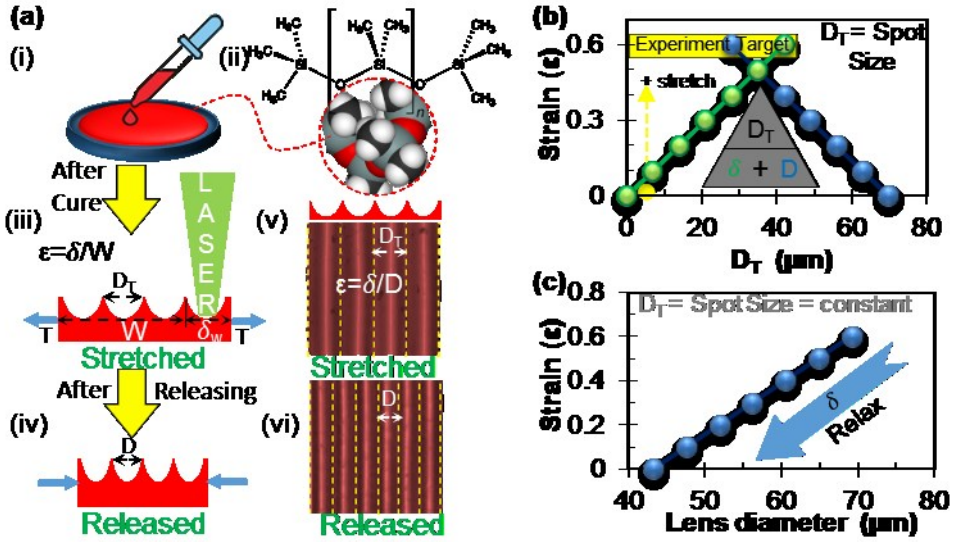

Figure 1. (a) Photonic diffuser design and fabrication (i) producing elastomer material, (ii) structural chemical formula and model of elastomer molecule, (iii) Schematic illustration of laser ablation on stretched elastomer for producing a photonic diffuser with its simulated structure in (v), (iv) the diffuser after releasing and its simulated structure in (vi). (b) The relation between the stretched lens diameter (D_T) during fabrication and changing strain and (c) their effect on the lens diameter (D) when releasing the applied strain.

Topographical Characteristics

The surface characteristics of two stretched diffuser elements (with 66% applied strain) had quite similar lenslet diameters with tolerance of 1 μm, but with different tip-widths (4.5 μm and 2 μm). The observed first and second batch stretched diffuser were obtained with tip widths of 4.5 μm and 2 μm, respectively (Figure 2a,i, c,i). These surface structures were measured orthogonally across the cylindrical lenslet axis to find their surface roughness and profile. The average roughness (Ra) values were

obtained to be 1.92 μm for the first batch stretched diffuser and 1.62 μm for second batch stretched diffusers (Figure 2a,iii, c,iii). The surface roughness is directly influenced by the depth of the lenses, which is affected by laser ablation power (See Figure S1 in Supporting Information).

The depth for the diffusers was measured with tolerance dimensions. These tolerance dimensions were computationally estimated based on the average mean depth calculation. As the laser power increases for the first fabricated diffuser (4.5 μm tip width), the depth started from 10 μm at a power of 4.5 W and kept rising to 20 μm at a power of 6 W (Figure 2a,iv). However, the depth in the second fabricated diffuser (2 μm) has the dimension of 7 μm at the power of 4.5 W and 25 μm at the power of 6 W (Figure 2**c**,**iv**). These greater variations could be due to the changing curing agent to resin (base) ratio which alters the properties of the resulting cured elastomer. As the ratio of curing agent to resin increases, a more rigid elastomer is produced [222]. Another effect could be that the elastomer plane, particularly on the fabricated face has an inaccurate flat surface.

Once both diffuser elements were released to 0% strain, their surfaces characteristics shrank and their profiles simultaneously extended in reverse. Upon observation under the microscope, the first released diffuser reduced the width of tip from 4.5 to 2.5 μm, while the second released diffuser reduced from 2 μm to <~1 μm (Figure 2b,i, d,i). In reverse, the depth of cylindrical lenslets were extended for both diffusers. The observed depth on first diffuser was elongated from 10 μm to 12 μm at the power of 4.5 W. Even at other powers, the net results observed that the depths elongated instantly by ~10% (Figure 2b,iv). On the other hand, the behavior of the depth elongation in the second released diffuser has extended by up to ~19% (Figure 2d,iv). These different observations in the reduction and extension could again be an indication of the dominant presence of such elastomer instability, either from the curing

process or deformation. For this reason, the topography characteristic of both diffusers were quite irregular at these applied strains, however, they maintained their form and transparency.

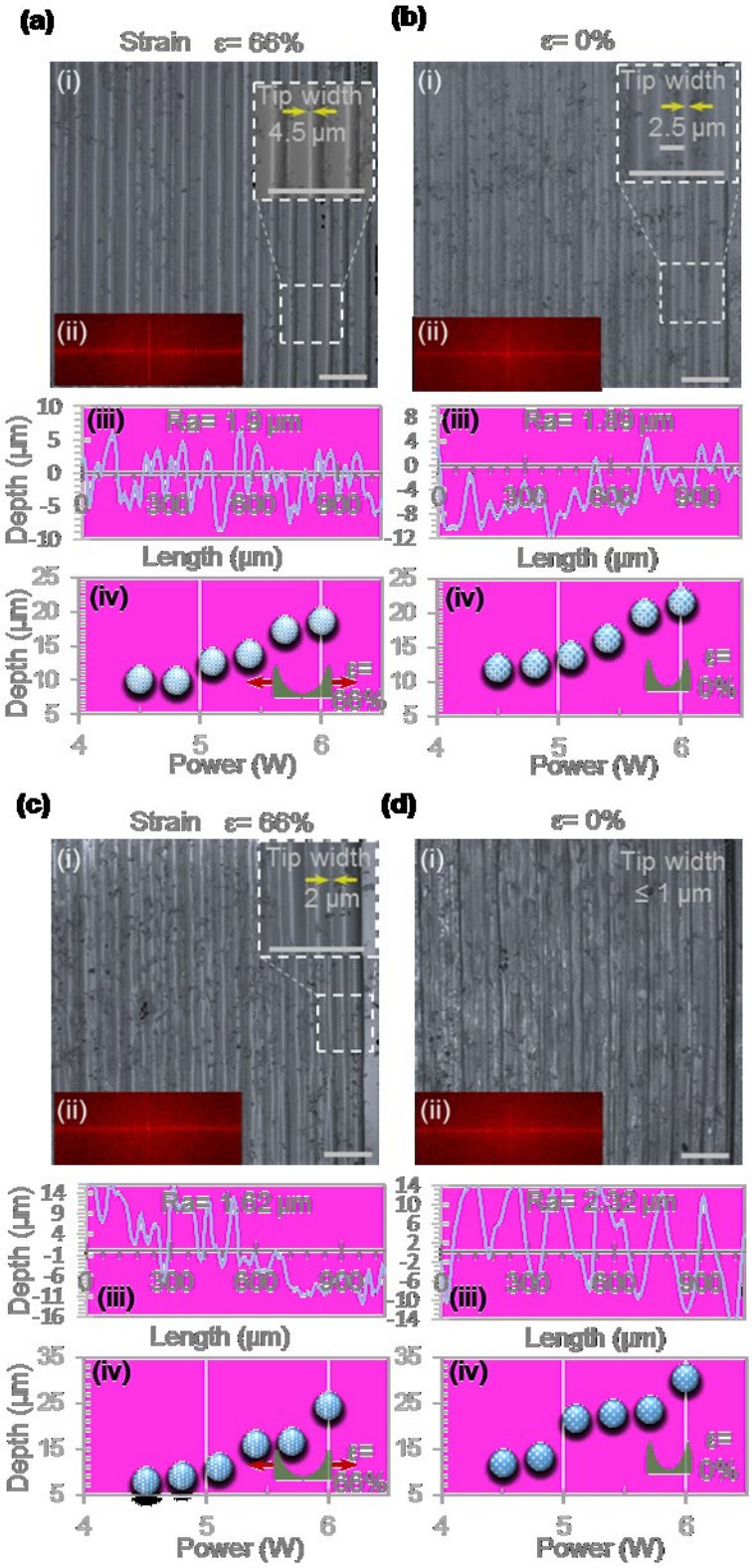

Figure 2. The surface characteristics of two diffuser samples. Optical images of two diffuser elements under their stretched and released conditions with two of identical tip widths. (a) The stretched first diffuser, (b) the released first diffuser, (c) the stretched second diffuser and (d) the released second diffuser. Each of these was

represented with (i) the captured optical image, (ii) FFT simulation generated from captured optical images in i, (iii) the roughness profiles, (iv) the average mean depth of lenslet arrays at different powers.

Wettability Characteristics

It is well known that liquid wetting on solids depends on both surface chemistry and physical factors. This work focused on physical factors [43, 223]. For the two diffuser elements, the surfaces decorated with identical cylindrical lenslet arrays but separated with different tip widths. Both tip width and lenslet depth play an important role in liquid wetting behaviour. In order to evaluate the relationship between stretched and released diffuser states, the working principle of wettability resistance in the stretched and released conditions is illustrated in Figure 3a which is following Cassie's theory where air can remain trapped below the droplet [224]. Theoretically, when the diffuser is being stretched, leading to enlarging the tips width and cylindrical lenslets diameter, more air remains trapped below the droplet, but the number of a contacted point with tips reduces. In this case, the stretched and released behaviour could affect correspondingly the wettability resistance, for that reason, the contact angle of water droplet was measured for the two diffusers, particularly at stretched and released states. These measurements also took into account various applied strains (0%, 33% and 66%) and three distinct orientations: by rotating the axes of the substrate from upward to sideways, and to downward orientations (Figure 3b, c and Figure S3 in supporting information).

On the first released diffuser element with various lenslet depths, the contact angle of the droplet achieved the value of 156 ± 1° when the parabolic profile of lenslet (or lenslet depth) was 22 μm (Figure 3b,i). This result suggests that superhydrophobic state existed with PDMS elastomer when microchannels were very close to each other

[217]. Reducing the depth of lenslet from 22 μm to 12 μm, slightly dropped down the contact angle by ~8°, which is a sign of less air being trapped. It seemed, in this case, that the pressure of water droplet will pass through the lens cavity as the pressure of air is insufficient to withstand it, resulting in that the tip penetrating the droplet and reducing the contact angle. Furthermore, the diffuser was oriented from flat (upward) position to a 90 degrees sideways position and a flipped downwards position resulting in lower contact angles, around ~7° at downward orientation and lesser angle around ~11° at sideways orientation (Figure 3b,ii, iii). On the other hand, once this diffuser was stretched with an applied strain of 66%, it has been observed that it reduced both the contact angle and the depth of the lenslet. By comparing the surface of diffuser under stretched and released states, the diffuser became capable of transiting between hydrophobic and superhydrophobic states, which such this behaviour cannot be generated by a rigid surface alone.

By reducing the tip width to ≤ 1 μm in the released second diffuser, the behaviour of wettability resistance was completely changed. It seems the droplet of water couldn't stand on tips and therefore the contact angle decreased to 109° ± 1°, which can be interpreted as the progressive sinking of the droplet inside the cavity of the lenslet (Figure 3c). Increasing the depth of lenslet by ~20 μm tended to obtain an extra contact angles of around 4°, in close agreement with the Wenzel's theory, particularly at the depth of surface [225]. However, the hydrophobicity tended to have a much larger contact angle of around 136° ± 1° when this diffuser was stretched to an applied strain of 66%, leading to an enlarged tip width of 2 μm. A comparison between the first and second batch diffuser associated with tip widths confirms that the hydrophobicity could be improved only if the width of the tips is larger than 2 μm. This is applied in case the lenslet diameter does not change. Finally, more details on how ablation power and

applied strain of 33% were studied and their effect on hydrophobicity was studied (See Supporting Information Figure S3).

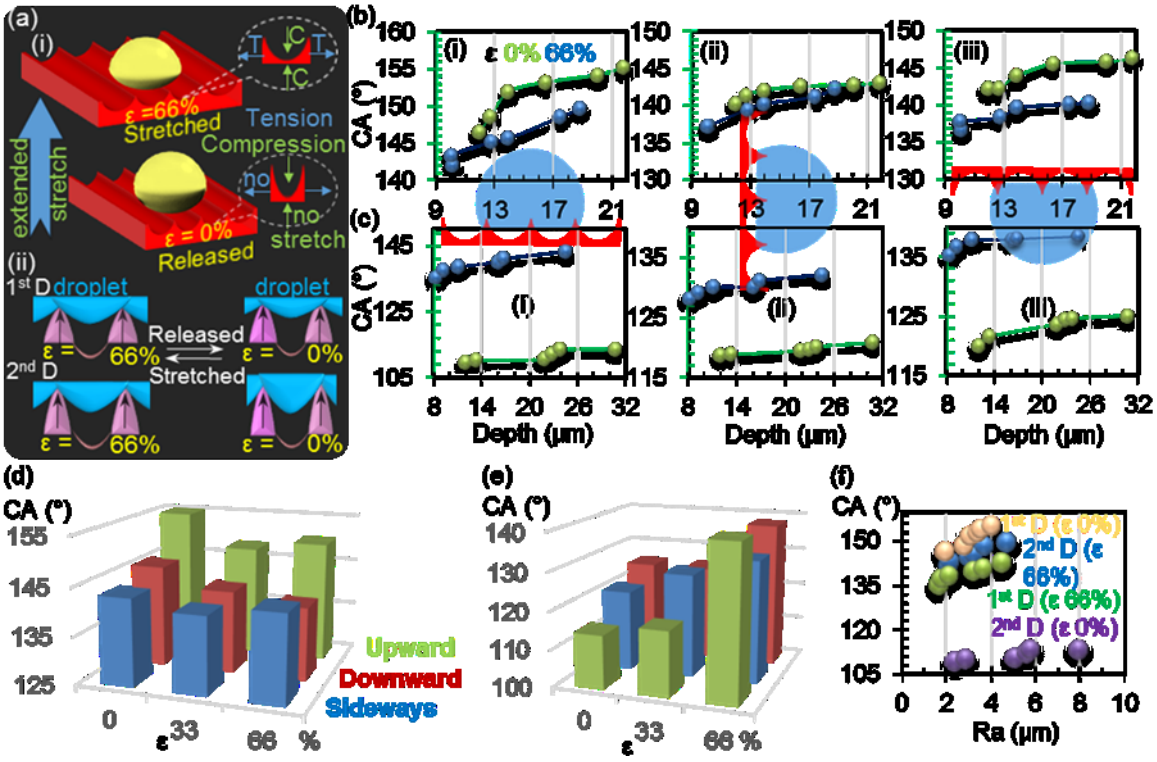

Figure 3. The wettability characteristics of diffuser elements. (a) Schematic of the photonic diffuser substrate when (i) it is strained from 0% to 66%. (ii) Schematic illustration to mimic how tips and lenslet depth react with droplet for both first diffuser (1st D) and second diffuser (2nd D) based on our experimental results. (b, c) the measurement of the contact angle on stretched and released (b) first diffuser and (c) second diffuser at different orientations: (i) upward, (ii) sideways and (iii) downward. (d, e) Comparison of contact angle for the first diffuser at the applied strain of 0%, 33% and 66% for the first diffuser (d) and second diffuser (e). (f) The relationship between average roughness (Ra) and contact angle for both diffusers once the structural periodicity is similar.

Optical Characteristics

Two distinct photonic diffusers were designed based on similar identical cylindrical lenslet arrays but were separated with two different tip widths; thus, avoiding hot spots

which are normally produced with a flat surface. These lenses are described as the plano-concave lenses which are typically used to diverge collimated beams of light perpendicular to the lens axis (Figure 4a). Each cylindrical lenslet is defined by a certain number of parameters, such as a parabolic profile (depth) and diameter of a lens. Once these diffusers were stretched uniformly and uniaxially along the cylindrical lens axis, so that its diameter extends and its depth shrinks, optical features were examined and compared against the relaxed diffuser. The stretching and releasing of diffusers was carried out mechanically, this affects the light distribution. To understand this behaviour, the working principle of the photonic diffuser is illustrated in Figure 4a. The schematic illustration presents how light propagates theoretically through the diffuser in both stretched and released states. It shows the stretched diffuser elongates the diameter of lens, allowing more distribution of light. To visualize this, the diffusion pattern of the diffuser was evaluated experimentally by an optical setup (Figure S4 in Supporting Information). In this optical setup, a collimated laser diode with 633 nm wavelength illuminated through the diffuser at a normal incident and the diffracted pattern was projected on to a screen. This projected pattern was captured by a digital camera and it was processed by employing image intensity processing to obtain its angle of diffusion and its intensity.

On the first type of diffuser, a strain of 66% was applied to stretch the series of diffusers which have different parabolic profile depths for their cylindrical lenslet. For an average lens depth of 19 μm, the stretched diffuser reached the diffusion angle of 67° (Figure 4b). By reducing the depth to 10 μm, it can be seem that the diffusion angle went down to 49°. Therefore, adjusting the lens depth gives the ability to produce different diffusers ranging from 49° to 67°. The diffusion angle at Full Width at Half Maximum (FWHM) was measured, and it was discovered that the diffuser maintained a good FWHM angle. For example, the diffusion angle was 67° while its FWHM was

maintained to be 50°. This diffusion is highly acceptable, and often beneficial for many applications. However, when this exact diffuser was released mechanically (strain 0%), it tuned the diffusion angle from 67° to 31° (Figure 4c). This confirmed that the diffuser has the capability to be a highly mechanically tunable diffuser. The distribution of light against the lens depth was unstable compared to the stretched diffuser. This is because the geometry of lenslet could become unstable in its shape and size. The reason geometry was unstable is that the lenslet fabrication was carried out at the stretched substrate and when it was released, it did not release uniformly.

On the second diffuser, the tip width was reduced to 2 μm at stretched state compared to the first diffuser which has the tip width of 4.5 μm. Contrary to the first diffuser, the diffusion angle of 48° was reached for the second stretched diffuser at a depth of 24 μm (Figure 4d) while its FWHM was measured to be around 26°. This confirmed that the width of the tips could also play an important role in the distribution of illumination. By increasing the depth of lenslets again for the second diffuser, more depth similarly keeps reducing the diffusion angle as observed in the first diffuser. However, the FWHM of diffusion angle was not particularly affected by the depth in this case. It was noticed that FWHM was calculated to be 26° and 24° for depth of 24 μm and 8 μm, respectively. Once this diffuser was released, the diffraction behavior related to depth was to diminish the distributing light in reverse because increasing the depth had less diffusion angle (Figure 4i).

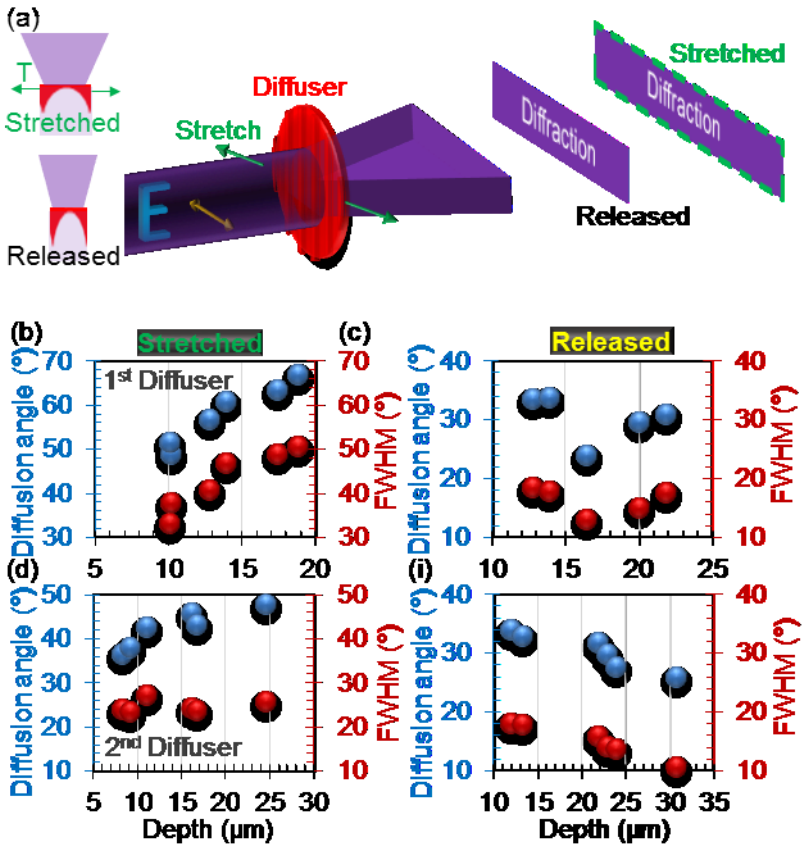

Figure 4. Optical characterization of the diffusers. (a) A schematic illustration of the diffraction of light passing through a released and stretched diffuser. (b-i) The angular diffusion measurement of the diffusers when illuminated with a collimated laser pointer (λ=633 nm). (b) The first and second diffuser have several parabolic depths at stretched states (b, d), and (c, i) once released, respectively. The diffusion angle represented with a blue colour and its FWHM appeared with a red colour.

Optical transmission measurements were also conducted on both diffuser elements at released states. The transmission of the visible spectrum was measured by employing an ocean optics spectrometer (2 nm resolution) which is connected to an optical microscope by fiber optic. This measurement was taken in the transmission mode with a 50× magnification objective to test the diffusers. The results showed that the first released diffuser offered superior optical transmission at minimum depth (Figure 5a). Generally, the transmission efficiencies of the first stretched diffuser are

rated between 73-84% (depending on the lenslet depth). The reason the lenslet depth reduces the transmittance is that the depth produced more scattering as shown on the previous result (Figure 4b-i). However, this is very high-efficiency rating due to the fact that the engineered lenslet is more efficient even in this case transmission is not a high enough due as laser produces a high roughness surfaces. But this rough surface of exact periodic-structure could play a great role in increasing diffusion angle (Supporting information Figure S5a). For further details in how laser power affect the percentage of transmission intensity was explained in supporting information (Supporting information Figure S6).

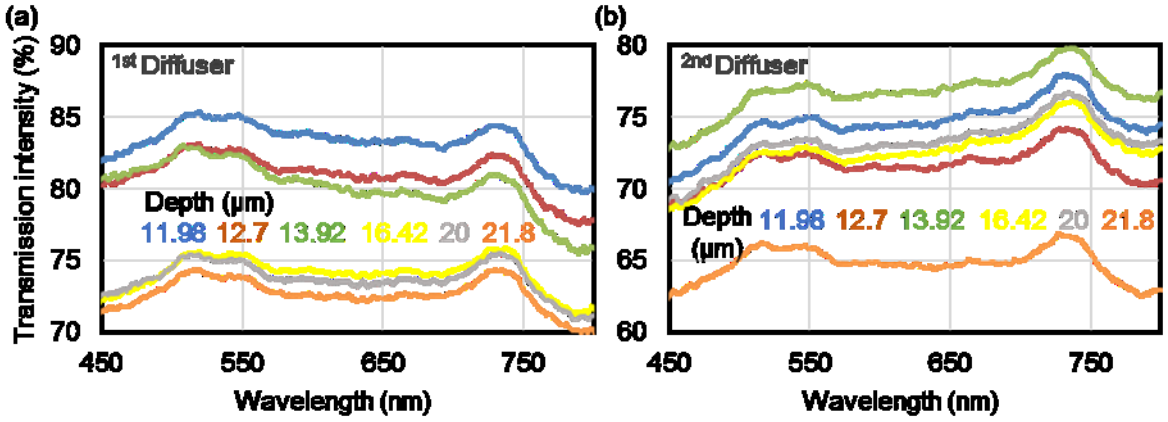

Figure 5. Optical transmission of diffuser elements across a visible wavelength spectrum for (a) first batch released diffusers and (b) the second batch released diffusers which had several lenslet depths.

Discussion

The new generation of stretchable diffuser elements developed based on an elastomer material enable a mechanically tunable diffuser. A key difference between our production method from traditional machining processes, such as single-point diamond turning, is that there is no mechanical contact with a substrate. These contact based methods lead to an intrinsic distortion of the design pattern on an elastomer

substrate while laser ablation does not. Laser ablation still leads to the generation of some roughness onto the cylindrical lens, particularly around the edge of the lens, thus, enhancing the diffusion of illumination. Moreover, stretching the elastomer substrate proved to be a feasible method for a considerable reduction in lenslet diameter and tip widths and potentially allowing the tip to be produced in a smaller scale.

For the wettability, these fabricated diffusers have the capability to switch mechanically between either hydrophobic to superhydrophobic or hydrophilic to hydrophobic based up on their design structure. On the first diffuser, the tip width structure was 2.5 μm and it was superhydrophobic (155°), but became hydrophobic when it was uniaxially extended (66%). This was due to the reduction in tip width and expansion of the lens diameter. The reason for the different wettability behavior was that the formed microgrooves had a width of 10 μm meaning the droplet could stand on more tips while in this case the microgrooves had the width of 70 μm. On the second diffuser, the tip width was around 2 μm and it became hydrophilic but if it was uniaxially stretched (66%), it switched from hydrophilic to a hydrophobic state. Closer inspection of the increasing lens depth shows an indication of more air trapping in the lens cavity, resulting in a rise in the contact angle following the Cassie's theory [224].

A stretchable diffuser, enables the production of tunable light distribution patterns. The advanced diffusion capability of a new class of diffusers makes them suitable for most applications that require mechanically stretchable diffusers including flexible OLEDs and a wearable strain sensors. Unlike the rigid diffusers [133, 214, 226], these stretchable diffusers tune the distribution of light based on mechanical applied strain while the recently developed diffuser as sensor controls the light diffraction based only on a swelling behaviour of hydrogel from chemicals [213]. However, it has limited control over the light distribution pattern, generally making only linear patterns but it is still suitable for both uniaxial and biaxial applied strain. Finally, these flexible and

stretchable diffusers are highly remarkable because such behaviour can not be generated by a rigid surface alone such as the transition between hydrophobic and superhydrophobic for surface wetting or their tuning angle for light diffusion.

6.5 **Conclusion**

The experiments establish the key principle that novel flexible and stretchable diffusers can be produced based on PDMS elastomer material. These diffusers confirmed that the tip widths, lens depths and diameters influence the distribution of light and surface wettability. Also, stretching the diffuser substrates mechanically offered both tunable light diffusions and switchable wettability. They provide, in wettability, a wide range of surfaces with hydrophilic to superhydrophobic properties and tuned the diffusion angle from 26° to 48°. For further work, more applied strain on diffuser could be investigated, and it is suggested that the high efficiency of these stretchable diffusers enable them to be utilized in a variety of optoelectronic and optomechanical applications.

Conflict of interests

The authors declare no competing financial interests.

Acknowledgments

TA and HB thanks Mr. S.Muthusankar for his work and support in this research.

6.6 **SUPPORTING INFORMATION**

Highly Flexible, Stretchable, Superhydrophobic and Tunable Optical Diffusers

Tawfiq Alqurashi[a,*] *and Haider Butt*[a,*]

ACS central Science, In press

Author Contributions

T.A. conceived the idea for the fabrication of flexible and stretchable optical diffusers. T.A. deigned the optical experimental setups and provided research direction under supervision of H.B. T.A. wrote the first draft of the paper and H.B proofread the writing of the paper.

[a]School of Mechanical Engineering, University of Birmingham, Birmingham, B15 2TT, UK

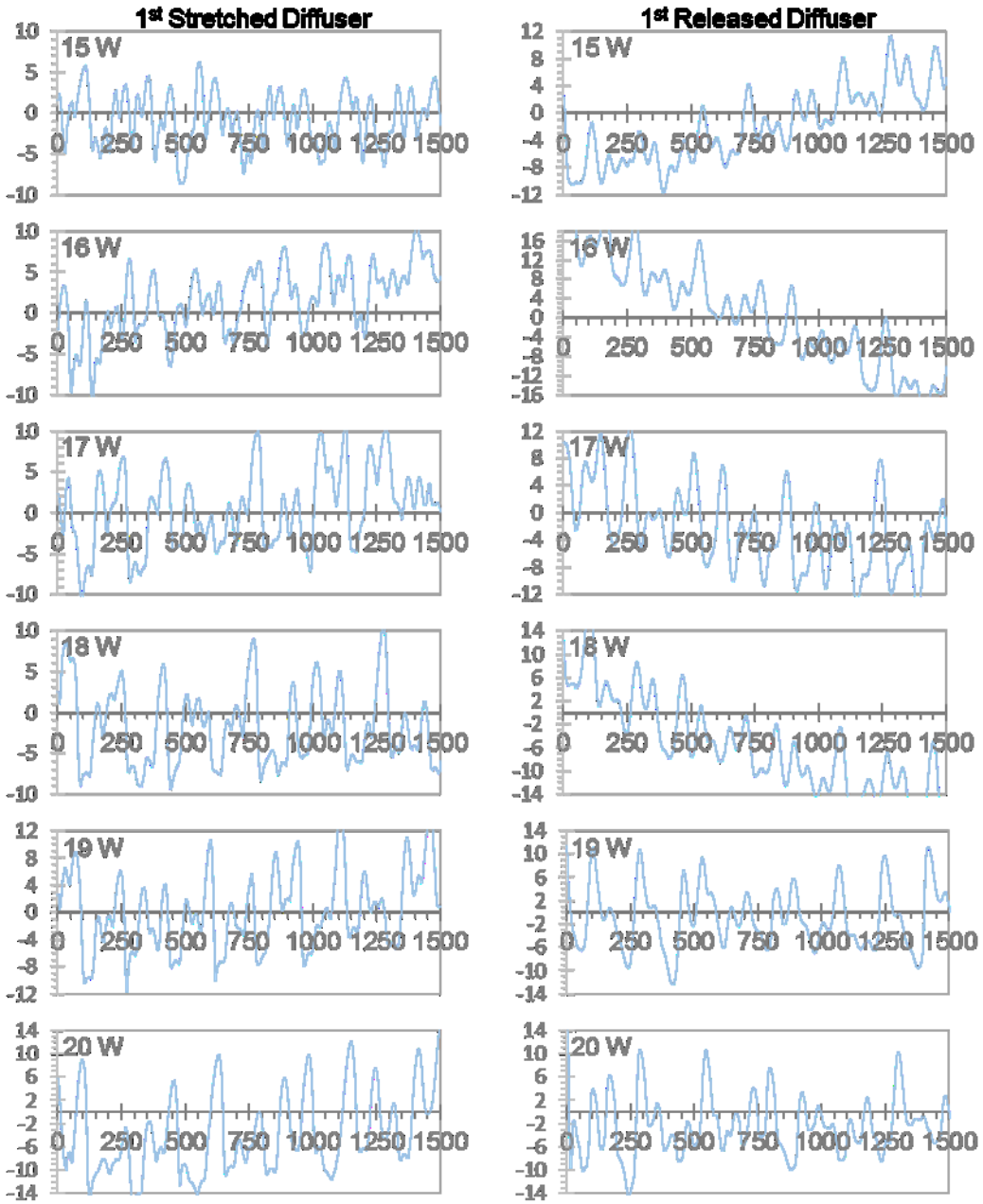

Figure S1. Roughness measurements for the first batch of fabricated optical diffusers including the first stretched diffuser (left column) and released diffusers (right column) at varied laser power (15, 16, 17, 18, 19, 20 W).

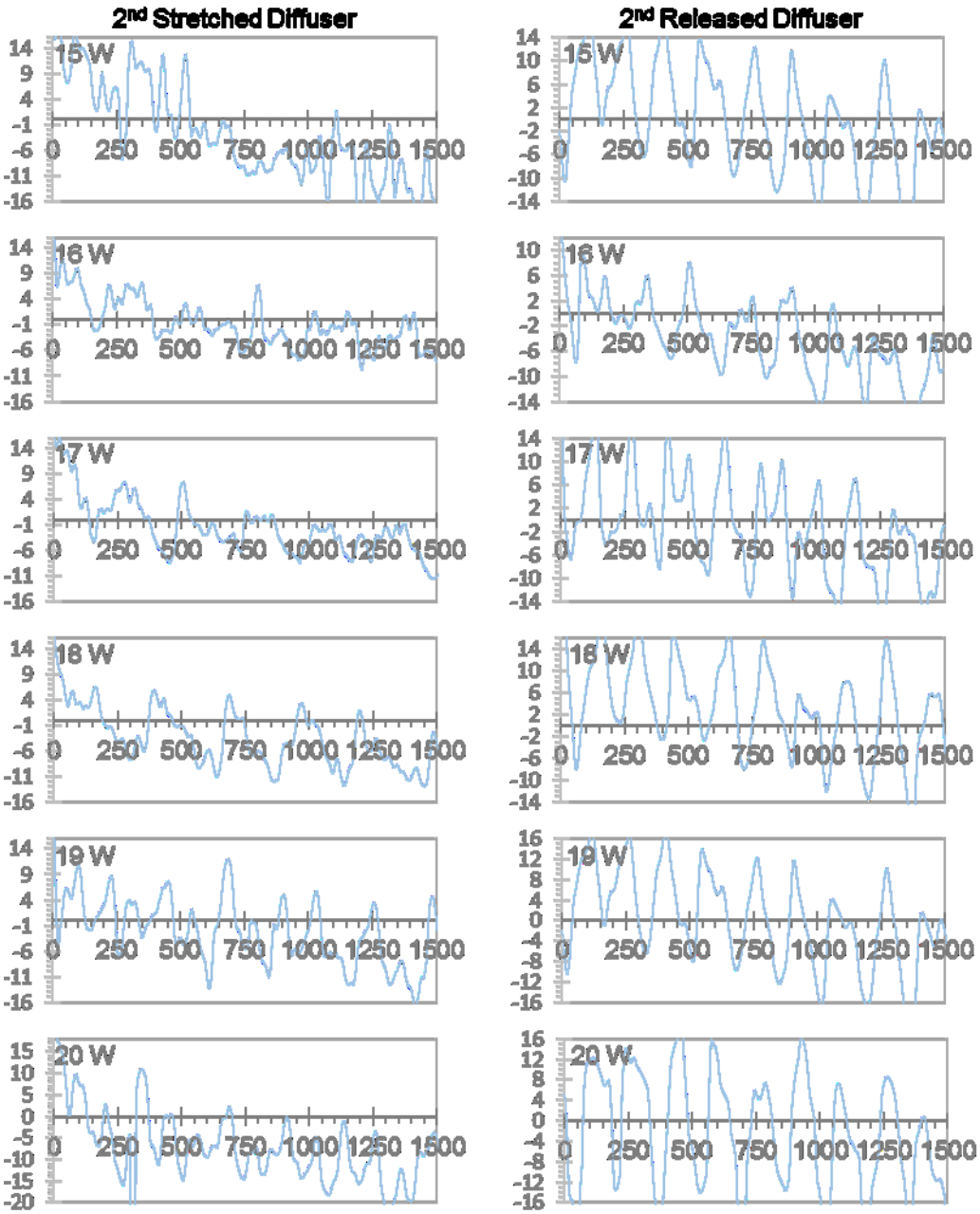

Figure S2. Roughness measurements for the second batch of fabricated optical diffusers including the second stretched diffuser (left column) and released diffusers (right column) at varied laser power (15, 16, 17, 18, 19, 20 W).

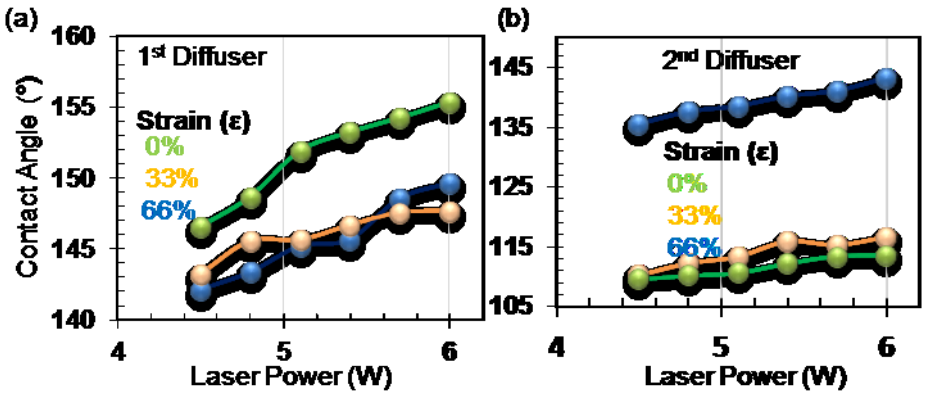

Figure S3. The contact angle measurements of droplet on surfaces of fabricated diffusers at different power. (a) First diffuser and (b) second diffuser.

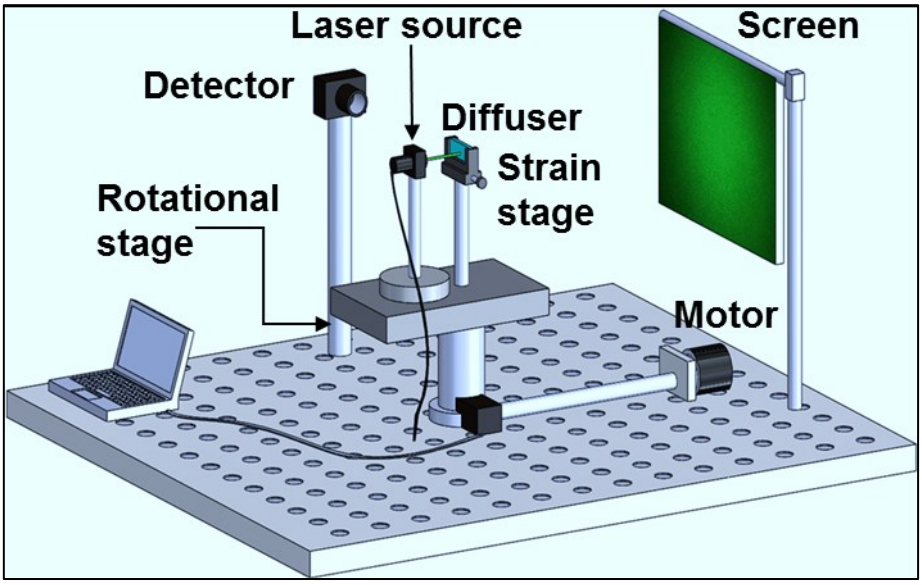

Figure S4. The optical setup for diffraction measurements.

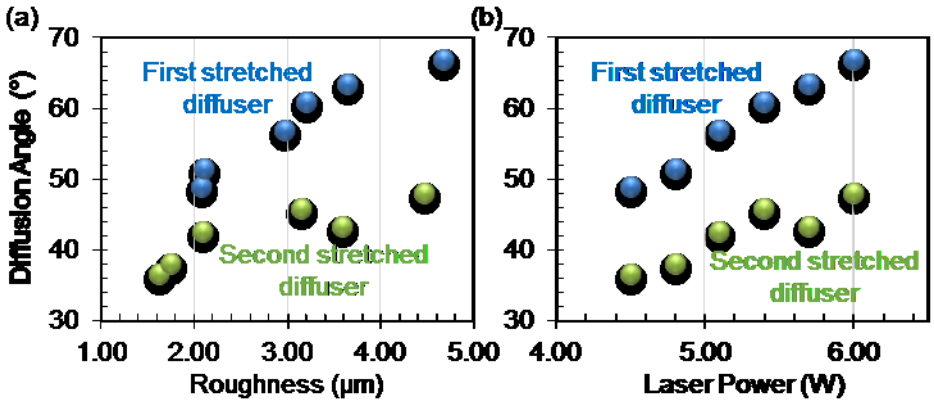

Figure S5. The measurements of diffusion angle for fabricated optical diffusers against (a) average roughness (Ra) and (b) laser ablation power (W).

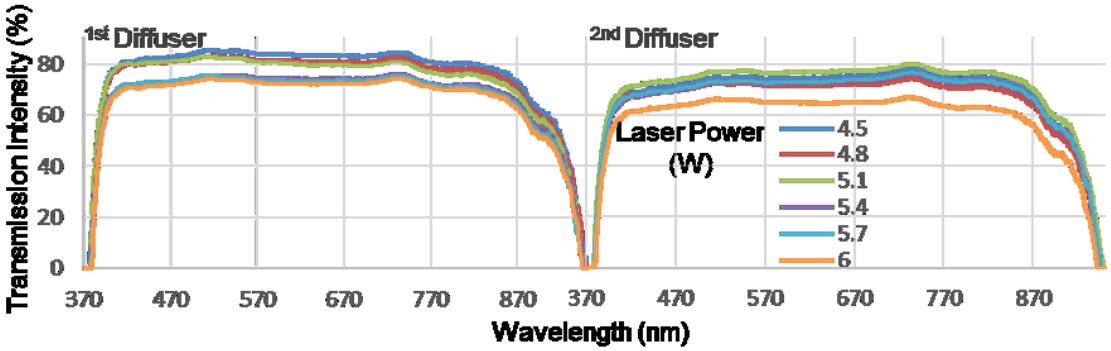

Figure S6. Transmission measurements of fabricated diffusers through different laser power (4.5, 4.8, 5.1, 5.4, 5.7, 6 W) for (a) first diffuser and (b) second diffuser.

Chapter 7: CONCLUSION AND FUTURE WORK

In this research study, the effect of three laser machining processes on transparent materials was characterised based on their optical properties. The laser machining was carried out on float glass, polycarbonate (PC), Polyethleneterephtalate Glycol (PETG) and Polydimethylsiloxane (PDMS) elastomer. It was found that the plastic material like PC and PETG became opaque after the laser processing. For that reason, only diffractive optical devices such as 1/2D diffraction gratings, Fresnel zone plate (FZP) lens and computer-generated holograms were fabricated on PC substrates. Optical diffusers were successfully fabricated on float glass and PDMS elastomer using three laser machining processes. The fabricated glass diffuser provides a solid device while fabricated elastomer diffusers provide highly flexible, stretchable and mechanically tunable photonic devices. However, the major challenge in using direct laser processing for manufacturing such photonic elements is the control and reproducibility of the optical microstructures and also minimizing the undesirable burrs on fabricated microstructure edges and cracking.

The FS laser machining produced micro and nano-scale surface-relief structures on the float glass surface. The surface-relief structures produced reduced illumination normal transmittance with haze boosting effects, and enlarged the angle of diffusion up to ~172°. The effect of FS laser beam polarization and hatch direction on transmission characteristics of the diffusers was also investigated. It was found that they have a significant influence on the transmission efficiency of optical diffusers. Additionally, FS laser processing could produce the diffractive optical devices such as 1D/2D gratings, a FZP lens and a computer-generated hologram on transparent PC materials. This fabrication approach allows production of microphotonic devices with nanoscale depth, where a few hundred nanometres in depth of grooves affected the

2-dimensional phase modulation and diffraction efficiency of the diffractive optical devices.

The micro surface features shaping a spiral pattern were textured on a float glass using a nanosecond laser texturing process. The textured float glass was investigated using an optical microscope system. This proved that the surface features have a direct relation with laser power and an inverse relation to the scanning speed. The characteristics of the fabricated diffusers can be altered by changing the laser processing parameters. Increasing the laser scanning speed along with lower laser power produces optical diffusers with higher efficiency and wider diffusion angle. By increasing the average roughness of a surface, the distribution of illumination can be precisely controlled in wide-ranging fields. The process limitation was to produce overlapping microstructures due to thermal effects compared to a femtosecond laser.

A direct CW CO_2 laser is the most cost-effective method among other laser sources, and it produced a pseudorandom surface-relief microstructure on float glass when laser scanning was linearly overlapped. The proposed approach of fabricating pseudorandom surface-relief microstructures have a direct influence on enhancing the optical performance of glass diffusers. The characteristics of diffusers can be altered by changing a design pattern including grid, linear and parallelogram. Increasing the number of fabricated patterns on both glass sides resulted in wider diffused light and improved homogeneity. This laser has the limitation to fabricate small microstructure features due to large beam size (~70 μm) compared to FS laser. Also, this laser has a continuous wave which it is not possible to play with a fabricated microstructure on the path of the laser.

However, flexible and stretchable diffusers can be produced by using CW CO_2 laser on the elastomer materials. These diffusers confirmed that the tips width, lens depths and diameters have played the main role in the distribution of light and surface

wettability. Also stretching the diffuser substrates mechanically offered both tunable light diffusions and switchable wettability. They provide, in wettability, a wide range of surfaces with hydrophilic to superhydrophobic properties and tuned the diffusion angle from 26° to 48°. For further work, more applied strain on the diffuser could be investigated, and this is suggested that the high efficiency of these stretchable diffusers enable them to have a great potential to be utilized in a variety of optoelectronic and optomechanical applications.

7.1 **Future Work**

This thesis presents three different laser machining processes to fabricate optical diffractive devices. It is suggested that many research directions can be carried forward based on the research findings.

i. Optical diffusers based on Polymethyl methacrylate (PMMA) material can be produced using these different laser machining processing due to a high transmission efficiency and a high-impact resistance.

ii. Optical diffuser based on microlens arrays can be produced on transparent materials using femtosecond laser processing providing the light diffraction with desired shapes.

iii. Optical diffusers and other optical diffractive devices can be produced as moulds on ultra-thin foil for replication. This eliminate the Gaussian profile in a cross-section of the foil by drilling through and it could produce pillars when the material will replicate this foil.

iv. More applied strain, either using tensile or compressive stress on flexible and stretchable diffusers could be investigated providing highly stretchable and tunable optical diffusers, tuning a high angle of diffusion.

v. Fabrication of flexible and stretchable diffusers with well-engineered microstructures using FS laser processing on different elastomer materials. This will produce optical diffusers with different diffused shapes.

vi. Volumetric diffractive optical devices can also be fabricated using FS laser processing inside the bulk of transparent materials allowing to control the formation of microstructure across the volume of the material. This can achieve interesting optical properties.

vii. Some light reflects back when incident on the optical diffuser. Therefore, coating an optical diffuser with an optical coating may reduce the reflection of light, and thus improving the transmission of light efficiency.

viii. Polishing the surface of diffractive optical devices after laser machining can eliminate the unwanted burrs from laser scanning path resulting in no light scattering.

References

1. Smith, W., *Modern Optical Engineering, 4th Ed*. Vol. PM180. 2007: McGraw-Hill. 768.
2. Helmenstine, A.M. *Huygens' Principle of Diffraction*. 2019 February 04, 2019.
3. Piaggio, H.T.H., *The Mathematical Theory of Huygens' Principle.* Nature, 1940. **145**(3675): p. 531-532.
4. Purcell, E.M. and D.J. Morin, *Electricity and Magnetism*. 3rd Edition ed. 2013: Cambridge University Press. 853 pages.
5. Flammer, J., M. Mozaffarieh, and H. Bebie, *The Interaction Between Light and Matter*, in *Basic Sciences in Ophthalmology: Physics and Chemistry*. 2013, Springer Berlin Heidelberg: Berlin, Heidelberg. p. 21-39.
6. Paton, J., *The Scattering of Light by Small Particles.* Nature, 1958. **182**(4648): p. 1470-1471.
7. Strutt, J.W., *XV. On the light from the sky, its polarization and colour.* The London, Edinburgh, and Dublin Philosophical Magazine and Journal of Science, 1871. **41**(271): p. 107-120.
8. Johnson, C.S. and D.A. Gabriel, *Laser Light Scattering*. 1994: Dover Publications.
9. Bohren, C.F. and D.R. Huffman, *Absorption and scattering of light by small particles*. 1983: Wiley.
10. Butt, H., et al., *Devitrite-Based Optical Diffusers.* ACS Nano, 2014. **8**(3): p. 2929-2935.
11. Murphy, K., et al., *Holographic beam-shaping diffractive diffusers fabricated by using controlled laser speckle.* Optics Express, 2018. **26**(7): p. 8916-8922.
12. Hu, J., et al., *Novel multifunctional microspheres of polysiloxane@CeO2-PMMA: Optical properties and their application in optical diffusers.* Optical Materials, 2013. **36**(2): p. 271-277.
13. Hu, J., Y. Zhou, and T. Zhang, *The novel optical diffusers based on the fillers of boehmite hollow microspheres.* Materials Letters, 2014. **136**: p. 114-117.
14. Hu, J., Y. Zhou, and X. Sheng, *Optical diffusers with enhanced properties based on novel polysiloxane@CeO2@PMMA fillers.* Journal of Materials Chemistry C, 2015. **3**(10): p. 2223-2230.
15. Deng, S., et al., *Laser directed writing of flat lenses on buckypaper.* Nanoscale, 2015. **7**(29): p. 12405-12410.
16. Rajasekharan, R., et al., *Can Nanotubes Make a Lens Array?* Advanced Materials, 2012. **24**(23): p. OP170-OP173.
17. Montelongo, Y., et al., *Computer generated holograms for carbon nanotube arrays.* Nanoscale, 2013. **5**(10): p. 4217-4222.
18. Quintián, F.P., M.A. Rebollo, and N.G. Gaggioli, *Diffusion of light transmitted from rough surfaces.* Journal of Modern Optics, 1997. **44**(3): p. 447-460.
19. Shih, T.-K., et al., *Fabrication of PDMS (polydimethylsiloxane) microlens and diffuser using replica molding.* Microelectronic Engineering, 2006. **83**(11): p. 2499-2503.
20. Scardaci, V., et al., *Carbon Nanotube Polycarbonate Composites for Ultrafast Lasers.* Advanced Materials, 2008. **20**(21): p. 4040-4043.
21. Aden, M., A. Roesner, and A. Olowinsky, *Optical characterization of polycarbonate: Influence of additives on optical properties.* Journal of Polymer Science Part B: Polymer Physics, 2010. **48**(4): p. 451-455.
22. Liu, S.-J., et al., *Rapid fabrication of surface-relief plastic diffusers by ultrasonic embossing.* Optics & Laser Technology, 2010. **42**(5): p. 794-798.
23. Wang, J.-H., et al., *One-step fabrication of surface-relief diffusers by stress-induced undulations on elastomer.* Optics & Laser Technology, 2009. **41**(6): p. 804-808.
24. Parikka, M., et al., *Deterministic diffractive diffusers for displays.* Applied Optics, 2001. **40**(14): p. 2239-2246.
25. Kim, G.H. and J.H. Park, *A PMMA optical diffuser fabricated using an electrospray method.* Applied Physics A, 2007. **86**(3): p. 347-351.
26. Ahn, S. and G. Kim, *An electrosprayed coating process for fabricating hemispherical PMMA droplets for an optical diffuser.* Applied Physics A, 2009. **97**(1): p. 125-131.

27. Wadle, S., et al. *Holographic diffusers*. 1994. SPIE.
28. Kim, S.I., et al., *Holographic diffuser by use of a silver halide sensitized gelatin process.* Applied Optics, 2003. **42**(14): p. 2482-2491.
29. Sakai, D., et al., *Direct Fabrication of Surface Relief Holographic Diffusers in Azobenzene Polymer Films.* Optical Review, 2005. **12**(5): p. 383-386.
30. Ahmed, R., et al., *Printable ink lenses, diffusers, and 2D gratings.* Nanoscale, 2017. **9**(1): p. 266-276.
31. Photonics, R. *Optical Diffuser Technologies*. Available from: https://www.rpcphotonics.com/pdfs/Optical_Diffuser_Technologies_Final_030215.pdf.
32. Chang, S.-I., et al., *Microlens array diffuser for a light-emitting diode backlight system.* Optics Letters, 2006. **31**(20): p. 3016-3018.
33. Wu, M.-H. and G.M. Whitesides, *Fabrication of Diffractive and Micro-optical Elements Using Microlens Projection Lithography.* Advanced Materials, 2002. **14**(20): p. 1502-1506.
34. Gimkiewicz, C., et al., *Fabrication of microprisms for planar optical interconnections by use of analog gray-scale lithography with high-energy-beam–sensitive glass.* Applied Optics, 1999. **38**(14): p. 2986-2990.
35. Stephen Chakmakjian, G.M.M.a.D.J.S., *Engineered microlens arrays provide new control for display and lighting applications.* Photonics Spectra, 2004. **18**(106): p. 5.
36. Penchev, P., et al., *Generic software tool for counteracting the dynamics effects of optical beam delivery systems.* Proceedings of the Institution of Mechanical Engineers, Part B: Journal of Engineering Manufacture, 2017. **231**(1): p. 48-64.
37. Bhaduri, D., et al., *An investigation of accuracy, repeatability and reproducibility of laser micromachining systems.* Measurement, 2016. **88**: p. 248-261.
38. Chryssolouris, E.L.K.E., *Laser machining - Theory and practice*. Mechanical Engineering Series. 1991: Springer-Verlag New York. XVIII, 274.
39. Patel, C.K.N., *Continuous-Wave Laser Action on Vibrational-Rotational Transitions of CO2.* Physical Review, 1964. **136**(5A): p. A1187-A1193.
40. Parandoush, P. and A. Hossain, *A review of modeling and simulation of laser beam machining.* International Journal of Machine Tools and Manufacture, 2014. **85**: p. 135-145.
41. Dubey, A.K. and V. Yadava, *Laser beam machining—A review.* International Journal of Machine Tools and Manufacture, 2008. **48**(6): p. 609-628.
42. Meijer, J., *Laser beam machining (LBM), state of the art and new opportunities.* Journal of Materials Processing Technology, 2004. **149**(1): p. 2-17.
43. Alqurashi, T., et al., *Femtosecond laser ablation of transparent microphotonic devices and computer-generated holograms.* Nanoscale, 2017. **9**(36): p. 13808-13819.
44. Bauer, F., et al., *Heat accumulation in ultra-short pulsed scanning laser ablation of metals.* Optics Express, 2015. **23**(2): p. 1035-1043.
45. Gusarov, A.V. and I. Smurov, *Thermal model of nanosecond pulsed laser ablation: Analysis of energy and mass transfer.* Journal of Applied Physics, 2005. **97**(1): p. 014307.
46. Navi, P. and A. Guidoum, *Proceedings of Third International Symposium on Wood Machining: 21-23 May 2007, Lausanne, Switzerland : Fracture Mechanics and Micromechanics of Wood and Wood Composites with Regard to Wood Machining*. 2007: Presses Polytechniques et Universitaires Romandes.
47. Yuan, L. and P.R. Herman, *Laser Scanning Holographic Lithography for Flexible 3D Fabrication of Multi-Scale Integrated Nano-structures and Optical Biosensors.* Scientific Reports, 2016. **6**: p. 22294.
48. Bertolotti, M., *Photon Statistics*, in *Photon Correlation and Light Beating Spectroscopy*, H.Z. Cummins and E.R. Pike, Editors. 1974, Springer US: Boston, MA. p. 41-74.
49. Boyd, K., et al. *Novel technique for the CO2 laser fabrication of optical devices with sub-micrometer ablation depth precision*. in *2014 The European Conference on Optical Communication (ECOC)*. 2014.
50. Rizzo, A., et al., *Laser micromachining of tapered optical fibers for spatially selective control of neural activity.* Microelectronic Engineering, 2018. **192**: p. 88-95.

51. Frank, A., et al., *Laser machining of sensing components on the end of optical fibres.* Journal of Micromechanics and Microengineering, 2013. **23**(4): p. 045021.
52. Takahashi, H., et al., *Novel laser machining of optical fibers for long cavities with low birefringence.* Optics Express, 2014. **22**(25): p. 31317-31328.
53. Zakariyah, S.S., et al., *CO2 laser micromachining of optical waveguides for interconnection on circuit boards.* Optics and Lasers in Engineering, 2012. **50**(12): p. 1752-1756.
54. Chen, F. and J.R.V. Aldana, *Optical waveguides in crystalline dielectric materials produced by femtosecond-laser micromachining.* Laser & Photonics Reviews, 2014. **8**(2): p. 251-275.
55. Li, L., et al., *All-laser-micromachining of ridge waveguides in LiNbO3 crystal for mid-infrared band applications.* Scientific Reports, 2017. **7**(1): p. 7034.
56. Vázquez, R.M., et al., *Fabrication of binary Fresnel lenses in PMMA by femtosecond laser surface ablation.* Optics Express, 2011. **19**(12): p. 11597-11604.
57. Luo, Z., et al., *Fabrication of parabolic cylindrical microlens array by shaped femtosecond laser.* Optical Materials, 2018. **78**: p. 465-470.
58. Luo, Z., J.a. Duan, and C. Guo, *Femtosecond laser one-step direct-writing cylindrical microlens array on fused silica.* Optics Letters, 2017. **42**(12): p. 2358-2361.
59. Chang, T.-L., et al., *Fabrication of diffraction grating in polydimethylsiloxane using femtosecond-pulsed laser micromachining.* Microelectronic Engineering, 2010. **87**(5): p. 1344-1347.
60. Machida, M., et al., *Shrinkable silver diffraction grating fabricated inside a hydrogel using 522-nm femtosecond laser.* Scientific Reports, 2018. **8**(1): p. 187.
61. Huang, T.-C., et al., *Fast fabrication of integrated surface-relief and particle-diffusing plastic diffuser by use of a hybrid extrusion roller embossing process.* Optics Express, 2008. **16**(1): p. 440-447.
62. Knowles, K.M., et al., *Light scattering and optical diffusion from willemite spherulites.* Optical Materials, 2016. **52**: p. 163-172.
63. Wu, C.Y., T.H. Chiang, and C.C. Hsu, *Fabrication of microlens array diffuser films with controllable haze distribution by combination of breath figures and replica molding methods.* Optics Express, 2008. **16**(24): p. 19978-19986.
64. Chang, S.I., et al., *Microlens array diffuser for a light-emitting diode backlight system.* Optics Letters, 2006. **31**(20): p. 3016-3018.
65. Lin, L., T.K. Shia, and C.J. Chiu, *Silicon-processed plastic micropyramids for brightness enhancement applications.* Journal of Micromechanics and Microengineering, 2000. **10**(3): p. 395-400.
66. Yeh, S.L., *A study of light scattered by surface-relief holographic diffusers.* Optics Communications, 2006. **264**(1): p. 1-8.
67. Allen, G.R., et al., *Led lamp with diffuser having spheroid geometry*. 2013, Google Patents.
68. Uehran, R.S., *LED lighted sign with a light diffuser*, in *US 6,829,852 B1*, Brooking, Editor. 2004, Daktronics, Inc.: US.
69. Han, Y., X. Zhao, and S. Qu, *Polarization dependent ripples induced by femtosecond laser on dense flint (ZF6) glass.* Optics Express, 2011. **19**(20): p. 19150-19155.
70. Tomita, T., et al., *Effect of surface roughening on femtosecond laser-induced ripple structures.* Applied Physics Letters, 2007. **90**(15): p. 153115.
71. Sugioka, K. and Y. Cheng, *Ultrafast lasers[mdash]reliable tools for advanced materials processing.* Light Sci Appl, 2014. **3**: p. e149.
72. Han, W., et al., *Continuous modulations of femtosecond laser-induced periodic surface structures and scanned line-widths on silicon by polarization changes.* Optics Express, 2013. **21**(13): p. 15505-15513.
73. Wang, H., et al., *Femtosecond laser-induced simultaneous surface texturing and crystallization of a-Si:H thin film: morphology study.* The International Journal of Advanced Manufacturing Technology, 2013. **65**(9): p. 1691-1703.
74. Gattass, R.R. and E. Mazur, *Femtosecond laser micromachining in transparent materials.* Nat Photon, 2008. **2**(4): p. 219-225.

75. Brown, M.S. and C.B. Arnold, *Fundamentals of Laser-Material Interaction and Application to Multiscale Surface Modification*, in *Laser Precision Microfabrication*, K. Sugioka, M. Meunier, and A. Piqué, Editors. 2010, Springer Berlin Heidelberg: Berlin, Heidelberg. p. 91-120.
76. Tuennermann, A., S. Nolte, and J. Limpert, *Femtosecond vs. Picosecond Laser Material Processing.* Laser Technik Journal, 2010. **7**(1): p. 34-38.
77. Righini, G.C., et al., *FIBER AND INTEGRATED OPTICS SENSORS: FUNDAMENTALS AND APPLICATIONS*, in *An Introduction to Optoelectronic Sensors*. 2009, WORLD SCIENTIFIC. p. 1-33.
78. Zhao, Q., et al., *Printable ink holograms.* Applied Physics Letters, 2015. **107**(4): p. 041115.
79. Zhao, Q., et al., *Printable nanophotonic devices via holographic laser ablation.* ACS nano, 2015. **9**(9): p. 9062-9069.
80. Chichkov, B.N., et al., *Femtosecond, picosecond and nanosecond laser ablation of solids.* Appl. Phys. A, 1996. **63**: p. 109-115.
81. Liu, X., D. Du, and G. Mourou, *Laser ablation and micromachining with ultrashort laser pulses.* IEEE Journal of Quantum Electronics, 1997. **33**(10): p. 1706-1716.
82. Chen, J.-T., et al., *Laser-induced periodic structures for light extraction efficiency enhancement of GaN-based light emitting diodes.* Optics Express, 2012. **20**(5): p. 5689-5695.
83. *On the Scattering of Light by small Particles*, in *Scientific Papers:*. 2009, Cambridge University Press. p. 104-110.
84. Cho, D.-H., et al., *Light diffusing effects of nano and micro-structures on OLED with microcavity.* Optics Express, 2014. **22**(S6): p. A1507-A1518.
85. Butt, H., et al., *Carbon Nanotube Based High Resolution Holograms.* Advanced Materials, 2012. **24**(44): p. OP331-OP336.
86. Butt, H., et al., *Visible Diffraction from Graphene and Its Application in Holograms.* Advanced Optical Materials, 2013. **1**(11): p. 869-874.
87. Bitterli, R., et al. *Refractive statistical concave 1D diffusers for laser beam shaping*. 2008.
88. Sun, Y.-L., et al., *Protein-based soft micro-optics fabricated by femtosecond laser direct writing.* Light Sci Appl, 2014. **3**: p. e129.
89. Fang, R., A. Vorobyev, and C. Guo, *Direct visualization of the complete evolution of femtosecond laser-induced surface structural dynamics of metals.* Light Sci Appl., 2017. **6**: p. e16256.
90. Zhao, Q.-Z., et al., *Direct writing computer-generated holograms on metal film by an infrared femtosecond laser.* Optics Express, 2005. **13**(6): p. 2089-2092.
91. Kerse, C., et al., *Ablation-cooled material removal with ultrafast bursts of pulses.* Nature, 2016. **537**(7618): p. 84-88.
92. Du, D., et al., *Laser‐induced breakdown by impact ionization in SiO2 with pulse widths from 7 ns to 150 fs.* Applied Physics Letters, 1994. **64**(23): p. 3071-3073.
93. Pronko, P.P., et al., *Machining of sub-micron holes using a femtosecond laser at 800 nm.* Optics Communications, 1995. **114**(1): p. 106-110.
94. Joglekar , A.P., et al., *A study of the deterministic character of optical damage by femtosecond laser pulses and applications to nanomachining.* Applied Physics B, 2003. **77**(1): p. 25-30.
95. Chimmalgi, A., et al., *Femtosecond laser aperturless near-field nanomachining of metals assisted by scanning probe microscopy.* Applied Physics Letters, 2003. **82**(8): p. 1146-1148.
96. Brabec, T. and F. Krausz, *Intense few-cycle laser fields: Frontiers of nonlinear optics.* Reviews of Modern Physics, 2000. **72**(2): p. 545-591.
97. Chris, B.S., B. André, and M. Eric, *Laser-induced breakdown and damage in bulk transparent materials induced by tightly focused femtosecond laser pulses.* Measurement Science and Technology, 2001. **12**(11): p. 1784.
98. Steinmeyer, G., et al., *Frontiers in Ultrashort Pulse Generation: Pushing the Limits in Linear and Nonlinear Optics.* Science, 1999. **286**(5444): p. 1507-1512.

99. Li, Q., K. Nakkeeran, and P.K.A. Wai, *Ultrashort pulse train generation using nonlinear optical fibers with exponentially decreasing dispersion.* Journal of the Optical Society of America B, 2014. **31**(8): p. 1786-1792.
100. Kumar, K., et al., *Quantized structuring of transparent films with femtosecond laser interference.* Light Sci Appl, 2014. **3**: p. e157.
101. Wu, D., et al., *In-channel integration of designable microoptical devices using flat scaffold-supported femtosecond-laser microfabrication for coupling-free optofluidic cell counting.* Light Sci Appl, 2015. **4**: p. e228.
102. Chichkov, B.N., et al., *Femtosecond, picosecond and nanosecond laser ablation of solids.* Applied Physics A, 1996. **63**(2): p. 109-115.
103. Stuart, B.C., et al., *Nanosecond-to-femtosecond laser-induced breakdown in dielectrics.* Phys Rev B Condens Matter, 1996. **53**(4): p. 1749-1761.
104. Osellame, R., G. Cerullo, and R. Ramponi, *Femtosecond Laser Micromachining: Photonic and Microfluidic Devices in Transparent Materials*. 2012: Springer Berlin Heidelberg.
105. Li, Y., et al., *Single femtosecond pulse holography using polymethyl methacrylate.* Optics Express, 2002. **10**(21): p. 1173-1178.
106. Feng, P., et al., *Femtosecond laser-induced subwavelength ripples formed by asymmetrical grating splitting.* Applied Surface Science, 2016. **372**: p. 52-56.
107. Kawamura, K.-i., et al., *Holographic encoding of fine-pitched micrograting structures in amorphous SiO2 thin films on silicon by a single femtosecond laser pulse.* Applied Physics Letters, 2001. **78**(8): p. 1038-1040.
108. Wang, C., et al., *Anisotropic optical transmission of femtosecond laser induced periodic surface nanostructures on indium-tin-oxide films.* Applied Physics Letters, 2012. **101**(10): p. 101911.
109. Matsuo, S., S. Juodkazis, and H. Misawa, *Femtosecond laser microfabrication of periodic structures using a microlens array.* Applied Physics A, 2005. **80**(4): p. 683-685.
110. Bricchi, E., et al., *Birefringent Fresnel zone plates in silica fabricated by femtosecond laser machining.* Optics Letters, 2002. **27**(24): p. 2200-2202.
111. Valle, G.D., R. Osellame, and P. Laporta, *Micromachining of photonic devices by femtosecond laser pulses.* Journal of Optics A: Pure and Applied Optics, 2009. **11**(1): p. 013001.
112. Zhu, Y., C. Romain, and C.K. Williams, *Sustainable polymers from renewable resources.* Nature, 2016. **540**(7633): p. 354-362.
113. Chen, J.-g., et al., *Low-loss planar optical waveguides fabricated from polycarbonate.* Polymer Engineering & Science, 2009. **49**(10): p. 2015-2019.
114. Takahiro, I., M. Tetsuya, and U. Tatsuo, *Wide-Viewing-Angle Polarizer with a Large Wavelength Range.* Japanese Journal of Applied Physics, 2002. **41**(7R): p. 4553.
115. Ueda, M., *A study on the characteristics of antiplasticized polycarbonates and their optical disk substrates.* Polymer Engineering & Science, 2004. **44**(10): p. 1877-1884.
116. Deng, S., et al., *Graphene nanoribbon based plasmonic Fresnel zone plate lenses.* RSC Advances, 2017. **7**(27): p. 16594-16601.
117. Di Fabrizio, E., et al., *High-efficiency multilevel zone plates for keV X-rays.* Nature, 1999. **401**(6756): p. 895-898.
118. Rajasekharan, R., et al., *Can nanotubes make a lens array?* Adv Mater, 2012. **24**(23): p. Op170-3.
119. Deng, S., et al., *Computational modelling of a graphene Fresnel lens on different substrates.* RSC Advances, 2014. **4**(57): p. 30050-30058.
120. Kong, X.-T., et al., *Graphene-Based Ultrathin Flat Lenses.* ACS Photonics, 2015. **2**(2): p. 200-207.
121. Ma, X., et al., *Analysis of optical characteristics of modulation devices with square and circle pixels for 3D holographic display.* Chinese Optics Letters, 2015. **13**(1): p. 010901-010901.
122. Larouche, S., et al., *Infrared metamaterial phase holograms.* Nat Mater, 2012. **11**(5): p. 450-454.

123. Wakunami, K., et al., *Projection-type see-through holographic three-dimensional display.* Nature Communications, 2016. **7**: p. 12954.
124. Hainich, R.R. and O. Bimber, *Displays: Fundamentals & Applications, Second Edition*. 2016: CRC Press.
125. Goodman, J.W., *Introduction to Fourier Optics*. 2005: W. H. Freeman.
126. Gerchberg, R.W. and W.O. Saxton, *A practical algorithm for the determination of the phase from image and diffraction plane pictures.* Optik (Jena), 1972. **35**: p. 237.
127. Ingersoll, L.R., *Polarization of Radiation by Gratings.* Polarization of Radiation by Gratings, 1920. **51**: p. 129.
128. AlQattan, B., et al., *Holographic direct pulsed laser writing of two-dimensional nanostructures.* RSC Advances, 2016. **6**(112): p. 111269-111275.
129. Zhou, G., et al., *Superhydrophobic self-cleaning antireflective coatings on Fresnel lenses by integrating hydrophilic solid and hydrophobic hollow silica nanoparticles.* RSC Advances, 2013. **3**(44): p. 21789-21796.
130. Xue, C.-H., X. Bai, and S.-T. Jia, *Robust, Self-Healing Superhydrophobic Fabrics Prepared by One-Step Coating of PDMS and Octadecylamine.* Scientific Reports, 2016. **6**: p. 27262.
131. Alqurashi, T., et al., *Femtosecond laser directed fabrication of optical diffusers.* RSC Advances, 2017. **7**(29): p. 18019-18023.
132. Wang, G., et al., *Robust superhydrophobic surface on Al substrate with durability, corrosion resistance and ice-phobicity.* Scientific Reports, 2016. **6**: p. 20933.
133. Alqurashi, T., et al., *Nanosecond pulsed laser texturing of optical diffusers.* AIP Advances, 2017. **7**(2): p. 025313.
134. Gauthier, A., et al., *Water impacting on superhydrophobic macrotextures.* Nature Communications, 2015. **6**: p. 8001.
135. Zhou, H., et al., *Fluoroalkyl Silane Modified Silicone Rubber/Nanoparticle Composite: A Super Durable, Robust Superhydrophobic Fabric Coating.* Advanced Materials, 2012. **24**(18): p. 2409-2412.
136. Lee, C. and C.-J. Kim, *Underwater Restoration and Retention of Gases on Superhydrophobic Surfaces for Drag Reduction.* Physical Review Letters, 2011. **106**(1): p. 014502.
137. Lu, Y., et al., *Robust self-cleaning surfaces that function when exposed to either air or oil.* Science, 2015. **347**(6226): p. 1132-1135.
138. Wu, G., et al., *A Versatile Approach towards Multifunctional Robust Microcapsules with Tunable, Restorable, and Solvent-Proof Superhydrophobicity for Self-Healing and Self-Cleaning Coatings.* Advanced Functional Materials, 2014. **24**(43): p. 6751-6761.
139. Keller, J.B., *Geometrical Theory of Diffraction*.* Journal of the Optical Society of America, 1962. **52**(2): p. 116-130.
140. Wisdom, K.M., et al., *Self-cleaning of superhydrophobic surfaces by self-propelled jumping condensate.* Proceedings of the National Academy of Sciences, 2013. **110**(20): p. 7992-7997.
141. Liu, Y., et al., *Pancake bouncing on superhydrophobic surfaces.* Nat Phys, 2014. **10**(7): p. 515-519.
142. Yu, E., et al., *Extreme wettability of nanostructured glass fabricated by non-lithographic, anisotropic etching.* Scientific Reports, 2015. **5**: p. 9362.
143. Raj, R., et al., *High-resolution liquid patterns via three-dimensional droplet shape control.* Nature Communications, 2014. **5**: p. 4975.
144. Tasso R.M. Sales, S.C., G. Michael Morris and Donald J. Schertler, RPC Photonics Inc., *Engineered microlens arrays provide new control for display and lighting applications.* Photonics Spectra, 2004. **38**(6).
145. Deng, S., et al., *Optical scattering from graphene foam for oil imaging/sensing.* RSC Advances, 2016. **6**(76): p. 71867-71874.
146. Bubb, D.M., et al., *Laser processing of poly(methyl methacrylate) Lambertian diffusers.* Applied Surface Science, 2010. **257**(1): p. 22-24.
147. Kosoglu, M.A., et al., *Fiberoptic Microneedles: Novel Optical Diffusers for Interstitial Delivery of Therapeutic Light.* Lasers in Surgery and Medicine, 2011. **43**(9): p. 914-920.

148. Khan, A.A., et al., *Tunable scattering from liquid crystal devices using carbon nanotubes network electrodes.* Nanoscale, 2015. **7**(1): p. 330-336.
149. Butt, H., et al., *Electrically Tunable Scattering from Devitrite–Liquid Crystal Hybrid Devices.* Advanced Optical Materials, 2017. **5**(1): p. 1600414-n/a.
150. Jain, A., *Experimental study and numerical analysis of compression molding process for manufacturing precision aspherical glass lenses*, in *Industrial and Systems Engineering*. 2006, The Ohio State University. p. 201.
151. Lin, C.-F., Y.-B. Fang, and P.-H. Yang, *Optical film with microstructures array for slim-type backlight applications.* Optik - International Journal for Light and Electron Optics, 2011. **122**(13): p. 1169-1173.
152. Liwei, L., T.K. Shia, and C.J. Chiu, *Silicon-processed plastic micropyramids for brightness enhancement applications.* Journal of Micromechanics and Microengineering, 2000. **10**(3): p. 395.
153. Heidrich, S., et al., *Optics manufacturing by laser radiation.* Optics and Lasers in Engineering, 2014. **59**: p. 34-40.
154. Wood, J.P., et al., *Nanosecond pulse lasers for retinal applications.* Lasers Surg Med, 2011. **43**(6): p. 499-510.
155. Jain, A., *Experimental study and numerical analysis of compression molding process for manufacturing precision aspherical glass lenses*. 2006, The Ohio State University.
156. Jwad, T., et al., *Laser induced single spot oxidation of titanium.* Applied Surface Science, 2016. **387**: p. 617-624.
157. Zhao, Q., et al., *Printable Nanophotonic Devices via Holographic Laser Ablation.* ACS Nano, 2015.
158. Bitterli, R., et al., *Fabrication and characterization of linear diffusers based on concave micro lens arrays.* Optics Express, 2010. **18**(13): p. 14251-14261.
159. Jaax, M., et al., *Optical and THz Galois diffusers*. Journal of the European Optical Society. Vol. 8. 2013.
160. Piao, M.-L., et al., *Full-color holographic diffuser using time-scheduled iterative exposure.* Applied Optics, 2015. **54**(16): p. 5252-5259.
161. Teague, E.C., et al., *Light Scattering from Manufactured Surfaces††Contribution of the U.S. National Bureau of Standards, not subject to copyright.* CIRP Annals - Manufacturing Technology, 1981. **30**(2): p. 563-569.
162. Beckmann, P. and A. Spizzichino, *The scattering of electromagnetic waves from rough surfaces*. 1963: Pergamon Press; [distributed in the Western Hemisphere by Macmillan, New York].
163. Sparvoli, M. and R.D. Mansano, *Glass Difractive Optical Elements (DOEs) with complex modulation DLC thin film coated.* Materials Research, 2008. **11**: p. 341-345.
164. Nixon, M., et al., *Real-time wavefront shaping through scattering media by all-optical feedback.* Nat Photon, 2013. **7**(11): p. 919-924.
165. Singh, A.K., et al., *Exploiting scattering media for exploring 3D objects.* Light Sci Appl., 2017. **6**: p. e16219.
166. Donati, G., *Optical imaging: Light scattering on tape.* Nat Photon, 2017. **11**(3): p. 141-141.
167. Méndez, E.R., et al., *Photofabrication of random achromatic optical diffusers for uniform illumination.* Applied Optics, 2001. **40**(7): p. 1098-1108.
168. Ahmed, R., A.K. Yetisen, and H. Butt, *High Numerical Aperture Hexagonal Stacked Ring-Based Bidirectional Flexible Polymer Microlens Array.* ACS Nano, 2017. **11**(3): p. 3155-3165.
169. Yi Wu, C., T.H. Chiang, and C.C. Hsu, *Fabrication of microlens array diffuser films with controllable haze distribution by combination of breath figures and replica molding methods.* Optics Express, 2008. **16**(24): p. 19978-19986.
170. Yi, L., A. Pukhov, and B. Shen, *Direct acceleration of electrons by a CO2 laser in a curved plasma waveguide.* 2016. **6**: p. 28147.
171. Goldman, L., et al., *Some Parameters of High Output CO2 Laser Experimental Surgery.* Nature, 1970. **228**(5278): p. 1344-1345.
172. Yilbas., S.H.G.F.B.C.J.V.T.B.S., *Comprehensive Materials Processing*. Vol. 9. 2014, Amsterdam: Elsevier. p. 5634.

173. *Silicate Glasses: A Class of Amorphous Materials*, in *Microstructuring of Glasses*. 2008, Springer Berlin Heidelberg: Berlin, Heidelberg. p. 3-56.
174. Coucheron, D.A., et al., *Laser recrystallization and inscription of compositional microstructures in crystalline SiGe-core fibres.* 2016. **7**: p. 13265.
175. Lawrence, J. and L. Li, *Modification of the wettability characteristics of polymethyl methacrylate (PMMA) by means of CO2, Nd:YAG, excimer and high power diode laser radiation.* Materials Science and Engineering: A, 2001. **303**(1): p. 142-149.
176. Temelkuran, B., et al., *Wavelength-scalable hollow optical fibres with large photonic bandgaps for CO2 laser transmission.* Nature, 2002. **420**(6916): p. 650-653.
177. Ehler, A.W., *High‐energy ions from a CO2 laser‐produced plasma.* Journal of Applied Physics, 1975. **46**(6): p. 2464-2467.
178. Lee, X.-H., et al., *Surface-structured diffuser by iterative down-size molding with glass sintering technology.* Optics Express, 2012. **20**(6): p. 6135-6145.
179. Eastham, L., *LSD expands possibilities for beam shaping and optical control*, in *LEDs*. 2004, LEDs & Lighting media group: UK.
180. Sales, T.R., et al., *Light tamers.* Photonics Spectra, 2004. **38**: p. 58-65.
181. Ding, L., et al., *Orthogonal Molecular Structure for Better Host Material in Blue Phosphorescence and Larger OLED White Lighting Panel.* Advanced Functional Materials, 2015. **25**(4): p. 645-650.
182. Guay, J.-M., et al., *Laser-induced plasmonic colours on metals.* Nature Communications, 2017. **8**: p. 16095.
183. Wang, Z.K. and H.Y. Zheng, *Investigation on CO2 laser irradiation inducing glass strip peeling for microchannel formation.* Biomicrofluidics, 2012. **6**(1): p. 012820.
184. Zheng, H.Y. and T. Lee, *Studies of CO 2 laser peeling of glass substrates.* Journal of Micromechanics and Microengineering, 2005. **15**(11): p. 2093.
185. Lim, H.S. and J. Yoo, *FEM based simulation of the pulsed laser ablation process in nanosecond fields.* Journal of Mechanical Science and Technology, 2011. **25**(7): p. 1811.
186. Malinauskas, M., et al., *Ultrafast laser processing of materials: from science to industry.* Light Sci Appl., 2016. **5**: p. e16133.
187. Malka, V., et al., *Principles and applications of compact laser-plasma accelerators.* Nat Phys, 2008. **4**(6): p. 447-453.
188. *Microstructuring Glasses Using Lasers*, in *Microstructuring of Glasses*. 2008, Springer Berlin Heidelberg: Berlin, Heidelberg. p. 175-196.
189. Kalampounias, A.G., et al., *Influence of cw CO2-laser radiation on the amorphous-to-microcrystalline phase transition in a-Si:H films: a Raman spectroscopic study.* Applied Physics A, 2014. **116**(1): p. 303-310.
190. Huygens, C., *Treatise on Light*. 2007, Gloucestershire: Echo Library. p. 139.
191. Barrio, R.A., et al., *Regular ring dynamics in AX 2 tetrahedral glasses.* Physical Review B, 1993. **48**(21): p. 15672-15689.
192. Domine, F., and Piriou, B., *Rarnan spectroscopic study of the SiOr-Al2O.-KrO vitreous system: distribution of silicon second neighbors.* American Mineralogist, 1986. **71**: p. 38-50.
193. Yadav, A.K. and P. Singh, *A review of the structures of oxide glasses by Raman spectroscopy.* RSC Advances, 2015. **5**(83): p. 67583-67609.
194. Umesaki, N., et al., *Raman spectroscopic study of alkali silicate glasses and melts.* Journal of Non-Crystalline Solids, 1996. **205**: p. 225-230.
195. Deschamps, T., et al., *Soda-lime silicate glass under hydrostatic pressure and indentation: a micro-Raman study.* Journal of Physics: Condensed Matter, 2011. **23**(3): p. 035402.
196. Prange, R.E. and T.-W. Nee, *Quantum Spectroscopy of the Low-Field Oscillations in the Surface Impedance.* Physical Review, 1968. **168**(3): p. 779-786.
197. Montelongo, Y., et al., *Plasmonic nanoparticle scattering for color holograms.* Proceedings of the National Academy of Sciences, 2014. **111**(35): p. 12679-12683.
198. Katz, O., et al., *Non-invasive single-shot imaging through scattering layers and around corners via speckle correlations.* Nat Photon, 2014. **8**(10): p. 784-790.

199. Katz, O., E. Small, and Y. Silberberg, *Looking around corners and through thin turbid layers in real time with scattered incoherent light.* Nat Photon, 2012. **6**(8): p. 549-553.
200. Yalikun, Y., et al., *An all-glass 12 [small mu]m ultra-thin and flexible micro-fluidic chip fabricated by femtosecond laser processing.* Lab on a Chip, 2016. **16**(13): p. 2427-2433.
201. Jiang, Y., et al., *Auxetic Mechanical Metamaterials to Enhance Sensitivity of Stretchable Strain Sensors.* Advanced Materials, 2018. **30**(12): p. 1706589.
202. Jinno, H., et al., *Stretchable and waterproof elastomer-coated organic photovoltaics for washable electronic textile applications.* Nature Energy, 2017. **2**(10): p. 780-785.
203. Ko, H.C., et al., *A hemispherical electronic eye camera based on compressible silicon optoelectronics.* Nature, 2008. **454**: p. 748.
204. Kim, D.-H., et al., *Epidermal Electronics.* Science, 2011. **333**(6044): p. 838-843.
205. Yokota, T., et al., *Ultraflexible organic photonic skin.* Science Advances, 2016. **2**(4): p. e1501856.
206. Yu, Z., et al., *Intrinsically Stretchable Polymer Light-Emitting Devices Using Carbon Nanotube-Polymer Composite Electrodes.* Advanced Materials, 2011. **23**(34): p. 3989-3994.
207. White, M.S., et al., *Ultrathin, highly flexible and stretchable PLEDs.* Nature Photonics, 2013. **7**: p. 811.
208. Yetisen, A.K., et al., *Wearables in Medicine.* Advanced Materials, 2018. **30**(33): p. 1706910.
209. Guo, J., et al., *Highly Stretchable, Strain Sensing Hydrogel Optical Fibers.* Advanced Materials, 2016. **28**(46): p. 10244-10249.
210. Kolle, M. and S. Lee, *Progress and Opportunities in Soft Photonics and Biologically Inspired Optics.* Advanced Materials, 2018. **30**(2): p. 1702669.
211. Espinha, A., et al., *Hydroxypropyl cellulose photonic architectures by soft nanoimprinting lithography.* Nature Photonics, 2018. **12**(6): p. 343-348.
212. Elsherif, M., et al., *Wearable Contact Lens Biosensors for Continuous Glucose Monitoring Using Smartphones.* ACS Nano, 2018. **12**(6): p. 5452-5462.
213. Elsherif, M., et al., *Glucose Sensing with Phenylboronic Acid Functionalized Hydrogel-Based Optical Diffusers.* ACS Nano, 2018. **12**(3): p. 2283-2291.
214. Alqurashi, T., et al., *Laser inscription of pseudorandom structures for microphotonic diffuser applications.* Nanoscale, 2018. **10**(15): p. 7095-7107.
215. Han, T.-H., et al., *Extremely efficient flexible organic light-emitting diodes with modified graphene anode.* Nature Photonics, 2012. **6**: p. 105.
216. Chen, J., et al., *Transparent triboelectric generators based on glass and polydimethylsiloxane.* Nano Energy, 2016. **30**: p. 235-241.
217. Yong, J., et al., *A simple way to achieve superhydrophobicity, controllable water adhesion, anisotropic sliding, and anisotropic wetting based on femtosecond-laser-induced line-patterned surfaces.* Journal of Materials Chemistry A, 2014. **2**(15): p. 5499-5507.
218. Hong, W., X. Zhao, and Z. Suo, *Formation of creases on the surfaces of elastomers and gels.* Applied Physics Letters, 2009. **95**(11): p. 111901.
219. Cai, S., et al., *Creasing instability of elastomer films.* Soft Matter, 2012. **8**(5): p. 1301-1304.
220. Jun, K., J. Kim, and I.-K. Oh, *An Electroactive and Transparent Haptic Interface Utilizing Soft Elastomer Actuators with Silver Nanowire Electrodes.* Small, 2018. **14**(35): p. 1801603.
221. Chen, Y.-C. and A.J. Crosby, *High Aspect Ratio Wrinkles via Substrate Prestretch.* Advanced Materials, 2014. **26**(32): p. 5626-5631.
222. Lisensky, G.C., et al., *Replication and Compression of Surface Structures with Polydimethylsiloxane Elastomer.* Journal of Chemical Education, 1999. **76**(4): p. 537.
223. AlQattan, B., A.K. Yetisen, and H. Butt, *Direct Laser Writing of Nanophotonic Structures on Contact Lenses.* ACS Nano, 2018. **12**(6): p. 5130-5140.
224. Cassie, A.B.D. and S. Baxter, *Wettability of porous surfaces.* Transactions of the Faraday Society, 1944. **40**(0): p. 546-551.
225. Lafuma, A. and D. Quéré, *Superhydrophobic states.* Nature Materials, 2003. **2**: p. 457.

226. Alqurashi, T., et al., *Femtosecond laser directed fabrication of optical diffusers.* RSC Advances, 2017. **7**(29): p. 18019-18023.